HWR No. 97-020

INVESTIGATIONS OF STREAM-AQUIFER INTERACTIONS USING A COUPLED SURFACE-WATER AND GROUND-WATER FLOW MODEL

by

Leticia Beatriz Vionnet
Thomas Maddock III
and
David C. Goodrich

Department of Hydrology and Water Resources
University of Arizona
Tucson, Arizona 85721

INVESTIGATION OF STREAM-AQUIFER INTERACTIONS USING A COUPLED SURFACE-WATER AND GROUND-WATER FLOW MODEL

by

Leticia Beatriz Vionnet
Faculad de Ingenieria y Ciencias Hidricas
Universidad Nacional del Litoral
Santa Fe, Argentina,

Thomas Maddock III
University of Arizona Research Laboratory for Riparian Studies
University of Arizona
Tucson, Arizona

and

David C. Goodrich
Southwest Watershed Research Center
USDA-ARS
Tucson, Arizona

Department of Hydrology and Water Resources

University of Arizona
Tucson, Arizona 85721

January 1997

ACKNOWLEDGMENT

This research was supported in part by the Fish and Wildlife Service. Its sponsorship and in particular, the continuous support we received from Steve Cullinan and Les Cunningham is gratefully acknowledged. The research was also supported in part by Microway Company with a gift of an I-860 board and software. Our thanks to Ann and Steve Freid. The views and conclusions contained in this document are those of the authors and should not be interrupted as necessarily representing the official policies, either expressed or implied, of the Fish and Wildlife Service or of the Microway Company

Particular thanks go to Laurel Lacher and Shlomo P. Neuman for listening, discussing ideas, and suggesting ideas.

TABLE OF CONTENTS

LIST OF ILLUSTRATIONS

LIST OF TABLES

ABSTRACT

A finite element numerical model is developed for the modeling of coupled surface-water flow and ground-water flow. The mathematical treatment of subsurface flows follows the confined aquifer theory or the classical Dupuit approximation for unconfined aquifers whereas surface-water flows are treated with the kinematic wave approximation for open channel flow. A detailed discussion of the standard approaches to represent the coupling term is provided. In this work, a mathematical expression similar to Ohm's law is used to simulate the interacting term between the two major hydrological components. Contrary to the standard approach, the coupling term is incorporated through a boundary flux integral that arises naturally in the weak form of the governing equations rather than through a source term. It is found that in some cases, a branch cut needs to be introduced along the internal boundary representing the stream in order to define a simply connected domain, which is an essential requirement in the derivation of the weak form of the ground-water flow equation. The fast time scale characteristic of surface-water flows and the slow time scale characteristic of ground-water flows are clearly established, leading to the definition of three dimensionless parameters, namely, a Peclet number that inherits the disparity between both time scales, a flow number that relates the pumping rate and the streamflow, and a Biot number that relates the conductance at the river-aquifer interface to the aquifer conductance.

The model, implemented in the Bill Williams River Basin, reproduces the observed streamflow patterns and the ground-water flow patterns. Fairly good results are obtained using multiple time steps in the simulation process.

CHAPTER 1

INTRODUCTION

1.1. RIPARIAN AREAS

Riparian ecosystems in the western United States generally consist of mildly sloping valleys bordered by sharply rising mountain ranges. A river system typically meanders through the lower elevations of the valley. The streams may be perennial, ephemeral (flowing only occasionally after a rainy episode), or intermittent (flowing only through some reaches along their entire length). Higher elevations enjoy higher precipitation while the valley floor receives less rainfall. Under natural conditions, the precipitation regime regulates streamflows. However, due to development, many streams that were once perennial have turned into intermittent or ephemeral along parts of their length or have seen their flows controlled.

Distinctive to these areas is their oasis-like appearance, in sharp contrast with the desert landscape of the surrounding areas. Riparian corridors are habitats of a great variety of vegetation species as well as animal species, some of them unique to these areas, which depend on the availability of water in the right amount and at the right time for their existence. Both, streamflows and shallow water tables provide the necessary source of water to sustain life in these ecosystems, that is why the conjunctive analysis of surface waters and ground waters is of primary importance.

Major hydrologic processes such as open-channel flow, deposition and erosion of stream sediments, evapotranspiration, seepage into saturated or unsaturated sediments, and saturated flow under the water table, all vast disciplines in themselves, intervene on the stream-aquifer interaction phenomenon.

The interaction between streams and the adjacent aquifer can be of significant magnitude to affect the river flow by attenuating peak flows, reducing flood waves celerity and extending the recession limb of the discharge hydrograph. By the same token, the subsurface portion of the system can either receive considerable amounts of water to replenish its storage capacity after the dry season or discharge water to the stream during low flow periods.

Evapotranspiration from dense vegetation stands is one of the factors affecting the stream-aquifer interaction process. The water intake by plants depletes the unsaturated portion of the soil and lowers the water table reducing, in turn, the water recharge to the stream and increasing the discharge from the ground-water system. Other natural factors influencing the transfer of water from or to streams include geologic characteristics, seasonal variations, changing stream levels, channel dimensions, stream geomorphology, bed materials, ground-water flow patterns and spatial variability of sediment hydraulic properties.

Anthropogenic factors may interfere with the process as well. Water resources development as a result of human activities materializes through water diversion and retention structures and well fields that supply water for various uses. All these man-made structures affect the stream-aquifer interaction to a degree that will depend on the magnitude of the development and on the storage and buffering capacity of the system.

The Lower Bill Williams River Watershed (Figure 1.1), is host to one of the few remaining riparian areas in the state of Arizona, the Lake Havasu National Wildlife Refuge, managed by the Fish and Wildlife Service (FWS). Located in west central Arizona, it is characterized by an arid to semiarid climate. Its drainage network is an intricate arrangement of washes which flow only occasionally and converge to the Bill Williams River, the main water conduit in the area.

Although categorized as a remote area, the basin did not escape development. With the construction of Alamo Dam in 1969, streamflows became entirely regulated and more recently, the establishment of agricultural activities at Planet Ranch, immediately upstream from the Refuge, added even more stress to the system (Figure 1.2). Therefore, cultural and natural water uses compete between each other along the 35 miles reach that separates Alamo Dam from Lake Havasu.

Some field observations indicate that the combined effect of regulated flows and ground-water withdrawals has adversely affected the hydrologic conditions at the Refuge, jeopardizing its natural assets. Surface flows have disappeared in places where they used to be perennial while water table declines, though unquantified, have occurred. A recent ground-water modeling study by Harshman and Maddock (1993) alerted the FWS about the long term damaging consequences to the river if pumping continues at present rates. The FWS took immediate action and negotiated with the Planet Ranch owners to discontinue pumping to put a halt to the Refuge deterioration. Consequently, at the present time, no ground-water is being extracted from the basin.

With different local characteristics, the above picture repeats in many

Figure 1.1: Bill Williams River Basin (after Wolcott et al. 1956)

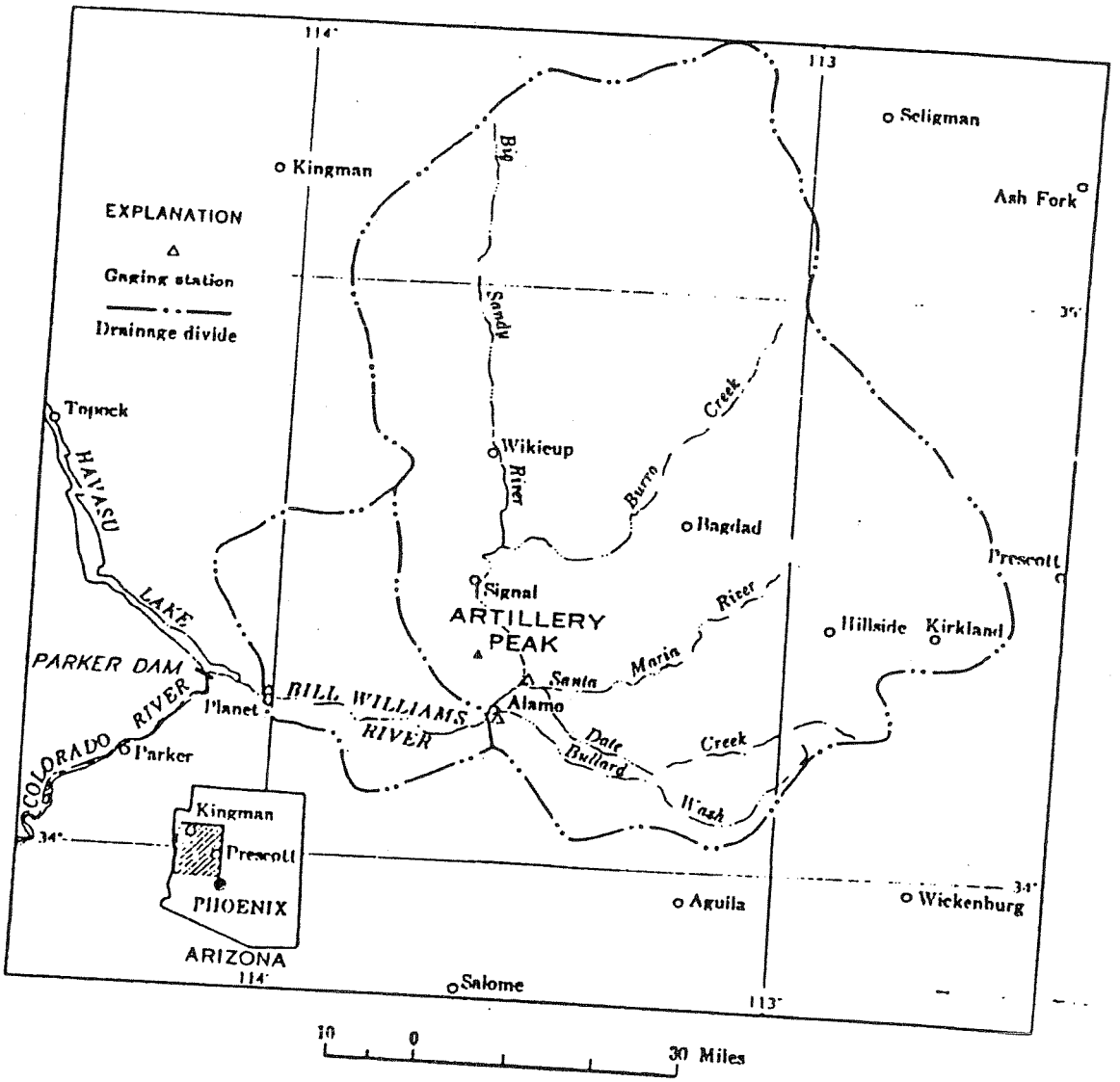

Figure 1.2: Lower Bill Williams Basin - Main features along the river

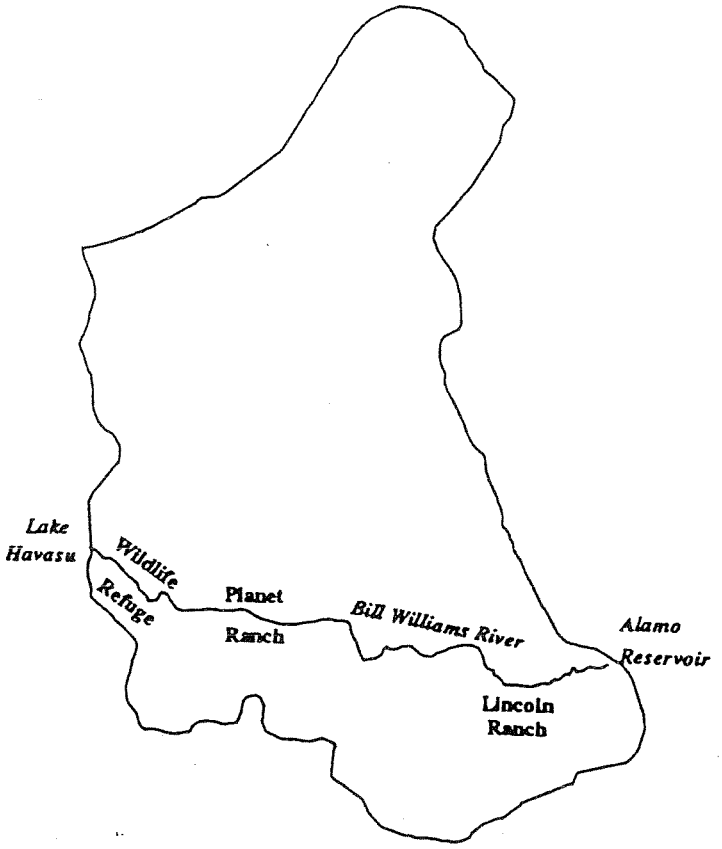

riparian areas throughout the western United States. The integral hydrologic study of these delicate systems can bring new light into the understanding of their functioning mechanisms which, in turn, may result in water management decisions and protective measures more wisely adopted.

1.2. THE STREAM-AQUIFER INTERACTION: BACKGROUND

Although the legal system in Arizona is still debating about the existence of a clear link between streams and aquifers, hydrologists are well ahead on this matter and have long recognized the undoubted relation between these two elements. Conjunctive analysis

of surface-water flow and ground-water flow in basin planning, development and management is greatly appreciated by hydrologists, particularly in areas of marginal or deficient rainfall. Because of that, this issue has been the focus of investigation for a few decades. However, in recent years the subject has gained strength motivated mainly by a generalized perception of a deteriorating situation in many riparian areas and a genuine will to protect them from further damage.

Different methods for assessing the interaction between surface and ground waters are available. They can be grouped in two major categories: field studies and numerical studies with distinct degrees of complexity. In addition, early research focused on the development of analytical techniques to evaluate the depletion of river discharge by pumping in nearby wells.

Basin scale field studies may be prohibitively expensive and time consuming. For these reasons, many field investigations are restricted to small areas within a seasonal time frame. Wilson and De Cook (1968), Cox and Stephens (1988) and Sophocleous *et al.* (1988), to name just a few, ventured into experimental stream-aquifer interaction studies.

In terms of streamflow depletion by pumping in nearby wells, some widely used techniques and principles include those by Theis (1941), Glover and Balmer (1954), Hantush (1959) and Glover (1974). The application of these techniques has been usually restricted to simple settings composed by a single well and a river section. Common simplifying assumptions behind some of them include fully penetrating streams, and isotropic and homogeneous aquifers of semi-infinite extent. In actuality, analytical solutions can be superimposed to study more complex systems, provided that they are linear. Recently, Sophocleus *et al.* (1995) evaluated the predictive accuracy of Glover's

(1974) stream-aquifer analytical model against the finite difference ground-water flow model MODFLOW (McDonald and Harbaugh 1988).

With the development of numerical models, many of the assumptions associated with stream flow depletion methods were not longer needed. Reduced costs and increased access to more powerful computers have favored the choice of numerical models. In general, two different approaches are followed in the mathematical modeling of the stream-aquifer interaction. The first is the single model approach, in which either a ground-water flow model or a surface water flow model is used. In general, ground-water models simulate streams in a simplified way through boundary conditions or source terms, giving poor or inadequate consideration to stream hydraulics, whereas most surface-water models treat all infiltrated water into the ground as a loss from the system. Therefore, neither a ground-water model nor a surface-water model seems to be fully appropriate to mimic the interaction between surface flows and subsurface flows.

Ground-water flow models such as MODFLOW (McDonald and Harbaugh 1988) and many others, can be used to simulate large scale systems. In the majority of MODFLOW applications, streams are simulated as having a constant stage over the whole simulation period, which in effect considers rivers as inexhaustible sources of water. With the introduction of the so called "stream package" (Prudic 1989) to be used with MODFLOW, a more realistic representation of streams is achieved. This package is not a true surface-water flow model but rather is a simple accounting routine that keeps track of flows in one or more streams which interact with the ground-water system. The river stage is allowed to vary and is calculated using Manning formula under the assumption of

a rectangular channel and steady flow conditions. Moreover, the amount of leakage through the streambed is limited to the available water on the stream.

The second approach in stream-aquifer modeling uses a ground-water flow model coupled with a surface-water flow model. The simultaneous solution of the ground-water flow equations and the unsteady open-channel flow equations can demand a great computational effort, which may not be justified in cases where the surface water system shows little variations. However, in situations where highly variable and dynamic seasonal effects are present, it is desirable that the stream-aquifer interaction be simulated with an adequate degree of sophistication and accuracy.

A source of difficulty in coupled modeling is given by the presence of multiple time scales in the representation of the river-aquifer interaction. In comparison with the characteristic time response of ground-water flows in the southwestern regions of the United States, surface-water flows are known to respond in very short times (on the order of hours or days). Then, it would be natural to assume that runoff processes will be unnoticed to ground-water systems. However, this is far from the truth in numerous real situations. In stream-aquifer interaction modeling, neglecting runoff and flood routing processes may lead to a misrepresentation of the interaction and, therefore, of the system dynamics. From a mass balance point of view, failure to incorporate runoff volumes can generate a water deficit that will be offset by other components of the system, namely baseflows and lower water tables, to satisfy the usually high evapotranspiration demand of riparian systems. From a mathematical point of view, the standard assumption set forth for modeling problems with disparate time scales is to drop the fast time scale and solve only for the slow time scale which, in turn, provides the sought long term behavior of the

system. However, in presence of nonlinearities, this aspect depends on whether or not the fast time scale effects accumulate to produce a cumulative effect that can influence the solution on the slow time behavior. Most of the stream-aquifer studies either neglect the fast time scale process (such as MODFLOW) or mainly focus on the passage and attenuation of a single flood wave through the system. Previous experience has shown that neglecting the flood routing process, when quantifying the stream-aquifer interrelationship in the long term, can deprive the system from an important amount of water that could otherwise satisfy evapotranspiration losses (Vionnet and Maddock 1992). Problems with streamflow calibration in ground-water modeling studies have been reported by Kraeger-Rovey (1975) and Vionnet and Maddock (1992). In both cases the calibration problems were attributed to the lack of runoff simulation in the model.

1.3. LITERATURE REVIEW

A survey of prior work on the stream-aquifer relationship can be discouraging, not because of the lack of material but because of its abundance. From site specific studies to theoretical studies, from field to modeling studies, from ground-water modeling to coupled modeling, from perennial to ephemeral streams, from clogging material characteristics to stream hydraulics and geomorphology, from infiltration under the streambed to recharge to shallow aquifers, all can be found under the single topic of stream-aquifer interactions. Because of the extensive volume of material available, this literature review is mainly restricted to numerical modeling studies. However, in the course of this work, more literature is analyzed and referenced.

Perhaps ground-water model applications can be counted by the hundreds, however those emphasizing the stream-aquifer relationship are less numerous. For instance Kraeger-Rovey (1975) developed a complex finite difference model to solve three-dimensional unsaturated or saturated flow that could be used in combination with a two-dimensional ground-water flow model. The model was applied to the Arkansas Valley in Southeastern Colorado. A negative pressure was considered at the bottom of the streambed to account for unsaturated conditions under the stream, an approach previously proposed by Bouwer (1964, 1966). Manning's equation was used to track down streamflows, approach later incorporated into MODFLOW by Prudic (1989). Kraeger-Rovey reported discrepancies between observed and computed discharges. Those discrepancies were attributed to a failure of the Kraeger-Rovey model to account for surface runoff and the lack of a dynamic equation to correctly describe the movement of a flood wave. More recently, Vionnet and Maddock (1992) implemented a ground-water flow model (MODFLOW) to study the ground-water system and the stream/aquifer interactions on the San Pedro River Basin in southeastern Arizona. The streams were simulated with the stream package (Prudic 1989) using baseflows as the input streamflow variable. Calibration problems were also encountered when trying to match simulated and observed baseflows. Those anomalies were explained by the lack of runoff representation in the model. Another ground-water flow modeling was reported by Sophocleus and Perkins (1993), who addressed the problem of declining streamflows in interconnected stream-aquifer systems in Central Kansas. The simulation model was a modified version of MODFLOW with the streamflow routing capabilities implemented by Prudic (1989). In what constitutes the first real application of the finite element ground-water flow model

MODXX (Jones 1992), Harshman and Maddock III (1993) evaluated the ground-water system and its relation to the stream system in the Bill Williams Basin. In this modeling activity, streams were represented by a modified version of the stream package.

Coupled modeling is not a new technique, but in the past it has been applied predominantly to simple cases. Most coupled models are solved with finite difference techniques (Pinder and Sauer 1971, Zitta and Wiggert 1971, Freeze 1972, Kraeger-Rovey 1975, Akan and Yen 1981, Miles and Rushton 1983, Swain and Wexler 1991,1993). Others are solved with the finite element method (Cunningham and Sinclair 1979, Crebas *et al.* 1984, Glover 1988, Defina and Matticchio 1994). In general all coupled models share common goals, which are achieving a better understanding of the stream/aquifer relationship and assessing the impact of man related activities. However, they differ in the model assumptions, in the numerical techniques employed and in the application cases.

Pinder and Sauer (1971) are usually credited for providing a breakthrough in stream-aquifer interaction modeling. They coupled a two-dimensional horizontal unconfined aquifer model mathematically represented by the well known Boussinesq equation, to a one-dimensional open channel flow model to analyze the system in the context of bank storage effects on flood wave propagation.

Similar lines of investigation to those of Pinder and Sauer were followed by Zitta and Wiggert (1971). Their model solved the one-dimensional open channel flow equations and the one-dimensional Boussinesq's equation in a direction perpendicular to the stream channel flow. Recharge from the stream to the aquifer was determined from the volume displaced per unit time by the fluctuations of the water table.

Another early contribution to the field of coupled models was made by Freeze in 1972, who quantitatively showed the importance of subsurface response in baseflow dominated streams and the mechanisms of baseflow generation. Freeze moved one step forward in the simulation of the subsurface flow component, incorporating unsaturated flow into the modeling process. Three-dimensional, transient saturated-unsaturated flow, represented by the Richards' equation, was coupled with one-dimensional, gradually varied, unsteady channel flow, mathematically represented by the one-dimensional Saint Venant equations. The model was applied to a hypothetical basin.

Akan and Yen (1981) presented a conjunctive surface-subsurface flow model which solved the one-dimensional Saint Venant equations coupled with the saturated-unsaturated flow equation. The authors emphasized more on some tests run to verify the individual components of the conjunctive model than on the model itself. The application of the conjunctive model was restricted to a very simple experimental test.

Another methodology employed in the study of stream-aquifer relations is the convolution equation. Hall and Moench (1972) used the convolution integral in the analysis of one-dimensional confined flow in a homogeneous isotropic aquifer of finite or infinite extent. The discharge into or out of the stream was obtained upon applying Darcy's law. Through the use of hypothetical examples, the authors succeeded in demonstrating the ability of the convolution method in the analysis of stream-aquifer relationships.

The boundary integral equation method (BIEM) has been used by Dillon and Liggett (1983) to simulate the interaction between an ephemeral stream and an unconfined aquifer through a semipervious streambed. The model developed by Dillon and Liggett

handled both, saturated and unsaturated conditions under the streambed, as well as the transition between these two states. The unsaturated flow portion was represented by a combination of the Green-Ampt model used to compute the time delay for recharge, and Darcy's law modified with a negative pressure at the bottom of the streambed to compute recharge. The paper also presents results obtained on a real case study conducted on a 3 km reach along the Little Para River in Australia.

Of the many factors that affect the transfer of water from ephemeral channels to the sediments under the channel, Reeder *et al.* (1980), Freyberg *et al.* (1980) and later Freyberg (1983) concentrated in the variability of the stream water levels. On one hand, Reeder *et al* (1980). investigated infiltration rates into initially unsaturated soils by numerically solving the one dimensional Richards' equation. On the other hand, Freyberg (1983) studied infiltration through a symmetric triangular cross section with vertical impermeable sidewalls and no overtopping. Freyberg used the Green and Ampt model to simulate infiltration into homogeneous sediments. This model, according to previous work by the same author, produced results that reasonably agree with numerical approximations to the Richards' equation. These findings agree with the conclusions later reported by Reid and Dreiss (1990) for their homogeneous fluvial sediments case.

Reid and Dreiss (1990) conducted a modeling study to analyze the effects of unsaturated, stratified sediments on ground-water recharge from intermittent streams. The paper concentrated more on alternative ways to represent river leakage. It also intended to examine how different fluvial stratigraphy may affect the timing and style of channel loss and ground-water recharge. The model used in the study was the finite element computer code UNSAT1 (Neuman 1972), which solves the nonlinear Richards' equation.

Reid and Dreiss also compared simulation results obtained with the two-dimensional model with results obtained with simplified methods for computing channel losses such as the Green-Ampt model and Darcy's law.

A recent model development by Swain and Wexler (1991,1993) who combined two public domain computer codes, MODFLOW and BRANCH, solving the ground-water flow and surface water flow equations simultaneously. BRANCH is a U.S. Geological Survey model that solves the one-dimensional Saint Venant equations for unsteady flow in open channels. The report presents a series of examples aimed at verifying the model that range from a flood wave propagation with bank storage to a real case application in Southwestern Florida. The main disadvantage of this model is that it possesses all the limitations inherent to MODFLOW to represent intricate geometries.

In summary, much of the work done after Pinder and Sauer (1971) and Freeze (1972) is rather similar with respect to the selection of the type of surface water and ground-water models and the methodology of their coupling. Subsequent modeling efforts differ in the character of the specific problems considered, in the modular structure of the model, and in the numerical algorithms and techniques used for their solution. All these aspects were remarked by Vasiliev(1987) on his review paper on stream-aquifer interaction modeling.

1.4. STATEMENT OF PURPOSE

The primary goal of the present study is the development of a robust finite element code for the simultaneous representation of ground-water flows and surface-water flows along with their interaction. The development is accomplished using state-of-the-art

numerical algorithms based upon well-established physical principles. Comparison with exact solutions of the proposed mathematical model and with published results, if any, is made whenever possible. It is shown that the coupled model presented here is able to capture the observed dynamics of the study area, to maintain full coupling between surface flows and ground-water flows, and to combine the time scales characteristic of both components. Furthermore, it only requires standard data that is relatively easy to obtain.

Seasonal processes and slow time processes are handled by the ground-water module. Aerial recharge and discharge, evapotranspiration, point sink/sources, line sources, prescribed head and prescribed flux boundary conditions are all included in the ground-water module. Confined flow as well as unconfined flow under the Dupuit assumption are modeled on a single aquifer system.

Surface flows are simulated using the one dimensional kinematic wave model that propagates streamflows over a non-erodable stream with rectangular cross-section. It is shown that this approximation of the fast time scale process is adequate to study channel flows in the study area. The application of several criteria based on normal flow conditions reveals that the leading mechanisms of flood waves movement are gravity and friction, giving rise to kinematic waves (Lighthill and Whitham 1955). Even with today's controlled flows at Alamo Dam, kinematic mechanisms are shown to capture surface-water flows adequately. Backwater effects such as those triggered by a downstream lake are considered negligible. Otherwise, the dynamic wave model should be considered.

The two main components of the integrated model are linked through a coupling term, mathematically represented by an expression analogous to Ohm's law. In employing such a relationship, it is assumed that all infiltrated water is instantaneously recharged to

the aquifer, that channel loss equals recharge to the aquifer, and that the transfer of water is controlled by saturated flow through low permeability streambed sediments. Nonetheless, it is shown that this formulation provides satisfactory results for a basin scale application like the one presented in Chapter 7. Needless to say that this approximation should not be used in cases where unsaturated sediments of considerable thickness separate the streambed from the water table.

The remaining purpose of this investigation is to provide some answers to some specific questions concerning wildlife refuges in arid to semi-arid regions. In particular, the present work concentrates on estimating the impact of ground-water exploitation and regulated streamflows on the Bill Williams River flows and the water table in the Refuge and its adjacent areas. Due to the small amounts of precipitation the study area receives, overland flow is not simulated. Moreover, ephemeral flows from tributaries to the Bill Williams are unquantified, however their magnitude is believed to be negligible compared to the main channel flows. Therefore, the single channel representation of the system is considered appropriate.

In summary, even though the model here discussed is developed with the final purpose of being implemented in the study area, it is general enough to be applied to many other cases, provided that its limitations are well understood.

1.5. REPORT OUTLINE

This report is divided into eight chapters and one appendix. Chapter 2 provides an overview of the study area including its location, topography, climate, geology and vegetation. Its ground-water hydrology and surface-water hydrology are described in

more detail. The complete mathematical setting of the ground-water flow and the coupling term are presented in Chapter 3. In particular, Section 3.3 on the coupling term covers some of the most interesting aspects of the stream-aquifer interaction. It also deals with a different interpretation of the classical representation of the interaction. This chapter concludes with the treatment of sink/source terms. Chapter 4 begins with an overview of the flood routing process. The unsteady open channel flow governing equations are given, with particular emphasis on the kinematic wave model and its range of applicability. The dimensional analysis of the governing equations is presented in Chapter 5. The next chapter is devoted to the discretization of the governing equations using the finite element method. The Bubnov-Galerkin method is implemented for the parabolic ground-water flow equation and the Petrov-Galerkin method is implemented for the hyperbolic-like behavior of the kinematic wave equation. Flux boundary computations, mass balance and time stepping algorithms are discussed in detail. Finally, the global structure of the integrated model is described. Chapter 7 presents the implementation of the coupled model to the Lower Bill Williams River Basin. The work includes the conceptualization of the system, the construction of the model grid, the definition of initial conditions, boundary conditions and aquifer properties, and the specification of all data related to the stream characterization. This chapter also includes the model calibration and simulations. Chapter 8 is the closure chapter while Appendix A details some of the different tests performed to validate both model components.

CHAPTER 2

DESCRIPTION OF THE STUDY AREA

2.1. LOCATION AND PHYSIOGRAPHY

The Bill Williams River drains portions of La Paz, Mohave and Yavapai counties in west-central Arizona. Its major tributaries include the Burro Creek, the Big Sandy River, the Date Creek and the Santa Maria River (Figure 1.1). Alamo Lake captures the surface flows from all these tributaries and adjacent areas and its releases give rise to the Bill Williams River. The river flows southwest for about 56 *km* and for most part traverses isolated terrain through a narrow channel confined between the rock walls of the mountains which it cuts. The Bill Williams River also passes through a 9.7 *km* long flood plain, the Planet Ranch Valley, located approximately 27-29 *km* downstream of Alamo Dam to finally discharge into Lake Havasu on the Colorado River (Figure 1.2).

The drainage area of the entire basin is quite large totaling 13,700 km^2 of which 12,250 km^2 drain to Alamo Lake. The Lower Bill Williams River Basin (LBWRB) is the watershed that encompasses all the drainage area below Alamo Dam and encloses 1450 km^2 (Rivers West 1990). The boundary and the complex drainage network of this subwatershed are shown in Figure 2.1. This study is particularly concerned with a portion of the LBWRB whose borders are approximately delineated by the boundary of the alluvial aquifer underlying the Bill Williams River, covering about 85 km^2.

Figure 2.1 - Lower Bill Williams River basin boundary and drainage network

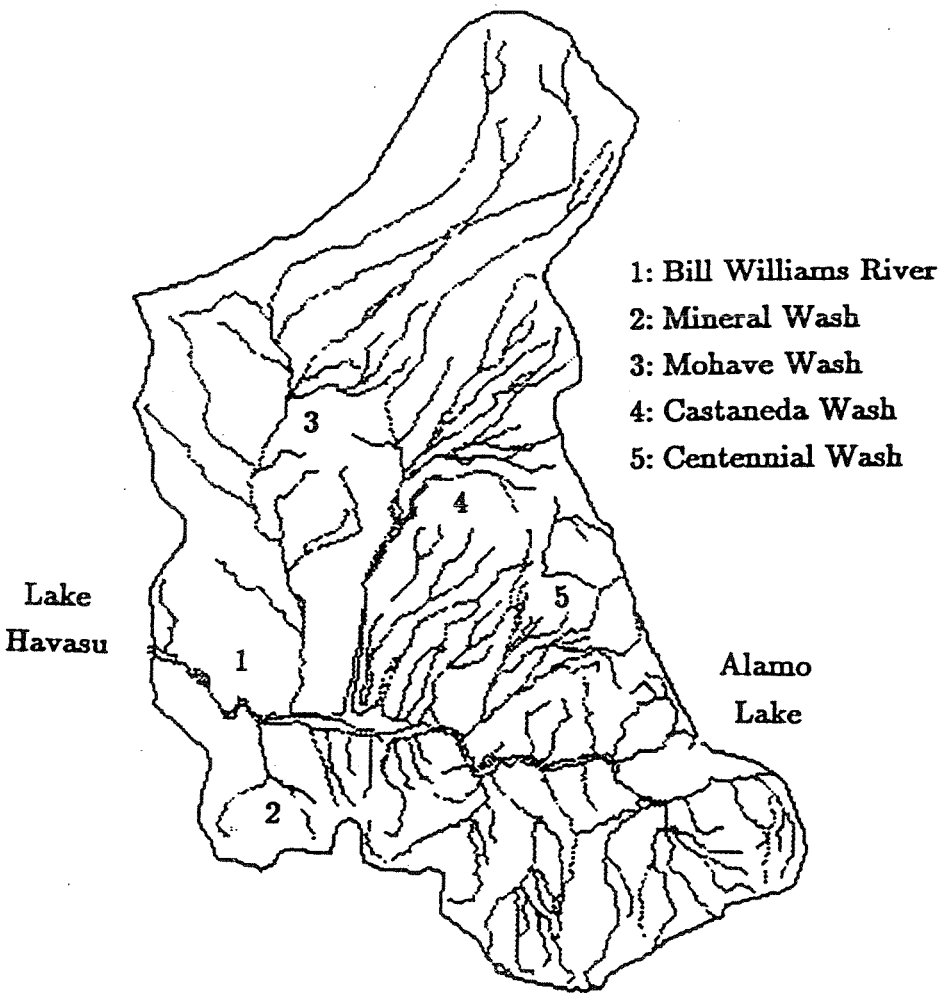

2.2. TOPOGRAPHY

The LBWRB lies within the Basin and Range Phisiographic Province of the Sonoran Desert (Anderson *et al.* 1992). This province is generally characterized by broad gently slopping valleys bordered by steep mountain ranges. The study area shares some of these phisiographic patterns but also has its own, typified by sharp canyon walls

constraining the river for several miles downstream of Alamo Dam. The Buckskin mountains bound the narrow valley from the south, and the Rawhide mountains and the Little Rock mountains limit the valley to the north (Figure 2.2).

Elevations range from about 1,525 *m* at the northernmost portion of the lower basin up to only 137 *m* at the junction of the Bill Williams River with Lake Havasu just north of Parker.

2.3. CLIMATE

Very hot summers and mild winters characterize the severe climate of the area. Summer temperatures in the lower elevations average 39.4-42.2°*C*, while winter day temperatures average 15.56-16.67°*C*.

The average annual precipitation is 137.2-195.6 *mm*, ranging between 6.9 *mm* and 254 *mm* (Bureau of Land Management 1988). The eastern portion of the watershed enjoys higher averages, in the order of 312.4-370.8 *mm*. The annual rainfall distribution shows two distinct rainy seasons which differ from each other in origin and intensity. Summer rains are often violent and usually last but a short period of time while winter storms may produce several days of gentle rain of moderate intensity.

Lake evaporation figures in the Bill Williams area have been estimated to be, on the average, 300 to 315 *mm/year* (Anderson *et al.* 1992).

Figure 2.2: Mountain ranges (after Harshman and Maddock 1993)

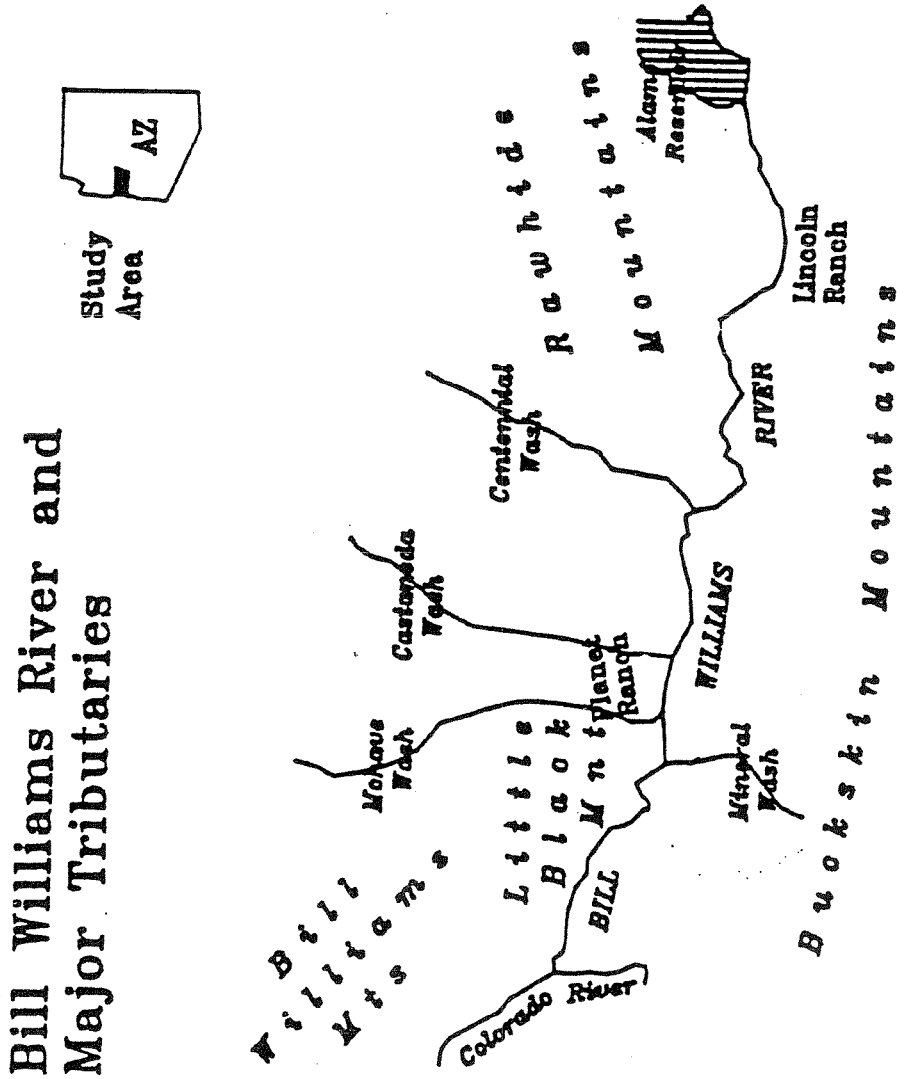

2.4. GEOLOGY

Three principal units can be defined in basins located within the Basin and Range province: 1) rocks of the mountains, 2) pre-Basin and Range sediments, and 3) basin fill deposits (Anderson *et al.* 1992).

Igneous, metamorphic and sedimentary rocks of various ages form the rocks of the mountains, which for all practical purposes do not yield water and act as boundaries to the ground-water flow in the basin.

The pre-Basin and Range sediments are composed by deposits that range in composition from silt, clay, and claystone to gravel and conglomerate. Their degree of consolidation varies from moderate to high. This type of sediment can reach several thousand meters in depth.

Basin fill deposits are the water bearing unit by excellence. Deposited during the late Terciary to Quaternary, they consist of weakly to highly consolidated gravel, sand, silt, and clay. Many investigators have divided the basin fill deposits into three general units: 1) lower basin fill, 2) upper basin fill, and 3) stream alluvium (Figure 2.3).

Lower basin fill deposits usually contain fine grained materials with a high degree of cementation, with their major depth development occurring toward the center of the valley. The upper basin fill materials, which overlie the former unit, are generally more coarse grained and less cemented than the lower basin fill. Together, both units have a considerable water storage capacity.

Finally, the stream alluvium, deposited during and after the establishment of the present surface drainage system, consists mainly of unconsolidated silt,

2.5. VEGETATION AND WILDLIFE: LAKE HAVASU NATIONAL WILDLIFE REFUGE

Migrant and resident wildlife species are attracted by the wetland and open waters of Lake Havasu and the Bill Williams River. The riparian habitat along the river represents the largest remaining riparian corridor along the highly regulated Lower Colorado River.

The Lake Havasu National Wildlife Refuge, managed by the U.S. Fish and Wildlife Service, covers over 2,428 *hectares* of land and extends approximately 19.3 *km* east from Lake Havasu. At its lower end, a cattail dominated marshland serves as the link between Lake Havasu and the river itself. Upstream of the marshy area the river supports dense forests of cottonwood (*Populus Fremontii*) and willow (*Salix Gooddingii)*. Abundant vegetation stands also develop between the dam and the Planet Ranch, whose aerial extent is comparable to that of the Wildlife Refuge.

The dominant vegetation species within the riparian stretches along the Bill Williams River consist mainly of mesquite (*Prosopis juliflora)*, cottonwood, salt cedar (*Tamarix sp.)* and willow, all vegetation types common to most southwestern riparian systems. In addition to these species, the study area sustains a considerable population of cattail (*Typhia spp.*) and bulrush (*Scripus spp.*), located in the marshy area at the downstream end of the Refuge, and small stands of smoketree (*Dalea spinosa*) and inkweed (*Suaeda torreyana*).

The Bureau of Land Management-BLM (1989) and Rivers West (1990) documented the area covered by native vegetation, upstream of the Planet Ranch and within the Refuge, respectively. Table 2.1.*a* and Table 2.1.*b* provide the aerial coverage of riparian vegetation categorized by composition of species.

2.5. VEGETATION AND WILDLIFE: LAKE HAVASU NATIONAL WILDLIFE REFUGE

Migrant and resident wildlife species are attracted by the wetland and open waters of Lake Havasu and the Bill Williams River. The riparian habitat along the river represents the largest remaining riparian corridor along the highly regulated Lower Colorado River.

The Lake Havasu National Wildlife Refuge, managed by the U.S. Fish and Wildlife Service, covers over 2,428 *hectares* of land and extends approximately 19.3 *km* east from Lake Havasu. At its lower end, a cattail dominated marshland serves as the link between Lake Havasu and the river itself. Upstream of the marshy area the river supports dense forests of cottonwood (*Populus Fremontii*) and willow (*Salix Gooddingii)*. Abundant vegetation stands also develop between the dam and the Planet Ranch, whose aerial extent is comparable to that of the Wildlife Refuge.

The dominant vegetation species within the riparian stretches along the Bill Williams River consist mainly of mesquite (*Prosopis juliflora)*, cottonwood, salt cedar (*Tamarix sp.)* and willow, all vegetation types common to most southwestern riparian systems. In addition to these species, the study area sustains a considerable population of cattail (*Typhia sp.*) and bulrush (*Scripus sp.*), located in the marshy area at the downstream end of the Refuge, and small stands of smoketree (*Dalea spinosa*) and inkweed (*Suaeda torreyana*).

The Bureau of Land Management-BLM (1989) and Rivers West (1990) documented the area covered by native vegetation, upstream of the Planet Ranch and within the Refuge, respectively. Table 2.1.*a* and Table 2.1.*b* provide the aerial coverage of riparian vegetation categorized by composition of species.

Table 2.1: Aerial coverage of riparian vegetation

Vegetation Type	Area (ha)
Salt Cedar/Willow	210.89
Mesquite/Salt Cedar	231.94
Mesquite/Salt Cedar/Willow	41.61
Mesquite	39.42
Mesquite/Inkweed	16.92
Hymenocleo Sp.	35.31
Cottonwood/Willow	26.57
Inkweed	2.88
Smoke Tree	1.05

(a) Upstream of the Planet Ranch (after BLM 1989)

Vegetation Type	Area (ha)
Cattail/Bulrush Marsh	135.55
Cottonwood/Willow/Salt Cedar	164.31
Willow/Salt Cedar	216.51
Salt Cedar	230.68

(b) Wildlife Refuge (after Rivers West Inc. 1990)

1 hectare=10,000 m^2

Riparian vegetation within the Refuge has been affected by high Alamo Dam releases during extended periods of time, causing considerable mortality of cottonwood and willow. More recent ground-water development may have also adversely impacted on vegetation development by lowering the water table and reducing soil moisture availability, both essential for plant survival

2.6. HYDROLOGY OF THE STUDY AREA

The description of the surface water system, the ground-water system and their interrelationship will set the framework for the necessary assumptions and simplifications later introduced in the implementation of the model. Actuality, no real physical dissociation between these two systems exists. However, for the sake of a better presentation of the available information, they will be described in separate sections and their link appropriately established.

2.6.1. Surface water hydrology

The drainage network of the basin looks overwhelmingly intricate (Figure 2.1), but when it comes to flowing streams, the arrangement of channels reduces to a handful of washes that drain the entire watershed and discharge into the BWR. They are the Mineral Wash to the south and the Castaneda, Centennial and Mohave Washes to the north.

Remote as the area is, it comes to no surprise that gaging stations are not common. None of the above washes has ever been gaged, however their ephemeral flows are deemed negligible compared to the BWR streamflows.

There is only one gaging station along the BWR with a period of records long enough for statistical analysis. The station at Alamo (USGS # 09426000) registered daily flows from 1940 to 1968. With the establishment of Alamo Dam, this station was moved a short distance downstream to the location that occupies today. Records at this new location represent daily dam releases and have been measured on a continuous basis since 1969. A second station was operative (USGS # 09426600) near Planet Ranch for a

number of years (1929-1946) and was abandoned ever since. In 1989 the Fish and Wildlife Service relocated this station and reinitiated streamflow recording.

The natural streamflow conditions were first altered in 1932 by Havasu reservoir, whose waters inundated about 6-8 *km* of land upstream of the river confluence shaping up the marsh that exists today. The normal operation elevation for that lake is about 137 *m*

Alamo Dam, with a normal operation elevation of 335 *m*, controls upstream flows modifying, in turn, the morphology of the stream. Up to what extent natural flows have been altered may be partially quantified by means of a monthly streamflow analysis. Figures 2.4.*a*, *b*, and *c* represent maximum, minimum, median and mean monthly flows, respectively, for the period 1940-1968 and the period 1969-1993. After 1969, maximum dam releases are higher than during the pre-dam era. The most dramatic change caused by the dam operation is reflected on minimum flows. During the post-dam period, zero flows are reported for a period of 7 consecutive months, situation that certainly did not occur prior to 1969. The picture is not that clear for median and mean flows. Median flows, which better represent seasonal patterns, suffered little modification except for the month of March, where the influence of high magnitude floods is noticeable. The same effect repeats on mean flows, with slightly higher flows during the dry months of the post-dam era. Figures 2.4.*c* and 2.4.*d* also show two distinct peaks, the first concentrated during the months of February, March and April, and the second, of much smaller magnitude, during August. Upstream flows are greatly depleted before they reach the Refuge. If they are not of a sufficient magnitude to overcome transmission losses at Planet Ranch, the river dries out along the 9.7 *km* reach of the Ranch. Surface flows reappear at the Refuge due

to the regulating flow effects of the Planet Ranch alluvial. In this area, alluvial deposits are 2 to 3 times deeper than elsewhere forming a bucket with an enormous buffering capacity.

Figure 2.4: Monthly streamflows at Alamo station

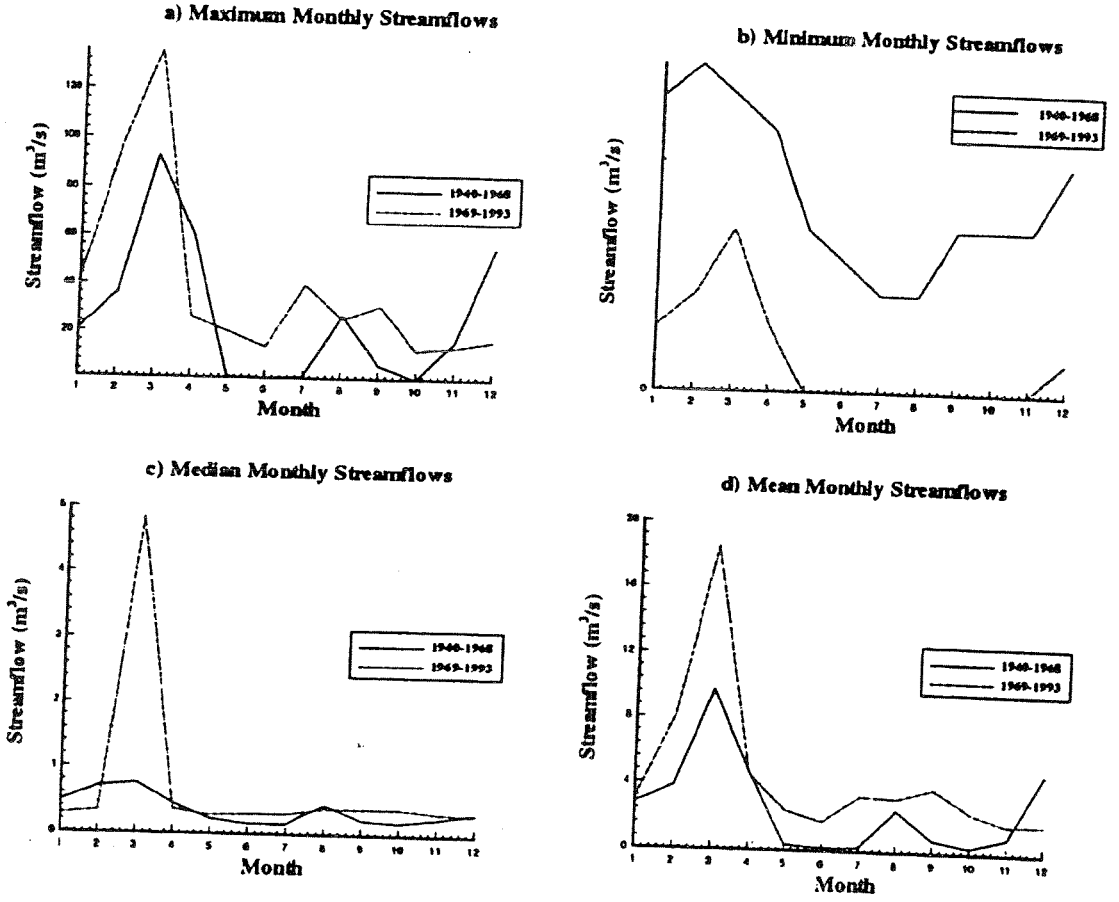

2.6.2. Ground-water hydrology

A fairly simple aquifer system hides behind a complex geology. The presence of an underlying regional aquifer interacting with the shallow alluvial aquifer is yet to be identified. The only assertion about it was made by the Corp of Engineers (1964), who stated that about 15 % of dam releases is lost to a highly fractured regional formation immediately downstream of the dam. Hence, the alluvial aquifer is the prevailing water bearing unit in the system.

Alluvial deposits range in depth from about 18 *m* at the canyon below the dam up to a maximum of 60-90 *m* at the Planet Valley (Wolcott *et al.* 1956, Turner 1962, CoE 1964, Wilson 1979).

Recent stream alluvium of unknown thickness, composed primarily of sand, forms the alluvial aquifer within the Refuge. Results of aquifer tests have been reported by several authors (Table 2.2). In all cases, hydraulic conductivity values show great disparity and seem to be unusually high, even for clean sand and gravel deposits.

Table 2.2 - Results of aquifer tests

Author	Test Location	Transmissivity (m^2/day)	Estimated Aquifer Thickness (m)	Hydraulic Conductivity (m/days)
Turner(1962)	Planet Ranch	38,612	23	1,645
	Planet Ranch	11,526	44	263
	Planet Ranch	16,173	12	1,327
CoE (1964)	Below Alamo Dam			1,829
Fogg *et al* (1976)	Planet Ranch		61	166-175
BLM (1988)	(estimated from tables)			2,696

The Planet Ranch alluvial and its flow dynamics provide unique characteristics to the system. It extents about 9.7 ***km*** parallel to the river and 2 ***km*** perpendicular to it. Assuming an average depth of 76 *m* and a specific yield of 0.20, the storage capacity of this bucket is estimated to be 2.9488×10^8 m^3. This formation acts as a flow attenuator and regulator, absorbing a great proportion of upstream and tributaries flows and releasing baseflows back to the river at a point downstream. During low flow periods the 9.7 ***km*** reach at the Ranch remains dry while during flood events the reach is completely covered with flood waters. The immense buffering capacity of the Planet Ranch alluvial manifests primarily in the streamflows registered at the Refuge, as drastic changes in dam releases are not proportionally corresponded by equal changes in the Refuge surface flows.

Sources of ground-water in the alluvial basin along the BWR include recharge from flood flows, underflow from tributaries, underflow from Alamo Dam, return flows from irrigation, and recharge from precipitation on the watershed.

Recharge from flood flows is the major source of ground-water, in particular at the Planet Valley. Transmission losses in that area are quite high, varying in magnitude with upstream flows. For instance, BLM (1988) reported that for a 2.97 m^3/s dam release, about 62 % of the streamflow is lost at Planet Valley. Although not necessarily all infiltrated water will percolate into the aquifer, the high permeability of the sediments and a shallow water table suggest that a good proportion of it makes its way to the water table. This point is illustrated in the following section.

Underflow from tributaries is poorly known. Turner (1962) estimated that during the months of October, November and December, approximately 9.87×10^5 m^3 per month enter Planet Valley from the north, while the Refuge receives about 9.0×10^5 $m^3/year$ of underflow from Mineral and Mohave washes. More recent studies have not reexamined these figures.

The loss of flow from Alamo Dam has been estimated at 0.79 m^3/s. However, this underflow is based on high hydraulic conductivity values and assumes no losses to the regional aquifer, which are likely to take place (Jackson and Summers 1989).

Return flows from irrigation and recharge from precipitation are only potential sources of ground-water. First of all, a low efficiency irrigation system and very dry conditions combine to prevent any irrigation water from reaching the water table. Secondly, there is virtually no recharge from precipitation in this arid region.

2.6.3. Historic water levels

Water level data in the study area are sparse. Nevertheless, two water level surveys conducted by the USGS in 1979 and in 1990 provide valuable information to delineate general ground-water flow patterns in the entire basin. No water level data prior to 1979 could be traced down. In 1979, a total of 59 wells were monitored. Figure 2.5 illustrates water level contours for that year generated with the inverse distance interpolation method. The location of the data points used in the interpolation as well as the boundary of the model area, introduced in Chapter 7, are also indicated in the graph. The steepest gradients occur in the northernmost portion of the watershed, where ground elevation reaches over 1500 *m* and some mountain front recharge is likely to take place. Hydraulic head gradients smooth down gradually toward the valley floor and are mild along the Bill Williams River. The water level drop between Alamo Dam and Lake Havasu is approximately 107 *m*. A small number and an uneven distribution of observation points in the 1990 survey introduce fictitious distortions to the ground-water pattern. Hence, this information is discarded for further analysis.

More valuable to the goals of this study are water level data obtained in the Planet Ranch area, where monthly static water levels have been recorded in 13 wells since 1985 by Ranch personnel (Hill 1992). Figure 2.6 shows the location of commercial wells within the irrigation fields. Due to some discrepancies between the well number reported by the Ranch manager and well records obtained from the Arizona Department of Water Resources (ADWR), the UTM well coordinates provided in the map were extracted from USGS topographic maps.

Figure 2.5: Water level contour map for 1979 conditions

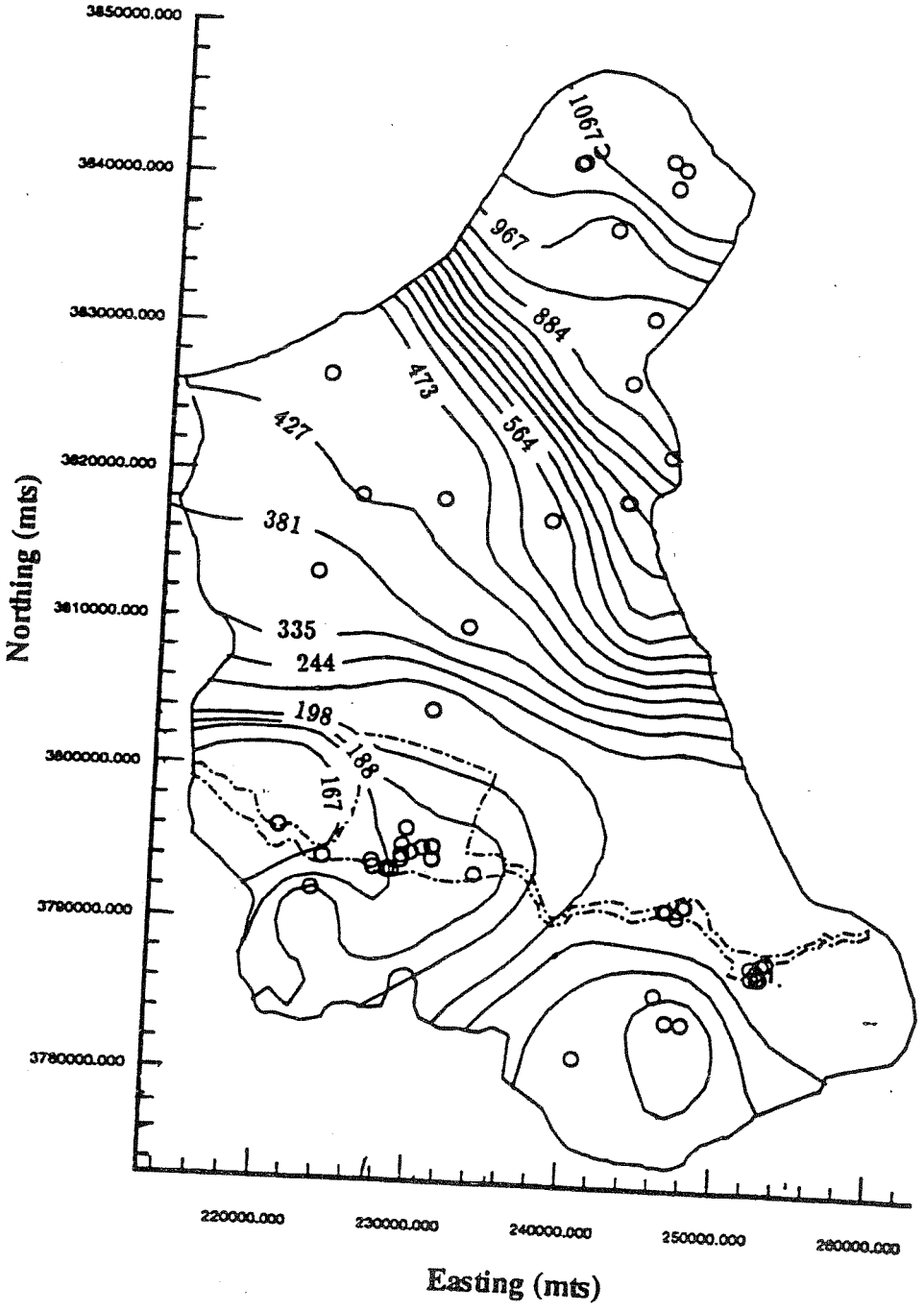

Figure 2.6: Well location at Planet Ranch

Well Number	Location		Distance from River (m)	Well Altitude (m)
	Easting (m)	Northing (m)		
2	234116	3793241	377	187
3	227159	3794051	294	178
4	228772	3793836	456	184
5	229056	3794122	54	183
6	229160	3795148	895	194
7	231082	3795030	1570	195
8	229763	3794583	723	186
9	230820	3794227	710	189
10	233074	3794740	921	
11	233318	3794371	996	
12	232503	3794660	1440	
13	231876	3794901	1715	
14	231208	3794223	808	189

In the presence of highly permeable materials, ground-water levels fluctuate rapidly in response to water use by riparian vegetation, water use for agricultural activities, changes in river stage and infiltration of runoff water.

Riparian vegetation, once present at the Planet Valley, was cleared out to allow for agricultural development, then ground-water level fluctuations are mainly due to the last three of the aforementioned factors.

Figures 2.7 to 2.9 show well hydrographs. Water level data cannot be fairly interpreted without regarding at simultaneous dam releases, graphed on Figure 2.10. Some relevant remarks can be drawn from the conjunctive evaluation of this set of graphs. First of all, the quick response of the ground-water system is worth noting. Depending on the magnitude of streamflow peaks, a one month lag between streamflow peaks and water level peaks is observed. This may just reflect the measurement interval, in which case the actual response could be either quicker or slower. This short term cause-effect behavior provides strong evidence of the close interrelationship between the two systems in this area, supporting the use of a coupled model to simulate the whole system dynamics.

Over time, dramatic water table recoveries occur after peak flows. Moreover, steady ground-water levels correlate with prolonged periods of high dam releases, as occurred from June 1985 to October 1986. A progressive water table decline is observed during long low-flow periods. Wells #3 and #4, the closest to the Refuge entrance, are subject to less drastic fluctuations, response that can be associated with geologic controls existing in that area. With the exception of these two wells, a general ground-water level decline trend is noticeable over the years. No matter how distant from the river, and

Figure 2.7: Well #2, #3 and #4 hydrographs - Period 1985-1992

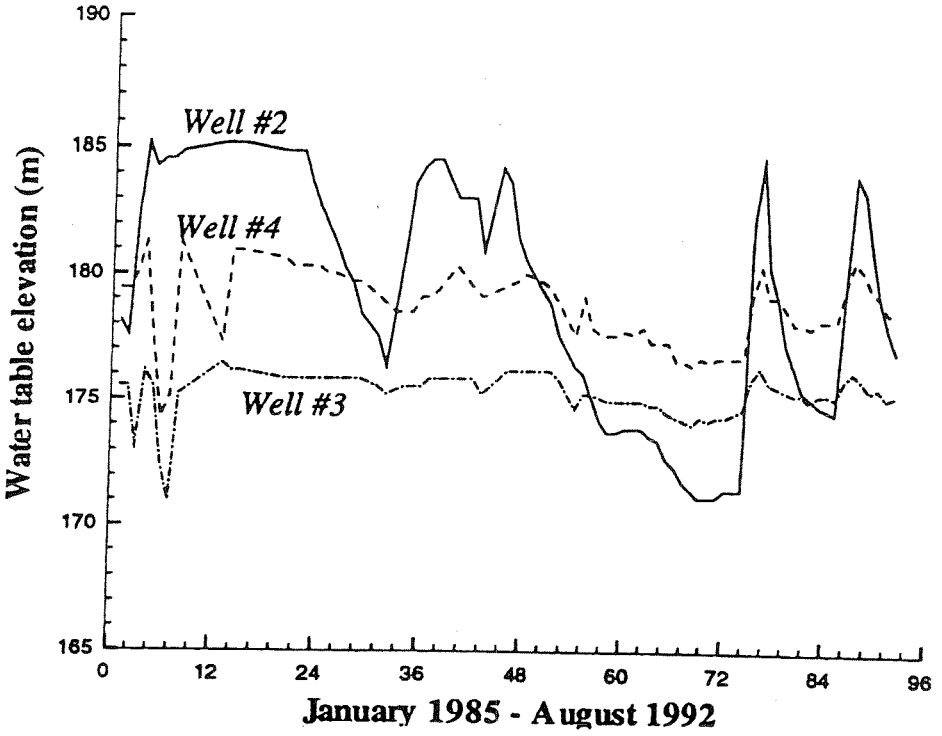

Figure 2.8: Well #5 and #6 hydrographs - Period 1985-1992

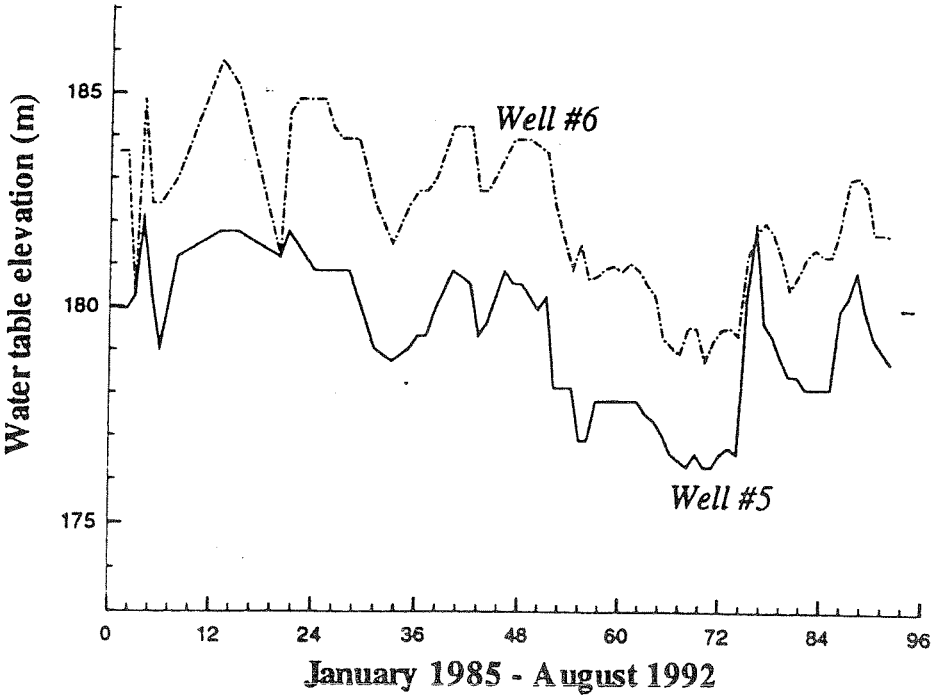

Figure 2.9: Well #8 and #9 hydrographs - Period 1985-1992

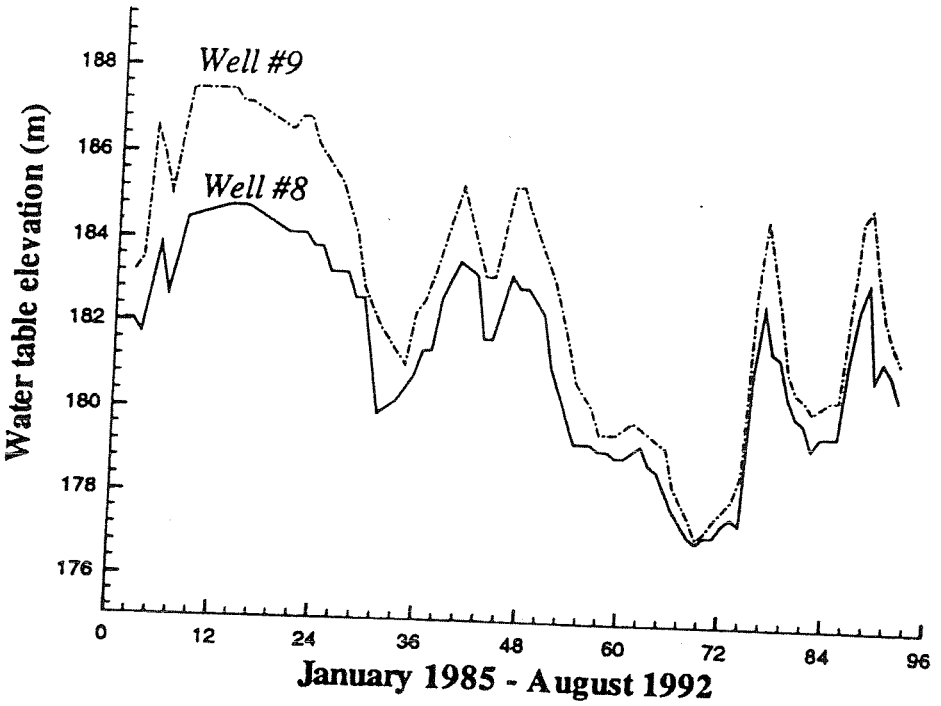

Figure 2.10: Streamflow at Alamo station - Period 1985-1992

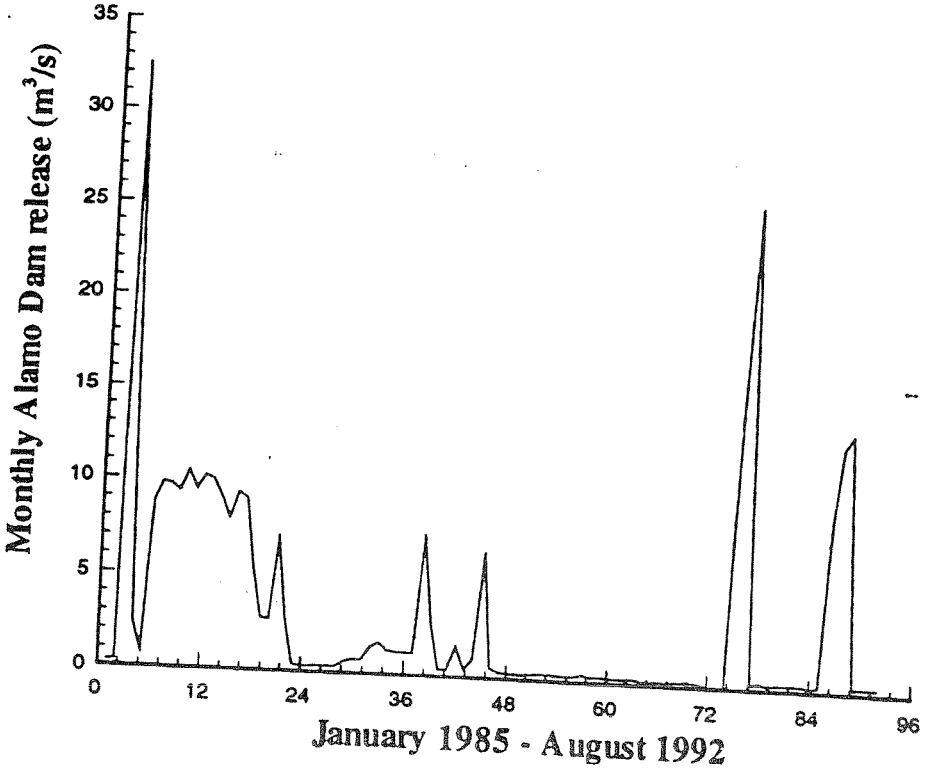

assuming an equal pumping regime, all wells seem to respond in a very similar and quick manner. This indicates the existence of a highly permeable aquifer.

2.6.4. Stream aquifer interactions

This description of the close relationship between stream and aquifer in the study area is largely based on interpretations of field data provided by Rivers West (1990) and on a site visit by the authors. At the present time, the system is no longer in a state of dynamic equilibrium and even though pumping activities have declined, a full recovery towards pre-development conditions will never occur as long as streamflows continue to be controlled.

Dry, losing and gaining stream reaches all occur along the Bill Williams River. During low flow periods, the river reach at Planet Ranch is completely dry, but is inundated during high flow periods. The stream is also dry within the Refuge along 6.5 *km* upstream from its confluence with Lake Havasu. Gaining conditions are observed two to three kilometers downstream from the Planet Ranch, where groundwater emerges from the alluvium converting the dry stream into a gaining one.

Two transmission losses studies were done on the site. The first was conducted by BLM (1988), and encompasses almost the entire length of the river from Alamo reservoir to Kohen Ranch. The study reports that for a 2.98 m^3/s dam release, 62 % of the water is lost on a 19 *km* reach that includes the Planet Ranch alluvium. This confirms the attenuating character and the buffering capacity of the alluvium at this location. The data reported by BLM is used to calculate transmission losses per unit length of channel (Table

2.3). The numbers in the table indicate that upstream from the Planet Ranch area the stream/aquifer system is also quite variable. Of much smaller dimensions than the Planet Ranch alluvial, the shallow aquifer at Lincoln Ranch (between kilometers 55.5 and 51.7) is also able to store water that is later released downstream where the stream gains water from the aquifer. For this particular flow release, 28 % of the water has infiltrated through the streambed between Alamo and Centennial Wash at the upstream end of the Planet

Table 2.3: Transmission losses

River Reach	Km	Discharge (m^3/s)	ΔL (km)	ΔD (m^3/s)	ΔD/ΔL ($m^3/s/km$)
Alamo	63.7	2.98			
			7.76	-0.40	-0.05155
	55.5	2.58			
			3.85	-0.14	-0.03636
	51.7	2.44			
			7.40	+0.22	+0.02973
	44.3	2.66			
			1.61	0	0.00
	42.6	2.66			
			2.25	-0.22	-0.9778
	40.4	2.44			
Centennial Wash			8.21	-0.29	-0.03532
	32.2	2.15			
			12.87	-1.84	-0.14287
	19.3	0.31			
			5.96	-0.14	-0.02349
Kohen Ranch	13.4	0.17			

Ranch. This distribution of gains and losses along the river may vary for different inflows, however it provides a good indication of the general behavior of the stream/aquifer system. Except at the Planet Ranch area, transmission losses are smaller than losses reported in other places of Arizona. For example, transmission losses for a steady inflow of 2.98 m^3/s computed at certain stream reaches of the Walnut Gulch Watershed in

Southeastern Arizona are around 0.5 $m^3/s/km$. Those calculations were performed following the methodology proposed by Lane (1980).

The second transmission losses study was performed by Rivers West (1990), but it only considered the stream reach within the Wildlife Refuge. They found that within the Refuge the rate of seepage from the stream varies from about 7.04×10^{-3} $m^3/s/km$ to about 6.34×10^{-2} $m^3/s/km$, depending on the location. This increase was attributed to a lack of hydraulic connection between the stream and the aquifer. In such a case the hydraulic gradient that drives the seepage becomes independent of the water table elevation and depends only on the water depth in the stream. Rivers West does not report what the dam release was at the time of their study. Consequently, the two studies are not readily comparable as different dam releases may yield different transmission losses.

Likewise, Rivers West (1990) conducted laboratory analyses of streambed material and material from the underlying stream alluvium. Their goal was to determine the hydraulic properties of both materials and characterize seepage under the presence of a restricting silt layer in the streambed. Grain size distributions for both samples are practically identical, however Rivers West claims that the arrangement of the fine portion of both samples differs substantially. A hydraulic conductivity of 0.0039 *cm/s* is reported for the alluvium, and a value of 0.00012 *cm/s* is given for the streambed sample. Results of this nature are really valuable, nevertheless, the manipulation, sieving and subsequent rearrangement of samples on the experimental device affect hydraulic conductivity values. In-situ measurements at various locations are highly recommended to confirm these findings. Lacher (1995) has determined in-situ hydraulic conductivity (K) at various sites on the Santa Cruz River. As expected, her results show variability of hydraulic

conductivity with depth and with test location. She also found that at some locations hydraulic conductivity values stayed fairly constant at ground level, 30 *cm* and 60 *cm* deep, at other sites the ground level value was one order of magnitude less than the K values at 30 *cm* and 60 *cm*, while at some other locations the lowest K was detected at 60 *cm* revealing the presence of clayed lenses within the coarser alluvium. Although every river system behaves differently, these findings reveal that, in actuality, the streambed is not uniformly carpeted by a constant thickness silty layer but rather is an heterogeneous array of surficial and interbeded low permeability lenses created during subsequent flood events. Streambed configurations of this kind were also identified in the San Pedro River, and the Bill Williams River is likely to be characterized by a similar streambed-underlying alluvium complex.

2.6.5. Natural and cultural water uses

Natural water uses refer to water requirements by riparian vegetation while cultural water uses represent water requirements for human activities development. In the following two sections, estimates of both uses are provided.

2.6.5.1. Natural water uses

Evapotranspiration (ET) losses due to phreatophytes and evaporation from bare soils are the main natural depletions of water supplies in the Bill Williams River Basin. Estimating its magnitude is then of primary importance whether for mass balance computations or for modeling purposes.

The terms consumptive use and ET are often used interchangeably. Consumptive use is defined as the sum of the volume of water evaporated from an area and that used directly in building plant tissue (Singh 1989). The evapotranspiration process is affected by climatic factors such as air temperature, wind, atmospheric pressure, humidity, and soil properties such as moisture and hydraulic conductivity.

A rigorous field study that assesses the factors affecting ET and precisely quantifies vegetation species in the study area is not available. However, due to their similar riparian vegetation, information gathered in nearby basins and throughout other basins in Arizona can be used in the Bill Williams River Basin.

The dominant vegetation species within the riparian stretches along the Bill Williams River consist mainly of mesquite, cottonwood, salt cedar and seep willow, all vegetation types common to most southwestern riparian systems. In addition to these species, the study area sustains a considerable population of cattail/bulrush, located in the marshy area at the downstream end of the Refuge, and small stands of smoketree and inkweed.

The Bureau of Land Management (1989) and Rivers West (1990) surveyed the acreage of native vegetation, upstream of the Planet Ranch and within the Refuge, respectively (see Tables 2.1.*a* and 2.1.*b*). Not reported in either one of these documents is the vegetation density. Turner (1962) provided some vegetation density figures, but they are considered outdated as the total acreage and distribution of riparian vegetation has changed over the last 30 years.

Seasonal consumptive use estimates were generated using the Blaney-Criddle method (Blaney and Criddle 1950):

$$E_T = \chi F = \sum_{i=1}^{12} k_i f_i \tag{2-1}$$

with,

$$f_i = \frac{T_i p_i}{100} \tag{2-2}$$

where E_T is the consumptive use in inches of water during the growing season, χ is an empirical consumptive use coefficient applicable to a particular vegetation species, F is the sum of monthly consumptive use factors f_i, T_i is the i^{th} mean monthly air temperature in °F, p_i is the mean percentage of annual daytime hours for the i^{th} month, and k_i is a monthly consumptive use coefficient. Although empirically derived, this formula has been widely used in the western United States. Moreover, it includes both meteorological and vegetation effects, represented by variables relatively easy to obtain.

Putman *et al.* (1988) computed "χ"values for phreatophytes species using data taken from Safford, AZ. It has been argued that such values may not be fully appropriate in the Bill Williams area because of the more stringent climatic conditions existing in that basin. However, "χ" estimates in nearby areas (Turner 1962) are practically identical to those reported by Putman *et al.* (1988). Table 2.4 provides the χ values used in this analysis.

Table 2.4: χ values

Vegetation Species	χ
Salt Cedar	1.357
Willow	0.886
Cottonwood	1.131
Mesquite	0.622
Salt Cedar	1.400
Cattail	0.569

Temperature data collected at Alamo Dam and at Lake Havasu weather stations have been used to compute the "f" factors upstream and downstream of the Planet Ranch, respectively. Tables 2.5.*a* and 2.5.b show monthly values of p_i, T_i and f_i as well as F for these two stations.

Annual consumptive use figures calculated with expression (2-1) are tabulated in metric units in Table 2.6.*a* and Table 2.6.*b*. A χ value for cattail/bulruch was unavailable, consequently a consumptive use of 1.61 *m/year* was adopted (Stromberg, personal communication, 1994). A vegetation density of 75 % was assumed for vegetation stands along the river upstream of Planet Ranch and 65 % density is set for riparian vegetation at the Refuge. These density figures are only estimates and should be verified by means of field vegetation surveys and aerial photographs. The estimated annual consumptive use by vegetation within the Refuge turned out to be 1.5328×10^7 m^3 or 12,426 *ac-ft*, about 6 % higher than the 11,712 *ac-ft* reported by Rivers West (1990). Precipitation can make up for some of the water consumed by native vegetation. However, due to minor amounts of rainfall falling in the area, its effect on ET losses is considered negligible.

2.6.5.2. *Cultural water uses*

Until recently ground-water pumping for irrigation of alfalfa at Planet Ranch was the primary anthropogenic water use in the BWR basin. In the past, irrigation has also occurred on cultivated fields upstream and downstream of the Ranch. Other uses have included ground-water extraction for domestic and stock water and surface water diversions. The 13 commercial wells supplying Planet Ranch (Figure 2.6) withdrew water

Table 2.5.a: Meteorological data for Alamo station
Latitude: 34° 14' Longitude: 113° 28' Elevation: 451.1 *m*
(Temperature reported in Celsius but calculation performed in Fahrenheit)

Month	Mean Temperature (°C)	Day Length (hours)	$f=T_F/100$
January	10.36	10.14	1.05
February	12.72	10.98	1.40
March	15.36	11.95	1.84
April	20.06	13.04	2.62
May	24.86	13.94	3.47
June	30.59	14.41	4.41
July	33.59	14.22	4.78
August	32.44	13.44	4.36
September	28.59	12.41	3.54
October	22.38	11.35	2.54
November	15.06	10.40	1.57
December	10.59	9.91	1.05
		Σf_i	**32.62**

Table 2.5.b: Meteorological data for Lake Havasu station
Latitude: 34° 27' Longitude: 114° 22' Elevation: 146.3 *m*
(Temperature reported in Celsius but calculation performed in Fahrenheit)

Month	Mean Temperature (°C)	Day Length (hours)	$f=T_F/100$
January	11.90	10.14	1.21
February	14.61	10.98	1.60
March	18.17	11.95	2.17
April	22.80	13.04	2.97
May	27.68	13.94	3.86
June	33.01	14.41	4.76
July	35.88	14.22	5.10
August	34.82	13.44	4.68
September	30.86	12.41	3.83
October	24.28	11.35	2.76
November	16.78	10.40	1.75
December	12.04	9.91	1.19
		Σf_i	**35.88**

Table 2.6: Annual consumptive use (CU)

Vegetation Type	CU ($\times 10^5$ m^3/year)	
	100 % density	75% density
Salt Cedar/Willow	64.58	48.44
Mesquite/Salt Cedar	62.82	47.12
Mesquite/Salt Cedar/Willow	10.81	8.10
Mesquite	6.56	4.92
Mesquite/Inkweed	2.82	2.12
Hymenocleo Sp.	5.88	4.42
Cottonwood/Willow	7.18	5.39
Inkweed	0.48	0.36
Smoke Tree	0.17	0.14
Total	**161.31**	**121.01**

(a) Upstream of the Planet Ranch (after BLM 1989)

Vegetation Type	CU ($\times 10^5$ m^3/year)	
	100 % density	75% density
Cattail/Bulrush Marsh	21.51	13.98
Cottonwood/Willow/Salt Cedar	52.93	34.40
Willow/Salt Cedar	69.99	45.49
Salt Cedar	91.34	59.37
Total	**235.78**	**153.24**

(b) Wildlife Refuge (after Rivers West Inc. 1990)

1 hectare=10,000 m^2

from the alluvial aquifer at an annual rate of 1.8503×10^7 m^3. This volume was used to irrigate 971.3 *hectares* (9.713 km^2) of alfalfa. Return flows from irrigated fields were likely to be very small or non-existent. The reasons for this are twofold: on one hand, the sprinkling irrigation system used in one of the driest spots in Arizona has a very low irrigation efficiency compared to other irrigation methods. On the other hand, assuming a 1.98 *ha-m/ha* of consumptive use for alfalfa, the reported total amount of ground-water withdrawn would be barely enough to meet crop demands.

CHAPTER 3

GROUND-WATER FLOW MODEL

3.1. INTRODUCTION

The objective of this chapter is to derive a proper ground-water flow equation along with the appropriate set of assumptions for the problem at hand. Particular attention is given to the boundary conditions as a means to define a well-posed problem. In the sense of Haddamard, a problem is well-posed when (*i*) the solution exists, (*ii*) the solution is unique, and (*iii*) the solution is stable. This means that the solution must depend continuously on the data and any perturbations on the parameters, boundary conditions or initial conditions produce small changes in the solution. The specification of data along any part of the boundary is of fundamental importance, and depends on the nature of the governing equations -- elliptic, parabolic, hyperbolic. In general, the boundary conditions are well established by the physics when the governing equations are derived from conservation laws. As it will be established in this chapter, the present problem is a case in point.

3.2. MATHEMATICAL DEVELOPMENT

The stream-aquifer interaction process occurs between a stream and its adjacent floodplain aquifer. In the latter, the flow is generally unconfined with the phreatic surface as its upper boundary. Actually, above the phreatic surface there is a capillary fringe

whose thickness is much smaller than that of the saturated domain below the water table. Hence, this fringe is commonly neglected in the derivation of the governing flow equations (Bear 1972).

In general, flow through porous media is a three-dimensional process. However, under special circumstances, geometric considerations allow to introduce a simpler and more advantageous approach. Most aquifers are thin compared to their horizontal dimensions, then the flow in the aquifer can be assumed as being mostly horizontal. The horizontal flow hypothesis implies that the flow velocities are horizontal and parallel to each other along any vertical line, this is the so-called Dupuit's hypothesis (Freeze and Cherry 1979). An obvious and a tremendous simplification is gained by using the Dupuit assumptions, which is the reduction of a three-dimensional problem to a two-dimensional one. If there is no vertical component, there is no vertical hydraulic gradient and, therefore, the hydraulic head $h = h(x, y, t)$ is independent of z. A word of caution should be brought up at this point since it is well known that the horizontal flow hypothesis fails in the vicinity of partially penetrating wells, springs, rivers or water divides (Bear and Verruijt 1987). Nevertheless, at some distance from sinks or sources, the hypothesis may again be valid. For example, according to Verma and Brutsaert (1971), the horizontal flow hypothesis is valid at a distance approximately equal to four times the aquifer thickness. Whenever justified on the basis of flow patterns and aquifer geometry, the assumption of horizontal flow greatly simplifies the mathematical formulation, and the error introduced by this assumption is indeed small in many practical cases (Bear and Verruijt 1987).

The mathematical details for the derivation of the two-dimensional flow equation for phreatic aquifers are omitted in this section, and only assumptions and final results are presented. For more details, the reader may consult the work of Bear (1972), De Marsily (1986) and Bear and Verruijt (1987). Following an Eulerian approach, the mass balance equation for confined aquifers is expressed as,

$$\nabla \cdot (\mathbf{K} \nabla \phi) + W = S_s \frac{\partial \phi}{\partial t} \tag{3-1}$$

where ∇ is the gradient operator, $\mathbf{K}$ is the hydraulic conductivity tensor, ϕ is the piezometric head, W is a source/sink term, t is the time, and S_s is the specific storage (Freeze and Cherry 1979),

$$S_s = \rho g(\alpha + n\beta_w) \tag{3-2}$$

In Equation 3-2, n denotes the porosity, ρ the water density, g the acceleration due to gravity, β_w the compressibility coefficient of the water and α the compressibility coefficient of the porous medium. Depending on the precise definition of α (Bear 1972), the α above may need to be replaced by $(1-n)\alpha$.

In order to develop the governing equation for a leaky-phreatic aquifer, the three-dimensional diffusion Equation 3-1 is first integrated over the vertical,

$$\int_{\eta(x,y)}^{h(x,y,t)} \left[\nabla \cdot (\mathbf{K} \nabla \phi) + W - S_s \frac{\partial \phi}{\partial t} \right] dz = 0 \tag{3-3}$$

where $h(x,y,t)$ indicates the elevation of points on the phreatic surface above some datum and $\eta(x,y)$ denotes the aquifer bottom elevation above the same datum (see Figure 3-1).

By employing the Leibnitz rule, the Dupuit's assumptions and the appropriate boundary conditions over $z = \eta$ and $z = h$ (Bear 1972), Equation 3-3 reduces to,

$$\nabla_2 \cdot \langle \mathbf{K} \rangle (h - \eta) \nabla_2 h + S_T + |\nabla_2 F| \frac{(\phi_1 - h)}{c_1} - \left[S_s (h - \eta) + S_y \right] \frac{\partial h}{\partial t} = 0 \qquad (3\text{-}4)$$

where,

$\langle \mathbf{K} \rangle$ is the vertically average hydraulic conductivity tensor,

S_y is specific yield

S_T is the integrated source/sink terms

$\phi_1(x, y, t)$ is the piezometric head of the underlying confined aquifer

$1/c_1$ is the coefficient of leakage

$F = z - h(x, y, t) = 0$ is the phreatic surface

$\nabla_2 = \left(\frac{\partial}{\partial x}, \frac{\partial}{\partial y} \right)$ is the gradient operator defined on the (x, y) plane

Figure 3.1: Aquifer cross section

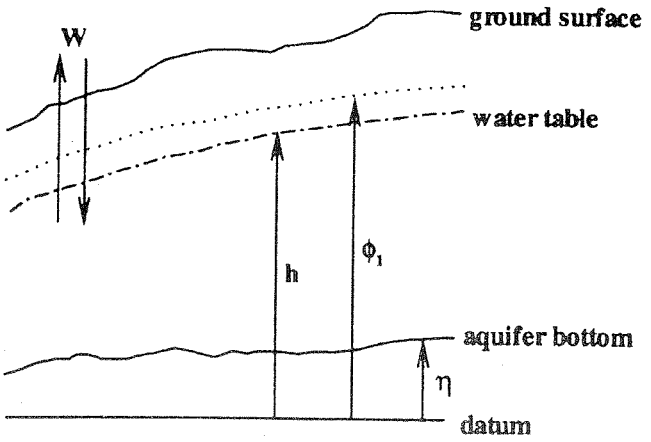

It turns out that, for all practical purposes, it suffices to consider $S_y >> S_s(h-\eta)$ (Bear 1972), in which case the transient term becomes $S_y \frac{\partial h}{\partial t}$. Moreover, whenever fluctuations in h are much smaller than the saturated thickness $h-\eta$, a less stringent simplification can be introduced. Under these circumstances, it is possible to approximate h by $\overline{h}$, where $\overline{h}$ represents the temporal mean value of h (Cunningham and Sinclair 1979). It follows that,

$$S_y + S_s(h-\eta) \approx S_y + S_s(\overline{h}-\eta) \equiv \overline{S} \tag{3-5}$$

where $\overline{S}$ is a constant independent of time. A deeper analysis on the significance of the aquifer material elasticity and the water compressibility in the context of unconfined flow can be found in Neuman (1972, 1973b), Streltsova (1975) and Neuman (1982). In any case, the term $S_y \frac{\partial h}{\partial t}$ (or eventually $\overline{S}\frac{\partial h}{\partial t}$) is used in the subsequent analysis.

For a non-leaky unconfined aquifer, Equation 3-4 can be written,

$$\nabla_2 \cdot \langle \mathbf{K} \rangle (h-\eta)\nabla_2 h + S_T - \overline{S}\frac{\partial h}{\partial t} = 0 \tag{3-6}$$

3.3. COUPLING TERM

The first part of this section discusses the physical and the mathematical aspects of the stream-aquifer interaction followed by a literature review on the topic. The third part intends to examine the classic representation of the coupling term.

Figure 3.2: Stream-aquifer interface conditions in western streams
a) gaining stream; b) losing stream; c) perched stream; d) dry stream

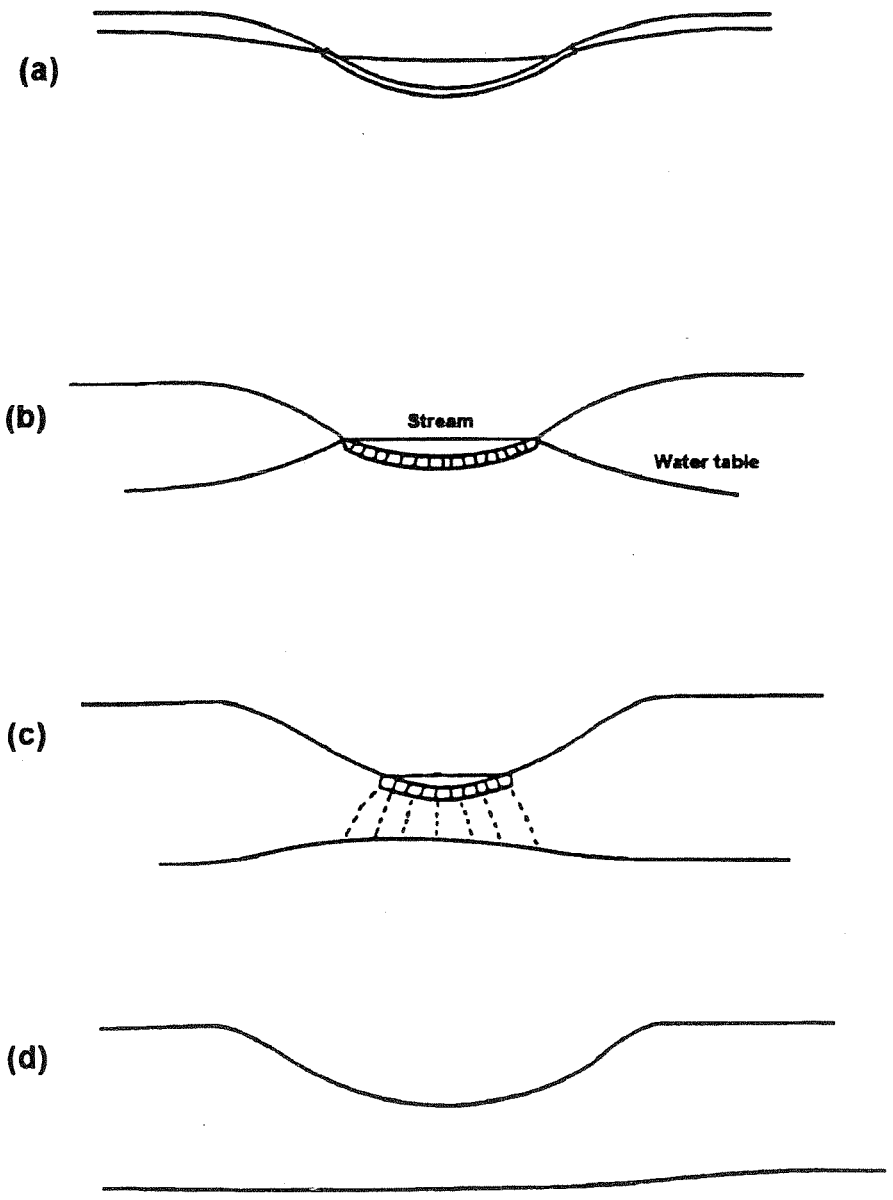

3.3.1. Introduction

The prevailing conditions in stream-aquifer systems in southwestern regions of the United States are sketched in Figure 3.2. Figure 3.2.*a* illustrates the situation of a gaining stream, Figure 3.2.*b* and Figure 3.2.*c* illustrate the case of a losing stream and Figure 3.2.*d* represents a dry stream.

By analogy to Ohm's law, the exchange of water between an aquifer and a stream may be formulated as (Bouwer 1978)

$$exchange = \frac{(h - h_s)}{R} = \frac{P}{R_f}(h - h_s) \qquad (3\text{-}7)$$

where R is the flow resistance factor, R_f is the resistivity factor, P is the wetted perimeter of the channel and h_s is the stream stage (see Figure 3.4.b)

Equation 3-7 has been and still is widely used in stream-aquifer modeling. The debate centers around two issues, first on how to determine the value of the resistance factor R_f, and second on how appropriate the expression is when non-saturated sediments underlay the streambed.

3.3.2. Background

Based on some field observations, Rushton and Tomlinson (1979) tested alternative non-linear relationships to Equation 3-7 of the exponential type and a combination of exponential and linear functions, but their results were not conclusive. Miles (1985) also experimented with non-linear relationships, and compared the results with those obtained with the Equation 3-7. Seepage calculated with both relationships was practically identical.

In her study of flow resistance, Strelsova (1974) proposed the method of additional seepage resistance in which the length of the flow path is increased to account for partially penetrating streams. Other authors (Miles and Rushton 1983) used an heuristic approach to determine the resistance coefficient. Crebas *et al.* (1984) borrowed some ideas from the drainage design theory and the method of additional resistances to develop expressions for R. In essence, they distinguished two major components in the resistance factor R, a horizontal resistance and a radial resistance. The horizontal resistance is due to the Dupuit-Forchheiner assumption of horizontal flow and the radial resistance is the additional resistance caused by the deformation of the flow pattern due to the geometry of the water conduit and inhomogeneities of the ground. Crebas *et al.* (1984) concluded that, because open channel seepage describes the water exchange per unit length of the channel in terms of local cross sections, the horizontal resistance is negligible and so the coefficient can be expressed as,

$$R = \left(\frac{1}{\pi K_1}\right)\ln\left(\frac{aD}{P}\right) + \frac{I}{P} \tag{3-8}$$

where K_1 is the hydraulic conductivity of the aquifer below the channel, D is the thickness of the aquifer below the channel, a is a geometrical shape factor, and I is the hydraulic impedance.

In natural channels, evidence exists about the reduction of the hydraulic conductivity of the outermost layer of channel bed material due to biological activity as well as inorganic sedimentary processes. This phenomenon is referred to as clogging. Settling of sediments and straining of suspended material as water moves through the soil, microbial transport and colonization, precipitation of chemical, can all cause such clogging

effect (Cunningham *et al.* 1987). In order to represent that effect mathematically, it is assumed that these materials form a thin layer of thickness e whose hydraulic conductivity K_e is usually one or two orders of magnitude smaller than that of the underlying sediments (Madlock 1965). Frequently, the magnitude of e is unknown, so e is combined with K_e in a single parameter $R_f = \frac{e}{K_e} = I$, the hydraulic impedance or resistivity introduced before. Under the presence of such a silty layer, the first term in Equation 3-8 can be one or two orders of magnitude smaller than the second one. Consequently, for all practical purposes no much is gained in retaining it.

Generally, the resistivity factor R_f or the conductance P/R_f is treated as a calibration parameter whose uncertainty is partially circumvented by means of a sensitivity analysis. Rushton and Tomlinson (1979) argued that this approach provides no insight into the physical processes involved, and the value obtained may disguise the influence of other aquifer or surface-water flow properties. Nevertheless, calibration is still a valid and widely used procedure.

Some of the assumptions behind expression Equation 3-7 are that the water is instantaneously recharged to the water table, that channel loss equals recharge to the aquifer, and that the transfer is controlled by saturated flow through low permeability streambed sediments. Therefore, the appropriateness of Equation 3-7 to handle the case portrayed in Figure 3.3.*c* needs to be reviewed. The presence of unsaturated materials, situation generally associated with ephemeral or intermittent streams, may invalidate some of the above assumptions. A distinction should be drawn between an unsaturated zone overlying deep groundwater and that overlying shallow groundwater. In the former, a

significant vadose zone separates the stream from the water table while in the latter the unsaturated portion of the soil is thin or absent. Then, an alternative mathematical formulation for the interaction may be selected. However, the advantages of such a selection must be weighted by considering the overall objectives of the study, the additional computational burden and, most important of all, the spatial and temporal scales being used.

Freeze (1972) and Kraeger-Rovey (1975) solved the three-dimensional Richards' equation at high computational cost. Pikul *et al.* (1974) followed a simplified approach coupling a one-dimensional saturated flow model to several one-dimensional vertical unsaturated column models. Even assuming that the downward flow under a stream is mainly a one-dimensional process, the solution to the Richards' equation would still be impractical to incorporate in basin-wide ground-water or coupled management models. Then, one may resort to more simple models such as infiltration formulas and infiltration-recharge transfer functions or the Bouwer's method. For example, the Smith and Parlange (1978) infiltration formula, implemented in the kinematic runoff and erosion model KINEROS (Woolhiser *et al.* 1990), or the Green-Ampt (GA) model, can be used to calculate channel losses. The well known GA model has been utilized, among others, by Freyberg *et al.* (1980), Freyberg (1983) and Reid and Dreiss (1990) to simulate stream-aquifer interactions. Reid and Dreiss (1990) demonstrated that the GA model performs well for settings with homogeneous sediments. However, it performs poorly for settings with low permeability streambed sediments or low permeability lenses under the streambed. This comes to no surprise as the GA model was conceived under the assumption of homogeneous sediments.

The delay and smoothing of infiltrated water that occurs in the unsaturated zone can be represented by a transfer function (Morel-Seytoux 1984, Besbes and De Marsily 1984). Linearity is the main assumption behind this procedure, i.e. the unsaturated hydraulic conductivity is assumed not to vary significantly. The recharge to the aquifer and the infiltration at a point are related by a convolution integral with a linear transfer function of the infiltration into the unsaturated zone. Besbes and De Marsily (1984) found that the linear transfer function of the infiltration into the unsaturated zone can be approximated by a gamma function depending on two parameters: k, a time constant to characterize the percolation velocity, and n, the number of linear reservoirs the unsaturated zone is divided into. At first glance, the transfer function method may be appealing. However, it has a few drawbacks. Without discussing the obvious non-linearity aspects, perhaps the most critical point of this approach is the need for data at a reasonable number of observation wells at small time intervals, data not readily available in many situations. Moreover, the method identifies only the temporal mean of the transfer function and does not account for its seasonal character. This problem was discussed by Morel-Seytoux (1984), who also addressed the issue of implementing the convolution equation in large scale problems, pointing that the use and saving of the past history of excess infiltration rates may be too costly.

Bouwer (1964, 1966) indicated that, in some cases, the flow occurring at negative pressure is only a small fraction of the total flow in a system which may be dominated by saturated flow conditions. This raises the question to whether or not the inclusion of the flow in negative pressure zones is always justified. Bouwer (1964, 1966) proposed to analyze the flow in negative pressure regions on the basis of saturated hydraulic

conductivity, setting the pressure head at the bottom of the streambed equal to a negative value ϕ_c, instead of zero. The critical pressure ϕ_c is given by,

$$\phi_c = \frac{\int_0^{\phi} K d\phi}{K_s} \tag{3-9}$$

where K_s is the saturated hydraulic conductivity of the sediments under the streambed. In essence, the $K - \phi$ relationship of these sediments is replaced by a step function through the integrated center ϕ_c, with the same area as that under the actual curve of ϕ versus K. Ignoring interfacial head losses in the contact area, Equation 3-7 is redefined as,

$$exchange = \frac{(h_s - h_b - \phi_c)}{R} \tag{3-10}$$

where h_b is the elevation of the top of the streambed sediments. Bouwer (1964, 1966) found that this method adequately reproduced laboratory and numerical results of seepage across a low permeability layer. Likewise, Reid and Dreiss (1990) showed that the Bouwer's method compared well with results obtained with a two-dimensional unsaturated model.

3.3.3. Boundary condition to simulate river-aquifer interactions

Practically all the mathematical formulations used in integrated ground-water/surface water models include the coupling term explicitly as a source term in the governing ground-water flow equation. This is the standard approach, however many models based on finite element approximations (e.g. Cunningham and Sinclair 1979, Glover 1988) do not take full advantage of one of the nicest properties of the method, which is the natural incorporation of boundary fluxes into the finite element equations.

In this work, the coupling term is not explicitly included in Equations 3-4 but rather is treated through a boundary flux integral. As it will become clear in Chapter 6, this integral arises naturally in the weak form of the governing equation.

To further illustrate this aspect, let the region Ω be bounded by a closed contour $\partial\Omega$ (Figure 3.3). Along this contour the necessary boundary conditions (BC) to supplement Equation 3-4 must be given in the form of known ground-water head (BC of the first kind or Dirichlet-I), or known ground-water flow through the boundary (BC of the second kind or Neumann-II), or a linear combination of both (BC of the third kind or Robin-III).

Figure 3.3 - Domain and boundaries showing the branch cut along the internal boundary

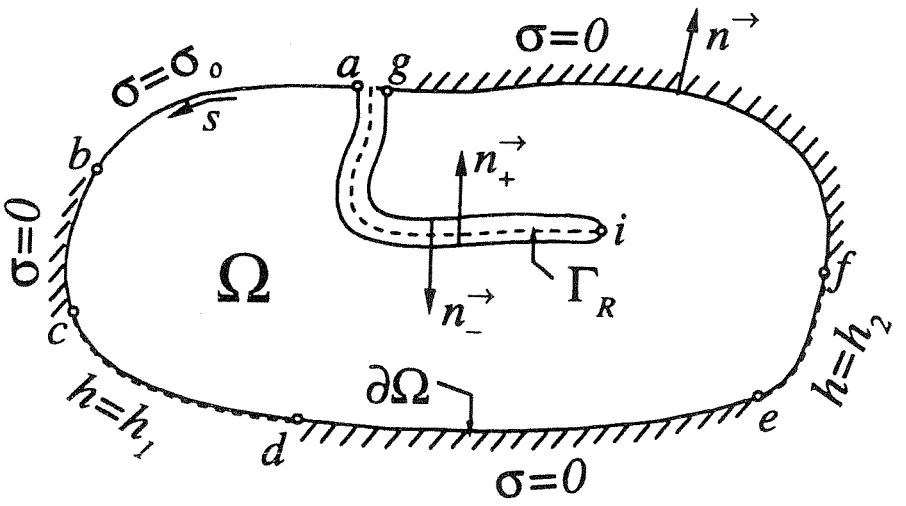

In order to develop a variational statement corresponding to Equation 3-4, the Green's first identity must be used (see Chapter 6, Section 6.2.1). It follows that a boundary term of the form $\int_{\partial\Omega} WK(h-\eta)\frac{\partial h}{\partial n}ds$ appears in the weak form of the equation.

Since $K(h-\eta)\frac{\partial h}{\partial n}$ represents the outgoing flux normal to the boundary, this term is naturally associated with the exchange of water between the aquifer and the river along the river portion Γ_R of the boundary $\partial\Omega$. This rather simple observation has profound meaning in the finite element approximation of the whole hydrologic system, as it will be seen in the following discussion.

Figure 3.4 shows the cases of a fully penetrating stream (*a*) and a partially penetrating stream (*b*). The application of the Green's first identity requires that Ω be a simply connected domain. When the stream fully penetrates the aquifer, it is necessary to introduce a branch cut in the domain along the internal boundary Γ_R representing the stream (Figure 3.3) to avoid the possibility of a multi-valued function *h* along this boundary. Then, and regardless of the degree of penetration of the stream, the natural inflow per unit length of channel is given by the sum of groundwater inflow from the left and the right channel banks (Vasiliev 1987). For case (*a*), the flow is essentially horizontal and continuity of flux through the thin layer of fine materials requires that (De Marsily 1986)

$$\left[-K(h-\eta)\frac{\partial h}{\partial n}\right]^{(-)} = \frac{K_e}{e}(h-h_s)(h_s-\eta)$$

$$= C^{-}(h-h_s) \qquad (3\text{-}11)$$

and similarly for the opposite side of the stream. The superscript minus is associated with the unit normal vector $\hat{n}$ pointing outwards from $\partial\Omega$ in negative direction, here assumed to the left (see Figure 3.5.*a*).

For the definition of the boundary condition along the interface between the stream and the aquifer, consider the control volume depicted in Figure 3.5.*b*. Mass conservation requires that, per unit length of channel,

$$-Flux\ in + Flux\ out = Rate\ of\ change\ of\ storage\ within\ the\ control\ volume$$

If the horizontal scale L is large enough to accept that the incoming flow is approximately

Figure 3.4.a: Schematic of a fully penetrating stream

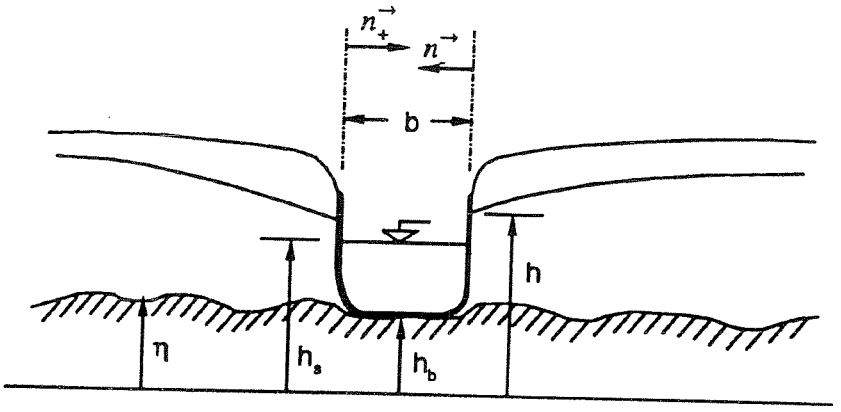

Figure 3.4.b: Schematic of a partially penetrating stream

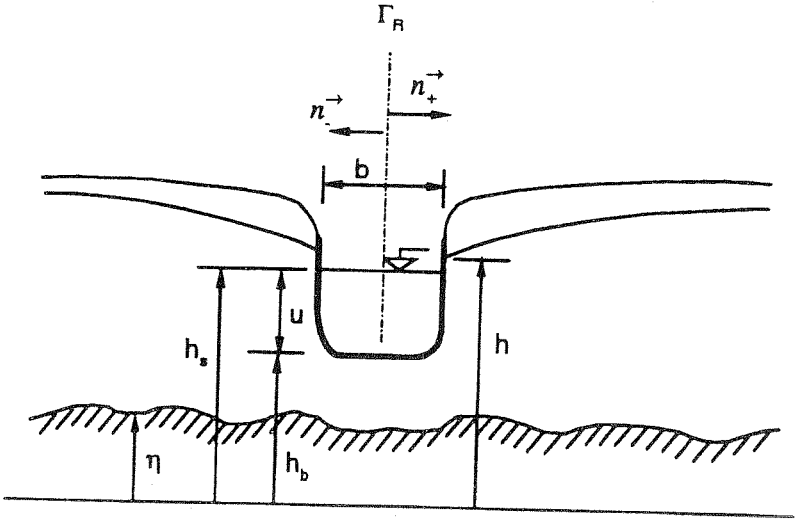

Figure 3.5.a: Semipervious boundary along a fully penetrating stream (modified after Bear and Verruijt 1987)

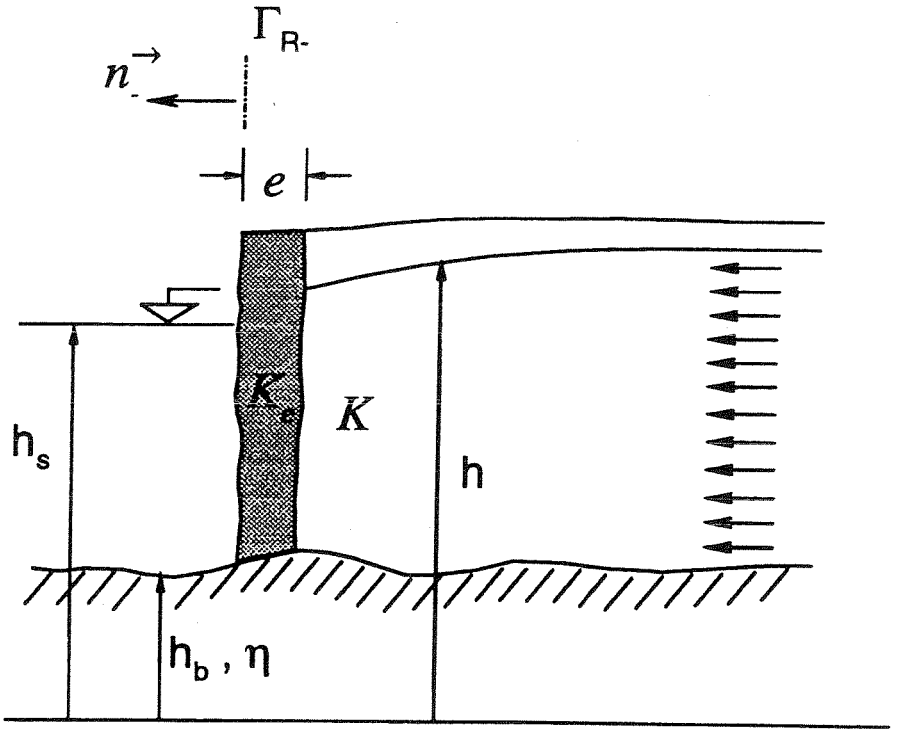

Figure 3.5.b: Control surface for a partially penetrating stream

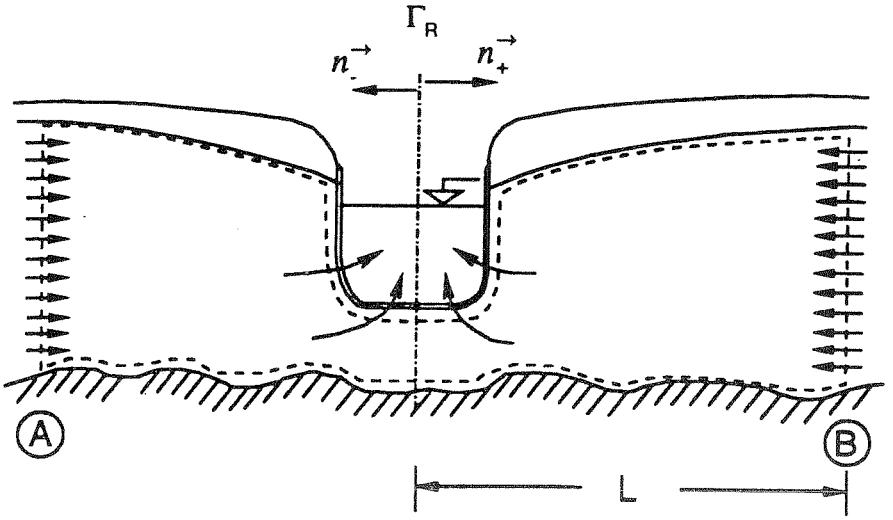

horizontal (see e.g. Verma and Brutsaert 1971), but small enough in comparison with the penetration depth (Carslaw and Jagger 1959), the storage effects are negligible and the mass balance reduces to,

$$-Flux\ in + Flux\ out \approx 0$$

which written in terms of Darcy's law and Equation 3-7 becomes,

$$\left[-K(h-\eta)\frac{\partial h}{\partial n}\right]^{(+)} + \left[-K(h-\eta)\frac{\partial h}{\partial n}\right]^{(-)} \cong \frac{K_e P}{e}(h-h_s) \qquad (3\text{-}12)$$

It must be pointed out that the slopes $\frac{\partial h}{\partial n}\Big]^{+}$ and $\frac{\partial h}{\partial n}\Big]^{-}$ above are evaluated at sections A and B, respectively (see Figure 3.5.*b*). Letting L go formally to zero, the necessary boundary condition to represent an interacting river-aquifer system for the case of a partially penetrating stream is given by,

$$\sigma^{-} + \sigma^{+} = C(h-h_s) \qquad (3\text{-}13)$$

where σ, later revised in Chapter 6, denotes the flux normal to the boundary contour Γ_R. Finally, for a non-interacting or hydraulically disconnected stream (Figure 3.2.*c*), the flux becomes independent of the head in the aquifer and is given by

$$\sigma = C(h_b - h_s) \qquad (3\text{-}14)$$

which remains constant as long as h_s remains constant. In a more realistic setting, Equation 3-10 should be used instead to account for unsaturated conditions.

3.4. BOUNDARY CONDITIONS

In the previous section, the equation that governs two dimensional ground-water flow through a porous medium was established. For a parabolic equation like Equation 3-4, the boundary conditions must be prescribed at all points along the boundary of the flow domain. Consider the idealized simply connected region Ω sketched in Figure 3.3, bounded by a close contour $\partial\Omega$. Along this contour either Dirichlet (*I*), Neumann (*II*), or mixed (*III*) boundary conditions are prescribed as follows,

$h = h_1$	on *cd*	(*I*)
$h = h_2$	on *ef*	(*I*)
$\sigma = \sigma_0$	on *ab*	(*II*)
$\sigma = 0$	on *bc*, *de* and *fg*	(*II*)
$\sigma^+ + \sigma^- = C(h - h_s)$	along Γ_R	(*III*)

if a partially penetrating stream is assumed and the stream is hydraulically connected to the aquifer or,

$\sigma^+ = C^+(h^+ - h_s)$	on *ia*	(*III*)
$\sigma^- = C^-(h^- - h_s)$	on *gi*	(*III*)

if a fully penetrating stream is considered instead. For a perched stream these conditions must be replaced by,

$\sigma = C(h_b - h_s)$	along Γ_R	(*III*)

3.5. SINK/SOURCE TERMS

For this study, the source/sink term, S_T, of Equations 3-4 and 3-6 is composed of three components. The first is point sinks or sources represent discharging and recharging wells, respectively. They are treated in the usual way by means of a finite summation,

$$Q = \sum_{j=1}^{N_w} Q_{w_j}(x_j, y_j; t)\delta(x - x_j, y - y_j) \tag{3-15}$$

where

N_w is the number of wells,

Q_{w_j} is the pumping or injection rate of well j located at (x_j, y_j), and

δ is the Dirac Delta function.

The second is the head dependent evapotranspiration. Quantification of water losses due to evapotranspiration in the floodplain alluvial requires knowledge of the relationship between the evapotranspiration rate E and the water table elevation h. The general nature of this relationship is shown in Figure 3.6 (Bouwer 1975). The deeper the roots, the greater the water table depth at which the vegetation can evapotranspire at potential rate. This is represented by the horizontal portion of the curves. When the water table drops below the root zone, the evapotranspiration rate reduces practically to zero. Actually, water uptake from the water table may cease but the plants make take up water from rain or water stored in the soil above the water table, process not taken into account in the present analysis. In mathematical terms, the E-h relationship can be approximated as (Trescott *et al.* 1976),

$$E = \begin{cases} 0 & h < h_{gd} \\ ET_m (h - h_g + d)/d & h_{gd} < h < h_g \\ ET_m & h_g < h \end{cases} \qquad (3\text{-}16)$$

where ET_m / d is the slope of the E-h relationship shown in Figure 3.7. This expression can be written in a more compact form by simply introducing appropriately chosen step unit functions.

Figure 3.6: Evapotranspiration rate-aquifer head relationship

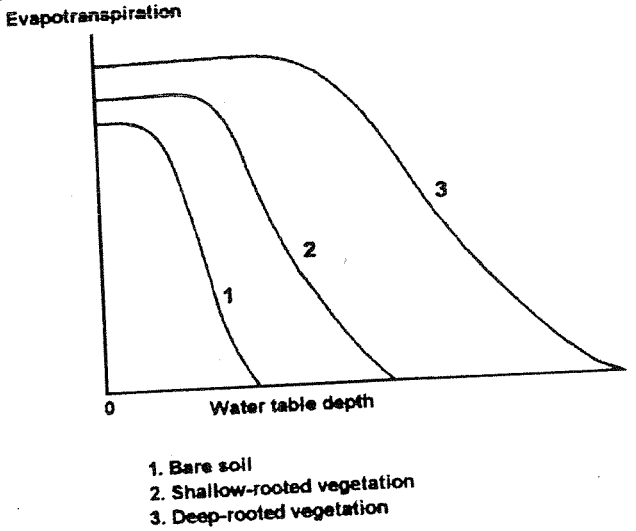

Figure 3.7: Conceptualization of the evapotranspiration rate-aquifer head relationship

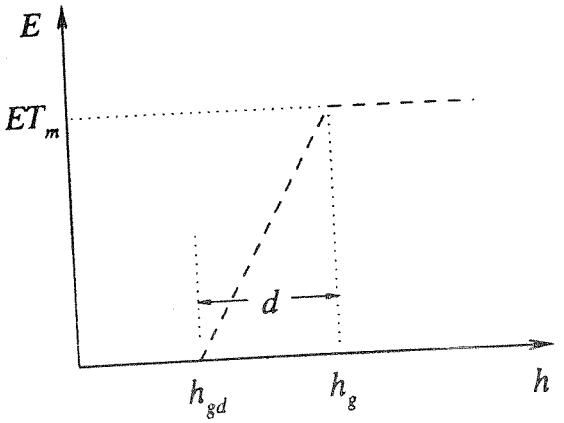

The third is the areally distributed recharge that most commonly occurs as a result of precipitation or irrigation that percolates to the ground-water system. R_G is the recharge influx in units of length per unit time. Like the pumping from a well, R_G is independent of head.

CHAPTER 4

SURFACE WATER MODEL

4.1. INTRODUCTION

Multiple time scale problems arise in a variety of physical situations, and the problem at hand is one example. Whereas the time variations in the surface water flow are in the order of hours or days, the ground-water time variations are in the order of weeks or even months. In situations such as this, when the time scales are very disparate, one may hope to be able to drop the fast time scale and solve only for the slow time scale which, in turn, will provide the sought long term behavior of the system. However, in presence of nonlinearities, this aspect depends on whether or not the fast time scale effects accumulate to produce a net effect that can influence the solution on the slow time behavior. Most of the stream-aquifer studies either neglect the fast time scale process or mainly focus on the passage and attenuation of a single flood wave through the system. Previous experience has shown that neglecting the flood routing process, when quantifying the stream-aquifer interrelationship in the long term, can deprive the system from an important amount of water that could otherwise satisfy evapotranspiration losses. This water deficit can be of fundamental importance in fragile riparian areas. The present goal is then to find the simplest representation of the fast time scale behavior preserving the true dynamics of the interaction between streams and aquifers.

Commonly, overland flow and flood wave propagation are modeled conjunctively. However, due to scanty precipitation and extremely hot conditions in the study area overland flow does not play a relevant role in the basin hydrology. The controlled flows of the main channel and their traveling downstream remain the dominant features of the surface water system. Compared to the main channel streamflows, tributary surface flows are also insignificant. This chapter is then devoted to the mathematical treatment of the one-dimensional unsteady channel flow as the only relevant mechanism of surface water flow.

4.2 FLOOD ROUTING

Flow routing is a procedure to determine the flow hydrograph at a point of a waterway given a known hydrograph at one or more points upstream, independently of the hydrograph generating process. When a flood is propagated, the changing magnitude, speed and shape of the flood wave as a function of time and distance are predicted. The method is not restricted to the propagation of waves along rivers or streams, it can be extended to reservoirs, canals, drainage ditches or storm sewers as well. The present work is strictly concerned with propagation of waves along streams.

Generally speaking there are two methods to trace a flow hydrograph through a hydrologic system, named "lumped" and "distributed" routing. Alternative names for these two approaches given in the literature are hydrologic routing and hydraulic routing, respectively.

Lumped system routing is based on the solution of the spatially lumped form of the continuity equation (Singh 1988),

$$\frac{dS}{dt} = I(t) - O(t) \tag{4-1}$$

where $I(t)$ is the input, $O(t)$ is the output, and $S(t)$ is the storage. This equation is coupled with an appropriate storage function, which can be represented as an arbitrary function of I, O and their time derivatives as follows

$$S = f\left(I, \frac{dI}{dt}, \frac{d^2I}{dt^2}, \cdots, O, \frac{dO}{dt}, \frac{d^2O}{dt^2}, \cdots\right) \tag{4-2}$$

The specific form of this function depends on the system being analyzed. This fact gives rise to different methods, among them the *level pool method* for reservoir routing and the well known *Muskingum method* for flow routing in channels (Chow *et al.* 1988).

The flow of water through channels is a distributed process. Actually, channel flow is three-dimensional as the flow velocity varies along the river, across it and with depth. However, in many practical applications, the velocity variations across the channel and with depth can be ignored and, for all practical purposes, the flow process may be considered one dimensional in the flow direction. With the contribution of Barre de Saint-Venant in 1871, the basic theory of one-dimensional analysis of flood wave propagation was formulated. The Saint-Venant equations are intrinsically complex and a profusion of simplified routing methods appeared in the literature thereafter. In the next sections, the Saint-Venant equations are set forth to later introduce the well-known kinematic wave simplified model used in this work. Available practical methodologies to establish the range of its applicability are reviewed and applied to the study case.

4.3. UNSTEADY OPEN CHANNEL FLOW - GOVERNING EQUATIONS

As it was previously stated, when the velocity variations on the channel cross section are neglected, the flow process on a channel can be treated as one dimensional. This kind of unsteady flow is mathematically governed by the one dimensional Saint-Venant equations, one for mass conservation and one for momentum conservation, that can be derived upon applying the Reynolds transport theorem to a fluid flowing through a control volume (Chow *et al.* 1988). The continuity and the momentum equations for an unsteady variable-density flow through a control volume and surface are written as,

$$\frac{d}{dt}\iiint_{c.v.} \rho dV + \oiint_{c.s.} \rho \mathbf{v} \cdot d\mathbf{A} = 0 \tag{4-3}$$

$$\sum \mathbf{F} = \frac{d}{dt}\iiint_{c.v.} \mathbf{v}\rho dV + \oiint_{c.s.} \mathbf{v}\rho \mathbf{v} \cdot d\mathbf{A} \tag{4-4}$$

where,

ρ is the density of the water,

$\mathbf{v}$ is the velocity vector,

dV is the elementary volume,

$d\mathbf{A}$ is the elementary area, and

t is time.

Equation 4-4 is Newton's second law written in the form of the Reynolds transport theorem, and states that the sum of the forces acting on the control volume is equal to the rate of change of momentum stored within the control volume plus the net outflow of momentum across the control surface. Choosing an appropriate control volume (Figure

4.1) and considering an incompressible fluid, Equations 4-3 and 4-4 are transformed as follows,

$$\frac{\partial A}{\partial t}+\frac{\partial Q}{\partial s}=q_l \tag{4-5}$$

$$\frac{1}{A}\frac{\partial Q}{\partial t}+\frac{1}{A}\frac{\partial}{\partial s}\left(\frac{Q^2}{A}\right)+g\frac{\partial u}{\partial s}-g(S_0-S_f)=\frac{q_t}{A}(v-v_t) \tag{4-6}$$

where,

A is the cross-sectional area,

$Q=Q(A)$ is the discharge,

$q_l=q_l(s,t)$ is the lateral inflow per unit length of channel,

s is the arc-length along the channel,

g is the acceleration due to gravity,

u is the water depth in the channel,

S_0 is the streambed slope,

S_f is the friction slope,

$q_t=q_t(t)$ is the uniform lateral inflow from tributaries,

$v=\frac{Q}{A}$ is the average velocity in the s-direction, and

v_t is the velocity component in -direction of lateral flow from tributaries.

Equations 4-5 and 4-6 are the full Saint-Venant equations written in conservation form. The source term $q_l(s,t)$ in the continuity equation is the sum of the rainfall rate $r_i(t)$, the uniform lateral inflow from tributaries $q_t(t)$ and the flux through the streambed $\sigma(s,t)$. The amount of precipitation fallen directly over stream channels is

Figure 4.1: Stream section

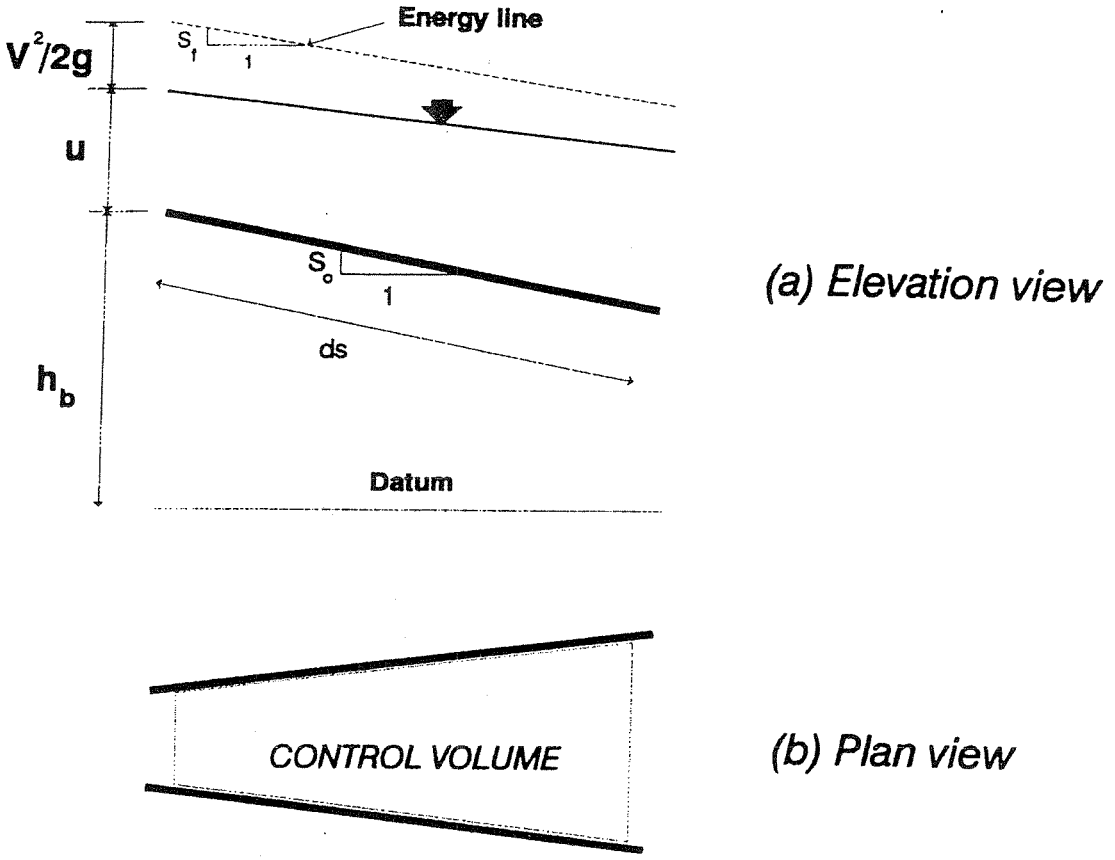

usually small and is neglected for calculation purposes. In the momentum equation, the first term represents local acceleration, the second convective acceleration, the third pressure, the fourth gravity, the fifth friction and the right hand side the momentum induced by the lateral inflow from tributaries q_t. This term is dropped from now on. Neither the shear force produced by the frictional resistance of wind against the free surface of the water nor the drag force caused by eddy losses in abrupt contractions or expansions of the channel has been considered in the momentum equation.

When all intervening forces are significant, the full Saint-Venant equations must be used, and the model is called the dynamic wave model. However, the relative magnitude of those terms with respect to one another allows to define simplified forms of the full system of equations, each giving rise to different one-dimensional distributed routing models. In some cases, inertia terms can be neglected and hence dropped from the momentum equation leaving the diffusion wave or zero-inertia model. If gravity and friction effects dominate balancing each other, the kinematic wave model is obtained. An important distinction between dynamic and kinematic waves is that dynamic waves possess at least two wave celerities, one for a wave moving forward, one for a wave moving backward. Kinematic waves move only forward with a single celerity. What this implies is that backwater effects such as tailing water from dam reservoirs can not be incorporated into the kinematic wave model.

4.4. THE KINEMATIC WAVE MODEL (KWM)

When friction and gravity effects dominate over inertia and pressure forces, the momentum Equation 4-6 reduces to,

$$S_0 = S_f \tag{4-7}$$

From Equation 4-7 it is obvious that the friction slope does not change with flow conditions. The discharge Q is then calculated by means of a constitutive relationship, replacing S_f by S_0, of the form,

$$Q = \gamma A^m \tag{4-8}$$

where γ and m are parameters related to the bottom slope, the surface roughness and to whether the Manning or Che´zy relationship is used. Table (4.1) provides values of m and expressions for γ for either case. In the table, C_h is the Chézy coefficient, P is the wetted perimeter of the channel, n is the Manning roughness coefficient, and $\bar{a}$ is a conversion factor ($\bar{a} = 1.49$ for English units, $\bar{a} = 1$ for metric units).

Table 4.1: Geometric parameters

	Chézy	Manning
γ	$C_h\sqrt{\frac{S}{P}}$	$\bar{a}\frac{1}{n}\frac{\sqrt{S}}{P^{2/3}}$
m	$\frac{3}{2}$	$\frac{5}{3}$

Equation 4-5 can now be expressed in terms of the cross sectional area as,

$$\frac{\partial A}{\partial t} + \frac{\partial Q}{\partial A}\frac{\partial A}{\partial s} = \sigma(s,t) \tag{4-9}$$

where holding s fixed, $\frac{\partial Q}{\partial A}$ is the wave celerity $c(A)$, and $\sigma = C(h - h_b - u)$ represents the coupling term defined in Section 3.3.3, with h_s replaced by $h_b + u$ (see Figure 3.4.b).

With the use of the constitutive relationship given by Equation 4-8, the wave celerity can now be related to the flow velocity v as follows,

Chézy $\rightarrow$ $c = \frac{3}{2}v$ (4-10)

Manning $\rightarrow$ $c = \frac{5}{3}v$ (4-11)

If Manning's relationship is adopted, Equation 4-9 becomes,

$$\frac{\partial A}{\partial t}+\frac{5}{3}v\frac{\partial A}{\partial s}=\sigma(s,t) \tag{4-12}$$

This implies that a kinematic flood wave travels faster than the mean flow. In the derivation of the wave celerity it was assumed that the wetted perimeter P remains constant as A varies, when in actuality, P changes as the cross-sectional area does. This situation is usually overlooked or not reported in the literature. If the variation of the wetted perimeter is taken into account, the wave speed is modified by a reducing factor as follows,

Chézy $\rightarrow$ $$c=\frac{3}{2}v(1-\tfrac{1}{3}R\frac{\partial P}{\partial A}) \tag{4-13}$$

Manning $\rightarrow$ $$c=\frac{5}{3}v(1-\tfrac{2}{5}R\frac{\partial P}{\partial A}) \tag{4-14}$$

which reduce to Equations 4-10 and 4-11, respectively when P is assumed constant. Here, R is the hydraulic radius of the channel ($R = A/P$). For the particular case of a triangular shaped channel, the second terms in Equations 4-13 and 4-14 can be easily evaluated (Lighthill and Witham 1955). The wave celerity reduces to $\frac{5}{4}v$ for Chézy and to $\frac{4}{3}v$ for Manning. Although interesting from a theoretical point of view, the variation of P in the celerity term is seldom considered in practical applications. The common approach is to assume the wave speed to be represented by either Equation 4-10 or Equation 4-11. In the present work the second equation is adopted.

A few final comments about the nature of kinematic waves are pertinent at this point. These waves are not dispersive, but due to the non-linearity of the governing equations, they may undergo some amplitude dispersion. Accordingly, continuous wave

forms can generate discontinuities. This phenomenon is described in the literature as shock waves, name first introduced by Lighthill and Whitham (1955). Shock formation is intrinsic to the hyperbolic nature of the equation governing kinematic wave theory. Moreover, shocks may be the manifestations of higher-order effects such as formation of monoclinal flood waves, bores, etc. Kinematic wave routing incorporating shock fitting has been pursued, among others, by Borah *et al.* (1980). However, whether the kinematic shock is as common in practice as calculations would seem to indicate is a matter of debate. According to Ponce (1991), the shock could occur under some highly selective conditions: 1) the wave is kinematic as opposed to diffusive or dynamic; 2) there is a low base-to-peak flow ratio; 3) there is a hydraulically wide and sufficiently long channel; and 4) there is a high Froude number, defined as the ratio between inertial and gravitational forces. These four physical conditions contribute to shock development. However, if only one or two of them occur simultaneously, the shock may not develop. Researchers seem to agree upon the fact that the formation of kinematic shocks is more a property of the mathematical equations and the methods adopted for their solution rather than an observable feature in natural processes.

4.5. APPLICABILITY OF THE KINEMATIC WAVE MODEL

The applicability of the kinematic wave as an approximation to the dynamic wave has been studied by many authors, among them Lighthill and Liggett (1967), Ponce et al. (1978), Mene´ndez and Norscini (1982), Fread (1983) and Ponce (1990).

Lighthill and Witham (1955) were the first to describe the competition between kinematic and dynamic waves in river flow under various flow conditions. On one hand

they showed how dynamic waves are subordinated when the mean flow velocity v_0 is well subcritical (F_δ<1) and, on the other hand, how both kinematic and dynamic waves can play equally relevant roles in supercritical flow situations ($F_\delta > 1$). The Froude number F_δ is defined as the ratio between the inertia force and the gravity force and is mathematically expressed as $F_\delta = v_0/\sqrt{gu_0}$, where g is the acceleration due to gravity and u_0 is the normal flow depth.

Henderson (1963) provided a qualitative criterion based on the bed slope. According to his analysis, the complete dynamic wave equations better describe flood waves in intermediate slopes, the diffusion wave model is more suited for gentle slopes, and the kinematic wave model better represents flood waves on steep slopes. This categorization should be considered with caution as steep slopes may result in supercritical flows and vice versa, contradicting criteria set by Lighthill and Witham (1955) and other authors.

In 1967, Woolhiser and Liggett defined a kinematic wave number k for overland flow problems. This parameter $k = SL_0/u_0F_\delta^2$, where L_0 is the length of the overland flow plane or channel, reflects the effects of the length and slope of the plane or channel as well as the normal flow variables. As k becomes large, usually greater than 10, the kinematic wave model can be used.

The criterion developed by Fread (1983) is based on estimating the magnitude of the terms in the conservation of momentum equation which are neglected by the kinematic and diffusion models.

Several investigators applied linear approximations to the Saint Venant equations to establish some applicability criterion. These approximations can be severe, nevertheless they are compensated by the advantage of obtaining a complete solution containing information about both, kinematic and dynamic waves. The application of linear stability theory to the governing equations led Ponce and Simons (1977) to an analytical solution of the linearized Saint Venant equations for a sinusoidal shaped wave propagating in a wide channel. Ponce *et al.* (1978) used this information to define a practical criterion for the applicability of kinematic and diffusion type models. They stated that for routing errors at a 5 % level, the following relationship must hold,

$$\frac{\tau S v_0}{u_0} \geq 171 \tag{4-15}$$

where τ is the duration of the inflow hydrograph and v_0, u_0 and S are as previously defined. If only a 1 % error is desired,

$$\frac{\tau S v_0}{u_0} \geq 873 \tag{4-16}$$

Menendez and Norscini (1982) incorporated a phase-lag δ between the h-wave and the v-wave and introduced a harmonic oscillation of the form,

$$h = \eta \exp[i(kx - \beta t)] \tag{4-17}$$

$$v = \varsigma \exp[i(kx - \beta t - \delta)] \tag{4-18}$$

into the linearized Saint Venant equations. Above, $k = 2\pi/\lambda$ is the wave number, λ is the wavelength, η ($\eta << d_0$) and ζ ($\varsigma << v_0$) are the initial amplitudes of the waves, δ is the phase between both waves, and β is a propagation factor, generally a complex number. After some algebra, two solutions are obtained, one for a wave moving forward and one

for a wave moving backward. Ultimately, these waves depend on two dimensionless numbers, namely, the Froude number and the dimensionless wave number,

$$\hat{\sigma} = \frac{ku_0}{S} \tag{4-19}$$

Because of its similarity with the kinematic flood wave, Menéndez and Norscini analyzed the behavior of the forward wave, defining the wave spectrum shown in Figure 4-2. Their criterion consists of finding the point that represents the case under study within the wave spectrum. To this aim, a series of steps must be followed, which are explained in the next section for the Bill Williams River study case.

4.6. KINEMATIC WAVES AND THE BILL WILLIAMS RIVER

In spite of the abundant evidence in favor of the kinematic wave model for flood routing in southwestern streams, some of the criteria presented in the previous section are applied to the study case to substantiate the use of such a model.

The analysis is carried over for pre-dam conditions simply because natural flood waves can be characterized with ease. If water discharge at Alamo is 1.13 m^3/s (40 cfs), $S = 0.003$, $n = 0.035$ and b (the width of a rectangular channel) is equal to 10 m, Manning's formula yields $u_0 = 0.21\,m$ and $v_0 = 0.54\,m/s$. Hence, the normal flow Froude number F_{δ_0} is equal to 0.38. Without any further analysis and according to Lighthill and Witham, subcritical flow conditions favor the kinematic wave theory.

Following Ponce *et al.* (1978) criterion, an accuracy of at least 95 % in the wave amplitude after one propagation period requires that,

$$\tau \geq \frac{171u_0}{Sv_0} = \frac{171 \times 0.21}{0.003 \times 0.54} \approx 0.26 days$$

or for a 99 % accuracy,

$$\tau \geq \frac{873u_0}{Sv_0} = \frac{873 \times 0.21}{0.003 \times 0.54} \approx 1.3 days$$

Thus the wave period, analogous to the duration of the inflow hydrograph, has to be at least longer than 1.3 days to satisfy the kinematic flow assumption.

Finally, use of the wave spectrum (Figure 4.2) developed by Menéndez and Norscini (1982) is as follows:

i) Draw a vertical line through F_{δ_0} that intercepts the different wave zones delineated in the spectrum and obtain values of $\hat{\sigma}_i$ at interception points;

ii) Use Figure 4.3 to get values of C_{δ_i}, the relative celerity, corresponding to F_{δ_0} and the $\hat{\sigma}_i$ obtained in *i*.

iii) Calculate the wave period by means of the relationships

$$C_{\delta_i} = \frac{c_i - v_0}{v_0}, \qquad c_i = \frac{\lambda_i}{\tau_i}$$

$$\hat{\sigma}_i = \frac{k_i u_0}{S} = \frac{2\pi u_0}{\lambda_i S_0}$$

which are combined to yield a relationship for τ_i,

$$\tau_i = \frac{2\pi u_0}{\hat{\sigma}_i S v_0 (1 + C_{\delta_i})} \tag{4-20}$$

For the case under analysis, it is enough to consider the first two intercepts. From the graphs,

Figure 4.2: Wave spectrum

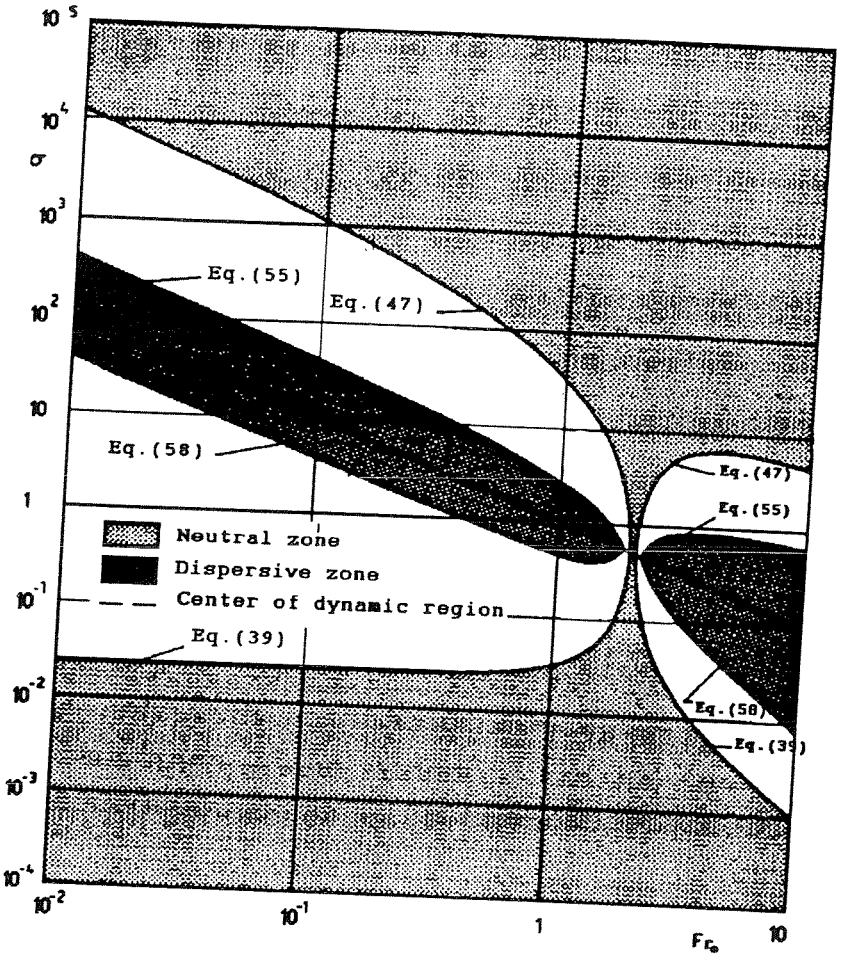

Figure 4.3: $\hat{\sigma} - F_{\delta_0} - C_{\delta_1}$ graph

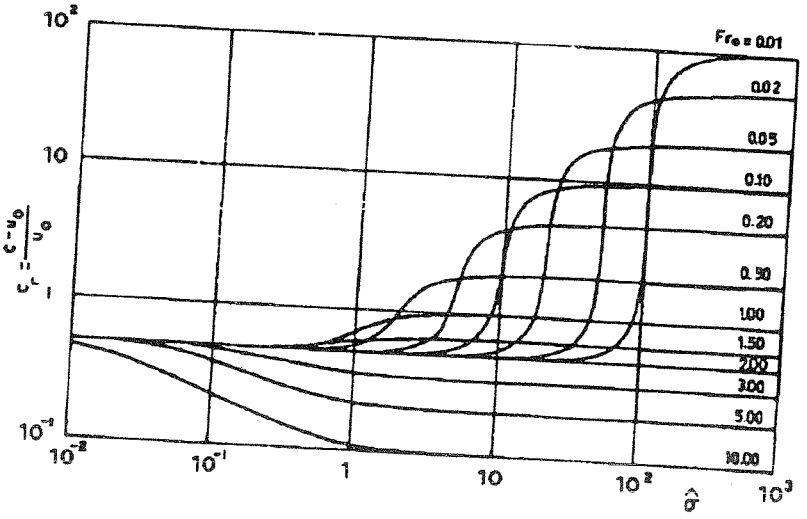

$$\hat{\sigma}_1 = 0.005 \qquad C_{\delta_1} = 0.5 \qquad \tau_1 = 1.26\,days$$

$$\hat{\sigma}_2 = 0.44 \qquad C_{\delta_2} = 0.5 \qquad \tau_2 = 0.014\,days$$

These results indicate that the Bill Williams River flood waves fall within the kinematic wave band if the wave period is greater than 1.26 *days*, a conclusion analogous to that previously obtained for a 95 % accuracy. Figure 4.4. shows two typical flood waves in the Bill Williams River whose duration exceeds both lower bounds calculated above.

The results of kinematic wave applicability criteria used in the BWR confirm the adequacy of such a model for flood routing purposes. This conclusion holds true for pre-dam conditions. During the post-dam period, the distribution of dam releases makes the definition of a wave period more difficult. However, it is assumed that the streambed characteristics and the channel slope, parameters that define the kinematic wave celerity, remain unchanged under controlled flow conditions.

As stated in Section 4.3, the kinematic wave model can not accommodate backwater effects such as tailing water from dam reservoirs. Consequently, in using this model any influence from Lake Havasu into the Bill Williams River is neglected. In the event such an effect becomes a modeling issue, the dynamic wave model should be used instead.

Figure 4.4: Flood waves in the Bill Williams River (pre-dam period)

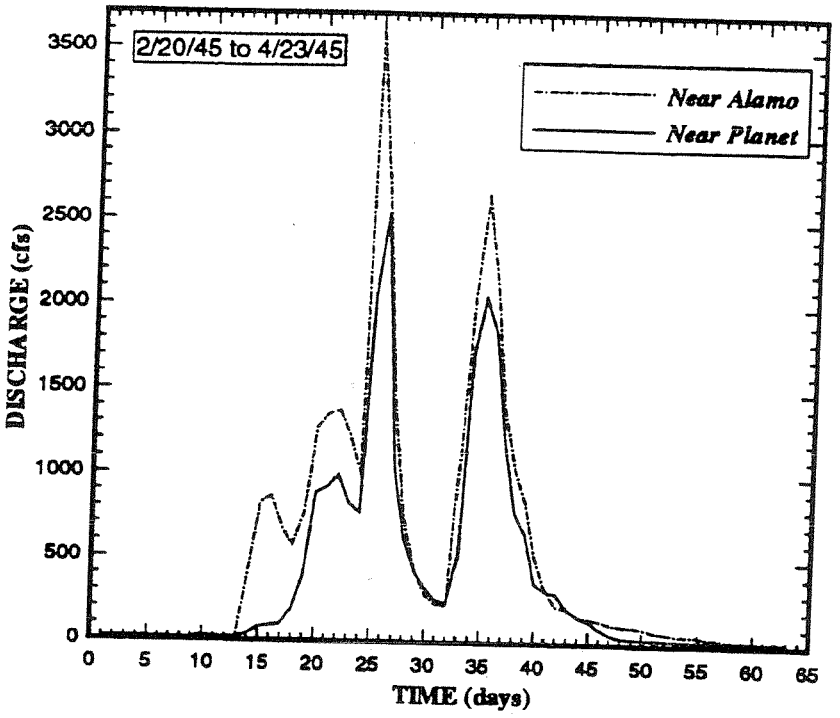

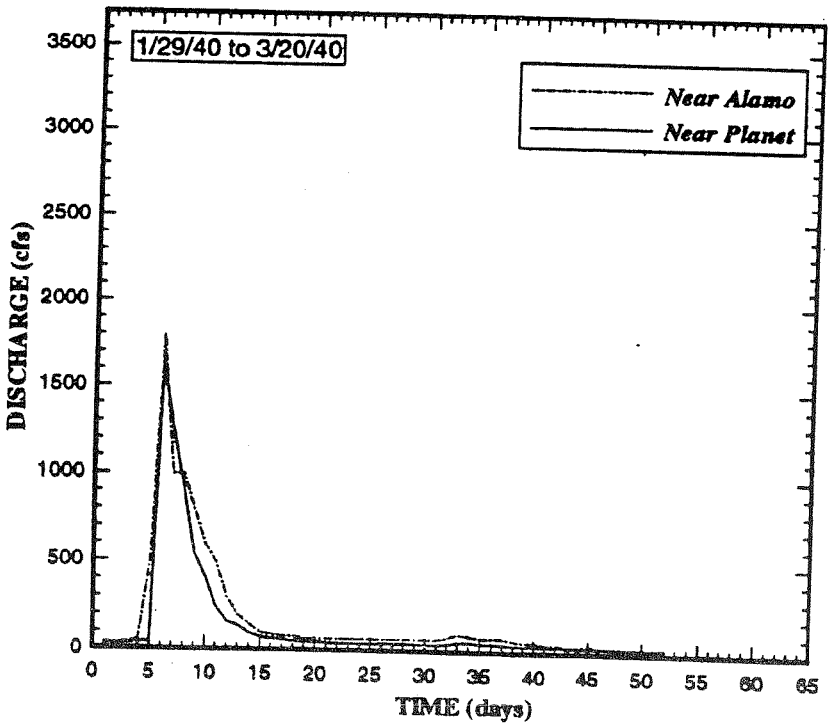

CHAPTER 5

DIMENSIONLESS FORM OF THE GOVERNING EQUATIONS

5.1. INTRODUCTION

In general, the variables in a physical phenomenon are known while the functional link among them are unknown. In some cases, analytical solutions of the governing equations can provide relationships among a set of groups of the intervening variables. Then, instead of altering the value of each variable in order to study the relationship between any pair of them, it is sufficient to explore the relationships among the groups. A good example is the Botzman's transformation that reduces the diffusion equation to an ordinary differential equation that can be readily solved in terms of the error function (Carslaw and Jaeger 1959). Another example is provided by the Theis' solution that relates the groups $s_d = 4\pi T/Q$, which is a dimensionless drawdown, and $t_d = 4Tt/Sr^2$, which is a dimensionless time, through the so called well function (for variables definition, see De Marsily 1986). However, most analytical techniques are available for very simple geometries. Oftentimes it is difficult to interpret the results in a physical context, specially when the solution is in the form of an infinite series of certain form of integral complicated function.

One way to circumvent the shortcomings of a pure mathematical approach is by means of numerical methods. When solving a problem numerically, it is customary to start

the analysis by employing a scaling process. Scaling reduces the likelihood of computing very small numbers and very large numbers during the solution procedure, an event that otherwise can greatly diminish accuracy. Actually, the technique of reproducing the behavior of a phenomenon on a different and more convenient scale is known as modeling. Any solution for a problem that has been worked out in a reduced formulation holds true for an infinite variety of actual systems which, although they differ physically, are simply scale models of each other. Then, the task is to express the governing equations in terms of non-dimensional variables. Perhaps the most critical aspect of the adimensionalization process is the choice of appropriate scales. If the scales are correctly chosen, the normalized variables and their derivatives should indeed be of order one. However, in certain cases, the solution of the problem exhibits a behavior that violates the original assumptions on the order of magnitude and new scales must be sought.

One of the main advantages of the nondimentionalization procedure is that the number of parameters which appear in a problem is reduced when dimensionless variables are employed. A word of caution is needed here; no parameters disappear, but they occur only in certain dimensionless combinations. It will be established in this chapter that the introduction of intrinsic reference quantities (scales) will render a properly nondimensionalized problem, which is better suited for its numerical treatment.

5.2. SCALES FOR THE KINEMATIC WAVE EQUATION

The adimensionalization of the KWM proceeds in the usual manner by defining the following normalized variables,

$$t' = \frac{t}{\tau_0} \qquad s' = \frac{s}{L_0} \qquad n' = \frac{n}{n_0} \qquad P' = \frac{P}{b_0} \qquad S' = \frac{S}{S_0} \qquad A' = \frac{A}{b_0 u_0}$$

where u_0 is the normal flow depth, b_0 is a characteristic river width, n_0 is a characteristic Manning's coefficient, and S_0 is a mean slope such that,

$$L_0 = \frac{u_0}{S_0}, \qquad \tau_0 = \frac{L_0}{v_0} = \frac{u_0}{v_0 S_0}$$

defines the characteristic horizontal length scale L_0 and the characteristic time scale τ_0, respectively. Using the above dimensionless variables with Equation 4-8 and the geometric parameters for Manning's equation (Table 4.1), Equation 4-12 is rewritten as,

$$b_0 S_0 v_0 \frac{\partial A'}{\partial t'} + b_0 S_0 \frac{\sqrt{S_0} u_0^{2/3}}{n_0} \frac{5}{3} \frac{\sqrt{S'} R'^{2/3}}{n'} \frac{\partial A'}{\partial s'} = \sigma' \sigma_0 \qquad (5\text{-}1)$$

where $R' = A'/P'$ is the dimensionless hydraulic radius. The velocity scale v_0 is naturally defined as $\sqrt{S} u_0^{2/3}/n_0$ and

$$v' = \frac{5}{3} \frac{\sqrt{S'} (R')^{2/3}}{n'} \qquad (5\text{-}2)$$

thus Equation 5-1 reduces to,

$$\frac{\partial A'}{\partial t'} + \frac{5}{3} v' \frac{\partial A'}{\partial s'} = \sigma' \frac{\sigma_0 L_0}{b_0 u_0 v_0} \qquad (5\text{-}3)$$

where σ_0 is the flux scale at the interface Γ_R, yet to be determined, and $\sigma = \sigma' \sigma_0$ is given by the relationship $C(h - h_s)$.

5.3. SCALES FOR THE GROUND-WATER FLOW EQUATION

In order to adimensionalize the ground-water flow equation, the following normalized variables are used,

$$\mathbf{K}' = \frac{\mathbf{K}}{K_0} \qquad Q' = \frac{Q}{Q^*} \qquad R' = \frac{R}{R^*}$$

$$(x', y') = (x, y)/L_0 \qquad t' = \frac{t}{\tau_0} \qquad \delta' = L_0^2 \delta$$

$$h' = \frac{h}{h_0} \qquad \eta' = \frac{\eta}{h_0} \qquad E' = \frac{E}{E^*}$$

where K_0 and h_0 are a characteristic hydraulic conductivity and a characteristic hydraulic head, respectively, and E^*, Q^* and R_G^* are scales to be determined. Rewritten in terms of dimensionless variables, the non-leaky unconfined aquifer flow equation [see Equations 3-5 and 3-6] results,

$$\frac{K_0 \tau_0 h_0}{S_y L_0^2} \nabla' \cdot \mathbf{K}'(h' - \eta') \nabla' h' + \frac{R_G^* \tau_0}{S_y h_0} R_G' - \frac{Q^* \tau_0}{S_y L_0^2 h_0} \sum_j Q' \delta' - \frac{E^* \tau_0}{S_y h_0} E' = \frac{\partial h'}{\partial t'} \qquad (5\text{-}4)$$

The surface water system imposes the selection of the time scale $\tau_0 = L_0 / v_0$, where v_0 is the mean velocity of the stream. This selection should not lead to the conclusion that ground-water flows and surface-water flows respond at the same rate. Multiplying both sides of Equation 5-4 by $S_y L_0^2 / K_0 \tau_0 h_0$ and introducing the selected time scale τ_0, the definitions of R_G^*, Q^* and E^* are immediate,

$$R_G^* = K_0 \frac{h_0^2}{L_0^2} \qquad E^* = K_0 \frac{h_0^2}{L_0^2} \qquad Q^* = K_0 h_0^2 \qquad (5\text{-}5)$$

Now, the coupling term is adimensionalized as follows,

$$\sigma' = \frac{\sigma}{\sigma_0} = -\frac{n_i T_{ij} \dfrac{\partial h}{\partial x_j}}{\sigma_0} = -n_i T_{ij} \frac{\partial h}{\partial x_j} \left(\frac{K_0 h_0^2}{L_0} \right)^{-1}$$

Then,

$$\sigma_0 = \frac{K_0 h_0^2}{L_0} \tag{5-6}$$

is the flux scale.

5.4. DIMENSIONLESS FORM OF THE GOVERNING EQUATION

Grouping Equations 5-3, 5-4, and using Equation 5-6, the final form of the governing equations are,

$$\nabla \cdot \mathbf{K}(h-\eta)\nabla h + R_G - \sum_{j=1}^{Nw} Q_j \delta(\hat{x} - \hat{x}_j) - E = P_e \frac{\partial h}{\partial t} \tag{5-7}$$

$$\frac{\partial A}{\partial t} + \frac{5}{3} v \frac{\partial A}{\partial s} = Q_a B_I (h - h_b - \varepsilon u) \tag{5-8}$$

where primes have been dropped for simplicity of notation.

Above, the P_e is a sort of Peclet number (Bear 1972) defined as,

$$P_e = \frac{L_0 v_0}{K_0 h_0 / S_y} = \frac{v_0}{\kappa_0 / L_0} = \frac{\textit{convective volumetric flux per unit area in the Stream}}{\textit{diffusive volumetric flux per unit area of aquifer}}$$

with the thermal diffusivity being replaced by the aquifer diffusivity $\kappa_0 = K_0 h_0 / S_y$. For instance, assuming $L_0 = 150\ m$, $v_0 = 0.5\ m/s$ and $\kappa_0 = 0.05\ m^2/s$, this parameter can be of O(1000), showing the disparity of the response of both systems.

The dimensionless group Q_a, termed here the flow number, is defined as,

$$Q_a = \frac{K_0 h_0^2}{v_0 b_0 u_0} = \frac{\textit{volumetric pumping rate}}{\textit{volumetric flow in the stream}}$$

The B_I is the Biot number or dimensionless conductance,

$$B_I = \frac{CL_0}{K_0 h_0} = \frac{C}{K_0 H_0 / L_0} = \frac{conductance\ at\ the\ river\text{–}aquifer\ interface}{conductance\ of\ aquifer\ across\ length\ L_0}$$

Finally,

$$\varepsilon = \frac{u_0}{h_0}$$

is a vertical scale distortion parameter.

CHAPTER 6

COUPLING OF THE GROUND-WATER AND SURFACE-WATER FLOW COMPONENTS USING THE FINITE ELEMENT METHOD

6.1. INTRODUCTION

Exact solutions to the governing equations of hydrologic processes can only be obtained in a limited number of cases. Those are likely posed on a simplified geometry, with boundary conditions easy to impose into the solution. In problems such as the simultaneous analysis of the ground-water system and the surface water system on a real watershed, numerical methods provide alternative means of finding solutions. The finite difference method, the Bubnov-Galerkin method and the Petrov-Galerkin method (Reddy 1993) are some of the techniques most frequently used by hydrologists and scientists in general to determine approximate solutions.

The finite element method (FEM) owes part of its popularity to its flexibility to handle complex geometries. Moreover, it incorporates boundary conditions of the second and third type into the governing equations very easily. These assets make the finite element method the method of choice to solve a broad family of hydrological problems.

In the following sections, the Bubnov-Galerkin method and the Petrov- Galerkin method are implemented for the parabolic ground-water flow equation and the hyperbolic kinematic wave equation, respectively. Flux boundary computations, mass balance and

time stepping algorithms are discussed in detail. Finally, the global structure of the integrated model is described.

6.2. GROUND-WATER FLOW COMPONENT

In the following sub-sections the Bubnov-Galerkin method is implemented for the parabolic ground-water flow equation.

6.2.1. Finite element formulation

Using Einstein tensor notation and lumping the source terms, Equation 5-6 is now rewritten in conservation form as,

$$P_e \frac{\partial h}{\partial t} + \frac{\partial q_i}{\partial x_i} - S_T = 0 \qquad (6\text{-}1)$$

where the flux is given by

$$q_i = -T_{ij} \frac{\partial h}{\partial x_j} \qquad (6\text{-}2)$$

and $T_{ij} = K_{ij}(h - \eta)$ is the transmissivity tensor.

The method of weighted residuals is used to obtain a system of algebraic equations that can be solved for the state variable h. Let the domain Ω with boundary $\partial\Omega$ be discretized into M elements and N nodes, and h be represented by the approximation,

$$h \cong h_\Delta = \sum_{j=1}^{N} h_j(t)\psi_j(x,y) \qquad (6\text{-}2)$$

over the partition Ω_e of the domain Ω, $h_j(t)$ are the unknown nodal hydraulic head values, and $\psi_j(x,y)$ are appropriate interpolation functions. Substitution of Equation 6-3 into Equation 6-1 produces a residual or approximation error. An integral formulation is then obtained by forcing the weighted average of the residual be equal to zero, i.e.

$$\iint_{\Omega} W\left(P_e \frac{\partial h_{\Delta}}{\partial t} + \frac{\partial q_i}{\partial x_j} - S_T\right) d\Omega = 0 \qquad (6\text{-}4)$$

where $W(x,y)$ is some weighting function. Upon applying Green's first identity over the simply connected domain Ω with boundary $\partial\Omega$, and dropping the subscript Δ from now on with the understanding that h is the approximation, Equation 6-4 becomes,

$$\iint_{\Omega}\left(P_e \frac{\partial h}{\partial t} W + T_{ij} \frac{\partial h}{\partial x_j} \frac{\partial W}{\partial x_i} - S_T W\right) d\Omega + \oint_{\partial\Omega} \sigma W ds = 0 \qquad -5)$$

where

$$\sigma = \hat{n} \cdot \hat{q} = -n_i T_{ij} \frac{\partial h}{\partial x_j} \qquad (6\text{-}6)$$

is the flux through the boundary $\partial\Omega$, $\hat{n} = n_i = (Cos\upsilon, Sin\upsilon)$ is the outward unit vector normal to $\partial\Omega$, and υ is the angle between $\hat{n}$ and the horizontal positive axis measured counterclockwise. Equation 6-6 implies that inflows are considered negative and outflows positive, in agreement with the Gauss divergence theorem. The weak form Equation 6-5 has two desirable characteristics. First, it requires weaker continuity of the state variable h, and second, flux boundary conditions are automatically incorporated in the integral equation. Therefore, the approximate solution of h is required to satisfy only Dirichlet boundary conditions. Taking advantage of such a property, the coupling term is treated

through a boundary integral over the internal boundary Γ_R, as it will become clear later on.

Different choices of the weighting function W give rise to different methods. In the context of the method of weighted residuals, the Galerkin's procedure is the method most frequently used to solve ground-water flow problems. In this method, the weighting function W is set equal to the approximation functions, i.e.

$$W = \{\psi_i\}_{i=1}^{N} \tag{6-7}$$

where by varying the subindex i from 1 to N, a system of N algebraic equations in the state variable h is obtained as follows,

$$P_e \iint_\Omega \frac{\partial h}{\partial t}\psi_i d\Omega + \iint_\Omega T_{ij}\frac{\partial h}{\partial x_j}\frac{\partial \psi_i}{\partial x_i}d\Omega = \iint_\Omega R\psi_i d\Omega - \iint_\Omega \left(\sum_{k=1}^{N_w} Q_k \delta_k\right)\psi_i d\Omega$$

$$-\iint_\Omega E\psi_i d\Omega + \oint_{\partial\Omega} n_i T_{ij}\frac{\partial h}{\partial x_j}\psi_i ds \qquad i = 1,\cdots,N \tag{6-8}$$

where the term S_T has been replaced by $R - \sum_{k=1}^{N_w} Q_k\delta_k - E$. Equation 6-8 written in matrix notation is

$$\mathbf{R}_c \cdot \frac{\partial \hat{h}}{\partial t} + \frac{1}{P_e}\mathbf{A}\cdot\hat{h} = \frac{1}{P_e}\hat{b} \tag{6-9}$$

Above, $\mathbf{R}_c$ is the capacitance matrix or mass matrix, $\mathbf{A}$ is equal to $\mathbf{M} + \mathbf{M}_0 + \mathbf{M}_{et}$ where $\mathbf{M}$ is the conductance matrix, $\mathbf{M}_0$ is the stream-aquifer contribution matrix, and $\mathbf{M}_{et}$ is the evapotranspiration contribution matrix, $\hat{b}$ is a load vector, and $h = (h_1,\cdots,h_N)$ is the vector of unknown nodal hydraulic heads.

For linear triangular elements, the element matrices can be evaluated exactly (see e.g. Istok 1989). The capacitance matrix is then expanded into,

$$R_{C_{ij}} = \iint_{\Omega_e} \psi_i \psi_j d\Omega = \frac{A^e}{12}(1+\delta_{ij}) \tag{6-10}$$

for the consistent formulation, where δ_{ij} is the Kronecker delta tensor and A^e is the area of the element, or

$$R_{C_{ij}} = \frac{A^e}{3}\delta_{ij} \tag{6-11}$$

for the lumped formulation, where the superscript e indicates element number.

As seen before, the matrix **A** is the sum of the conductance matrix plus the contributions from non-linear sources. For an inhomogenous anisotropic aquifer with $T_{xx} \neq T_{yy}$, and (x,y) principal directions (i.e. $T_{xy} = T_{yx} = 0$),

$$T_{ij}\frac{\partial h}{\partial x_j}\frac{\partial W}{\partial x_i} = T_{xx}\frac{\partial h}{\partial x}\frac{\partial W}{\partial x} + T_{yy}\frac{\partial h}{\partial y}\frac{\partial W}{\partial y} \tag{6-12}$$

Then,

$$M_{ij} = \iint_{\Omega_e}\left(T_{xx}\frac{\partial \psi_i}{\partial x}\frac{\partial \psi_j}{\partial x} + T_{yy}\frac{\partial \psi_i}{\partial y}\frac{\partial \psi_j}{\partial y}\right)d\Omega$$

$$= \frac{1}{4A^e}\left[\tilde{T}_x b_i b_j + \tilde{T}_y c_i c_j\right] \tag{6-13}$$

where ~ means the average $\left(\sum_{k=1}^{3}(T_x)_k\right)\Big/3$. Analytical expressions to evaluate the derivatives of the approximation functions b_i and c_i are well known and can be found in Istok (1989). Equation 6-13 is valid not only for the linear case but also for the non-linear case, the non-linearity being embedded in the transmissivity values.

The matrix $\mathbf{M}_{et}$ has components,

$$M_{et_{ij}} = \frac{ET_m^e}{d^e} \iint_{\Omega_e} \psi_i \psi_j d\Omega = \frac{ET_m^e}{d^e} \frac{A^e}{12}(1+\delta_{ij}) \tag{6-14}$$

where ET_m and d are defined in Section 3.4.

The stream is represented by one-dimensional elements along which h_s is approximated using one dimensional linear interpolation functions $\{\phi_i(s)\}_{i=1}^{NSR}$, where NSR stands for the number of stream reaches determined by the finite element partition. Then $\mathbf{M}_o$ has components,

$$M_{0_{ij}} = C^s \int_0^{\Delta s} \phi_i \phi_j ds = C^s \frac{\Delta s}{6}(\delta_{ij}+1) \tag{6-15}$$

Here the superscript s indicates a stream element, Δs is the length of the stream element and C^s is the average conductance coefficient over the element.

Finally, the vector $\hat{b}$ contains all those contributions from boundary terms and source terms that do not depend on the solution.

6.2.2. Time integration

The time integration scheme is based on the theta method with either lumped or consistent formulation. Equation 6-8 is valid for either a confined or an unconfined aquifer, with the understanding that a non-linear system of equations results in the latter case. Then, the set of equations to be solved is,

$$\left[\mathbf{R}_c + \omega_1 \mathbf{A}^{n+1}\right]\hat{h}^{n+1} = \left[\mathbf{R}_c + \omega_2 \mathbf{A}^n\right]\hat{h}^n + \omega_2 \hat{b}^n + \omega_1 \hat{b}^{n+1} \tag{6-16}$$

where the superscript n denotes the time level $t_n = n\Delta t$, $\omega_1 = \theta\Delta t/P_e$ and $\omega_2 = (1-\theta)\Delta t/P_e$. Steady state solutions are obtained with $\theta = 1$, corresponding to the Backward Euler or fully implicit algorithm, and transient solutions are obtained with $\theta = \frac{1}{2}$, which corresponds to the well-known Crank-Nicolson-Galerkin.

In general, $\mathbf{A}$ depends on h in some non-linear fashion, and so does the load vector $\hat{b}$. In this case, a Picard iteration is used to advance the solution one time step where the coefficient matrix $\mathbf{A}^{n+1} = \mathbf{A}(\hat{h}^n)$ and the vector $\hat{b}$ are updated at each iteration to reflect the most recent estimate of head and thereby saturated thickness (Pinder and Gray 1977). The scheme is first rewritten as,

$$\left[\mathbf{R}_c + \omega_1 \mathbf{A}^{\upsilon}\right]\hat{h}^{\upsilon+1} = \left[\mathbf{R}_c - \omega_2 \mathbf{A}^{n}\right]\hat{h}^{n} + \omega_2 \hat{b}^{n} + \omega_1 \hat{b}^{\upsilon} \qquad (6\text{-}17)$$

where $\mathbf{A}^{\upsilon} = \mathbf{A}(\hat{h}^{\upsilon})$, $\hat{b}^{\upsilon} = \hat{b}(\hat{h}^{\upsilon})$, and υ is the iteration level. Then, the Picard iteration proceeds as follows,

Step 1: Assume that at time $t = t^n$, the head $\hat{h}^n$ is known.

Step 2: Compute the modified matrix $\tilde{\mathbf{R}} = \mathbf{R}_c - \omega_2 \mathbf{A}^n$.

Step 3: Compute the constant vector $z = \tilde{\mathbf{R}} = \mathbf{R}_c - \omega_2 \hat{b}^n$

Step 4: Initialize iteration $\upsilon = 0$, $\hat{h}^{\upsilon} = \hat{h}^n$

Step 5: Form $\mathbf{A}^{\upsilon} = \mathbf{A}(\hat{h}^{\upsilon})$

Step 6: Compute $\tilde{\mathbf{A}}^{\upsilon} = \mathbf{R}_c + \omega_1 \mathbf{A}^{\upsilon}$

Step 7: Evaluate $\hat{b}^{\upsilon}$ and form right hand side vector $z' = z + \omega_1 \hat{b}^{\upsilon}$

Step 8: Apply boundary conditions and store $\hat{h}^{\upsilon}$

Step 9: Solve $\tilde{\mathbf{A}}^{\upsilon}\hat{h}^{\upsilon+1} = z'$

Step 10: Check if the desired accuracy has been reached, i.e.

$$\frac{\left\|\hat{h}^{\upsilon+1} - \hat{h}^{\upsilon}\right\|}{\left\|\hat{h}^{\upsilon+1}\right\|} < \varepsilon_1$$

no $\rightarrow$ $\upsilon = \upsilon + 1$, return to Step 5

yes $\rightarrow$ Advance the solution $\hat{h}^{n+1} = \hat{h}^{\upsilon+1}$, then continue

Step 11:

$$\frac{\left\|\hat{h}^{n+1} - \hat{h}^{n}\right\|}{\left\|\hat{h}^{n+1}\right\|} < \varepsilon_2$$

yes $\rightarrow$ steady state solution has been reached

no $\rightarrow$ $t^{n+1} = t^n + \Delta t$. If $t^{n+1} < t_{end}$ return to *Step 1*,

Otherwise end time integration.

6.2.3. Accurate boundary flux calculation

There are many practical situations, particularly in the mass-balance computation, in which the flux is desired at nodes or part of the boundary where Dirichlet data are prescribed. However, these fluxes are not given directly by the finite element solution and must be obtained *a-posteriori* once the values of the unknown dependent variable have been determined.

Full credit of the analysis that follows must be given to Carey (1982) and Carey *et al.* (1985). Carey detailed a technique to obtain very accurate fluxes from finite element solutions. This technique, implemented on the model, is illustrated with the help of Carey's example. Let a one-dimensional problem be posed as,

$$-u'' + u = x \qquad \text{on} \quad 0 < x < 1 \tag{6-18}$$

subject to $u(0) = u(1) = 0$, whose exact solution is $u = x - \frac{Sinhx}{Sinh1}$. The weak form statement reads,

$$\int_0^1 (-u'' + u)v dx = \int_0^1 xw dx \tag{6-19}$$

for all admissible test functions v. Integrating the above expression by parts,

$$\int_0^1 (u'v' + uv)dx - u'v\Big|_0^1 = \int_0^1 xw dx \tag{6-20}$$

If u is restricted to satisfy the homogeneous boundary conditions $u(0) = u(1) = 0$, the test function v must be zero at both ends. However, if v is allowed to take the values $v(0) = v(1) = 1$, two expressions for the boundary fluxes are obtained. To be specific, introducing a finite element basis $\{\phi_i\}_{i=0}^N$ of piecewise linear functions on the interval [0,1], with compact support on the node i, where $x_i = i\Delta x$, and $\Delta x = 1/N$ for $i = 0,\cdots,N$ and choosing $v = \phi_i$ the Galerkin procedure yields,

$$\int_0^1 (u'\phi_i' + u\phi_i)dx + u'(0)\phi_i(0) - u'(1)\phi_i(1) = \int_0^1 x\phi_i dx \qquad i = 0,\cdots,N \tag{6-21}$$

Setting $i = 0$ and $i = N$, the two formulas to estimate the fluxes at both boundaries are,

$$\sigma_0 = \int_0^1 x\phi_0 dx - \int_0^1 (u'\phi_0' + u\phi_0)dx \tag{6-22}$$

$$\sigma_N = \int_0^1 x\phi_N dx - \int_0^1 (u'\phi_N' + u\phi_N)dx \tag{6-23}$$

where the one-dimensional fluxes are defined as $\sigma = -n_i \frac{\partial u}{\partial x_i}$, in agreement with Equation 6-6 (the transmissivity is here trivially set equal to one). Expanding the dependent variable

u in the standard fashion, $u \approx u_\Delta = \sum_j u_j \psi_j(x)$, where $\Delta\ (= \Delta x)$ is the partition norm of the interval [0,1], and u_Δ is the approximation function to $u(x)$, Equations 6-22 and 6-23 become,

$$\sigma_0^\Delta = \frac{\Delta x^2}{6} - \frac{1}{\Delta x}(u_0 - u_1) - \frac{\Delta x}{6}(2u_0 + u_1) \tag{6-24}$$

$$\sigma_N^\Delta = \frac{\Delta x}{6}(3 - \Delta x) - \frac{1}{\Delta x}(u_N - u_{N-1}) - \frac{\Delta x}{6}(2u_N + u_{N-1}) \tag{6-25}$$

where σ_i^Δ is the discrete approximation to σ at the boundaries $i = 0$ and $i = N$. The performance of this technique is now assessed by means of the estimation of the flux calculation error at node $i = N$. First, a way to measure the error must be introduced.

It is customary to seek asymptotic estimates of the error in the finite element approximation, where the error is a function defined as the difference between the exact and the approximate solution. Ordinarily, these estimates will be of the form,

$$\|e\| \le c\Delta^p \tag{6-26}$$

where c is the asymptotic error constant, p is the rate of convergence and $\|e\|$ is a nonnegative number called norm (Dahlquist and Bjorck 1974). Equation 6-26 will plot as a straight line of slope p and intercept $\log(c)$ on a log-log plot,

$$\log\|e\| = \log(c) + p\log(\Delta) \tag{6-27}$$

For example, let $\|e_1\| = \left|-u'(1) - \sigma_N^*\right|$ be the error when the flux is computed differentiating the resulting finite element solution, where $\sigma_N^* = -u_\Delta'(1)$. Let $\|e_2\| = \left|-u'(1) - \sigma_N^\Delta\right|$ be the error when the flux is computed using Equation 6-25. In both expressions $-u'(1)$ is the

Figure 6.1: Rate of convergence for flux calculations using the derivative method and the accurate method - 1D problem

One-dimensional example

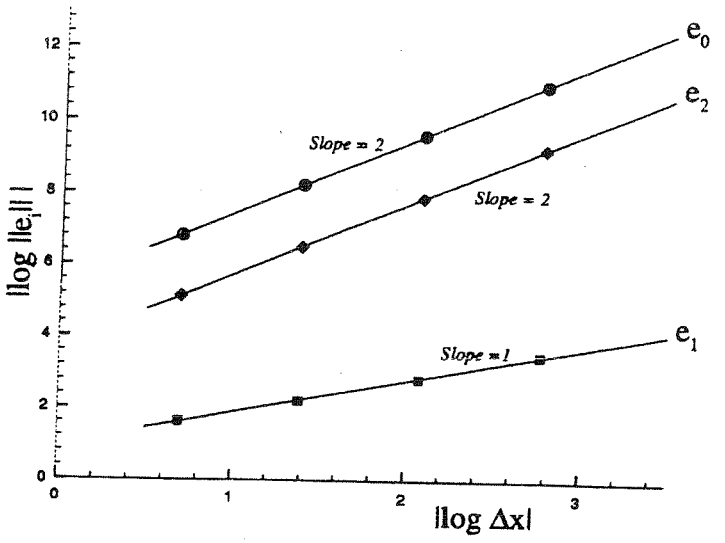

exact flux. Figure 6.1 shows $|\log\|e_1\||$ and $|\log\|e_2\||$ plotted against $|\log\Delta|$. The error committed in the numerical solution of equation 6-18 at point $x = 0.5$, $|\log\|e_0\|| = |u(0.5) - u_\Delta(0.5)|$ is also plotted. The graph shows that the rate of convergence for both, the technique just described and the solution itself is equal to two. Meanwhile, the differentiation of the finite element solution method yields a rate of convergence of order one.

The foregoing ideas can be extended to two-dimensional problems as well (Carey *et al.* 1985). However, the procedure is less direct. The flux now appears on a contour integral along the boundary of the domain rather than explicitly as a point value. The procedure starts with the weighted residual statement of Equation 6-1, i.e. Equation 6-5

$$\oint_{\partial\Omega} \sigma W ds = \iint_{\Omega} \left[S_T W - \left(P_e \frac{\partial h}{\partial t} W + T_{xx} \frac{\partial h}{\partial x} \frac{\partial W}{\partial x} + T_{yy} \frac{\partial h}{\partial y} \frac{\partial W}{\partial y} \right) \right] d\Omega \qquad (6\text{-}28)$$

This expression and the computed solution can be used to obtain an approximation to the normal flux. To do so, the expansion $h \approx h_\Delta = \sum_j h_j \psi_j(\hat{x})$ is introduced in the right hand side of Equation 6-28 and the weight function W is set equal to ψ_i, the global basis function for the boundary node i. It is understood that ψ_i is only non-zero on those elements immediately adjacent to node i, and in particular, on those parts of the boundary $\partial\Omega$ adjacent to node i. Equation 6-28 becomes,

$$\oint_{\partial\Omega} \sigma \psi_i ds = \iint_{\Omega} \left[S_T \psi_i - \left(P_e \frac{\partial h}{\partial t} \psi_i + T_{xx} \frac{\partial h}{\partial x} \frac{\partial \psi_i}{\partial x} + T_{yy} \frac{\partial h}{\partial y} \frac{\partial \psi_i}{\partial y} \right) \right] d\Omega \qquad (6\text{-}29)$$

This can be expressed directly in terms of the finite element spatial discretization as,

$$\oint_{\partial\Omega} \sigma \psi_i ds = b_i - \sum_{j=1}^{N} (R_{C_{ij}} P_e \frac{dh_j}{dt} + M_{ij} h_j) \qquad i = 1, \cdots, NEC \qquad (6\text{-}30)$$

where NEC is the number of nodes with prescribed essential boundary conditions along $\partial\Omega$ and the $R_{C_{ij}}$ are given by Equations 6-10 and 6-11, and the M_{ij} by Equation 6-13.

Let now $\phi_i(s)$ be the restriction of ψ_i to the boundary $\partial\Omega$, i.e. $\phi_i(s) = \psi_i(\hat{x})$ whenever $\hat{x} \in \partial\Omega$, s being the arc-length along $\partial\Omega$. Expanding the flux in the usual form, $\sigma \approx \sum_n \sigma_n \phi_n(s)$, the left hand side of Equation 6-30 becomes,

$$\sum_{n=1}^{NEC} \left(\int \phi_i \phi_n ds \right) \sigma_n = \sum_{n=1}^{NEC} T_{in} \sigma_n \qquad i = 1, \cdots, NEC \qquad (6\text{-}31)$$

where T is the tridiagonal banded matrix, tridiag $\left[\frac{\Delta s}{6}(1,4,1)\right]$, symmetric and strictly diagonally dominant, with leading coefficients $\Delta s/3$ in the first and the last rows. The

system Equation 6-31 can be solved easily by means of the Gaussian elimination method. In matrix form, Equation 6-31 is written as,

$$\mathbf{T} \cdot \hat{\sigma} = \hat{r}_0 \tag{6-32}$$

where $\hat{r}_0$ is the "residual vector" defined as $r_{0_i} = b_i - \sum_{j=1}^{N} (R_{C_{ij}} P_e \frac{dh_j}{dt} + M_{ij} h_j)$.

The method can now be extended to transient problems just by introducing a backward difference to evaluate the time derivative. Finally, the solution to Equation 6-32 is given by,

$$\hat{\sigma} = \mathbf{T}^{-1} \cdot \hat{r}_0 \tag{6-33}$$

In this work, the boundary flux is approximated using the standard Galerkin basis functions for linear triangular elements. At the endpoints, the normal and hence σ is not uniquely defined. However, Carey *et al.* (1985) proposed a way to overcome such difficulty. Their approach states that, whenever a good approximation to the flux value at the corner point is obtained, the method just described yields the optimal rate of convergence. The method implemented here is as follows: initially the fluxes at the first and last node of the portion of the boundary with prescribed Dirichlet data are computed by direct differentiation of the finite element solution. These values are then used as boundary conditions in the system Equation 6-33. This method is very stable and produces superior accuracy for the calculation of the flux through any boundary segment (for more details see Carey *et al.* 1985).

In order to illustrate the capabilities of the algorithm, the following test problem is solved using two different discretizations, $\Delta = \frac{1}{8}$ and $\Delta = \frac{1}{4}$,

$$\nabla^2 u = 4 \qquad \text{in } \Omega = [(0,1) \cup (0,1)]$$

with

$$\sigma = 0 \text{ on } x = 0 \text{ and } y = 0, \quad \sigma = -2 \text{ on } y = 1, \text{ and } u = 1 + y^2 \text{ on } x = 1,$$

whose solution is $u = x^2 + y^2$. The absolute value of the logarithm of the error in the calculated flux is plotted against the logarithm of the mesh size (Figure 6.2). A marked improvement on the convergence rate is observed for the accurate method given by Equation 6-33, with a rate of approximately 3.4, in comparison with the asymptotic rate $O(\Delta)$ obtained by differentiating the finite element solution. The numerical finite element solution u_Δ, computed at $(x = 0.5, y = 1)$, converges with the expected optimal rate $O(\Delta^2)$. For more details see Carey *et al.* (1985). These ideas are now applied to the estimation of the closure error on the water budget.

Figure 6.2 - Rate of convergence for flux calculations using the derivative method and the accurate method - 2D problem

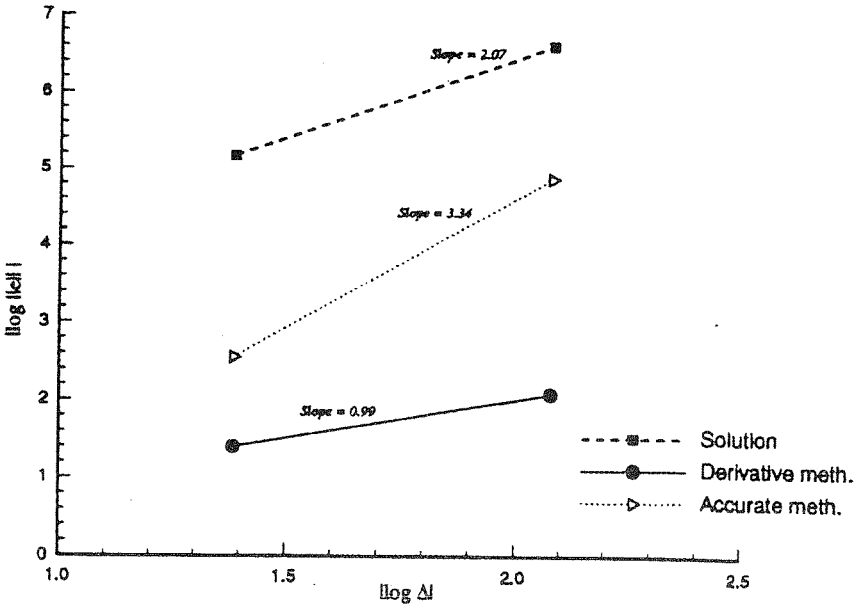

6.2.4. Mass balance

The water budget, here called mass balance, is generally a summary of all inflows and outflows to the region. It can be done with volumes of water and/or volumetric flow rates. The model mass balance not only provides a hydrologic budget analysis but also furnish an indication of the accuracy of the numerical solution.

The following analysis deals with volumes of water. However, it can be easily extended to volumetric rates. Equation 6-1 is integrated over the domain Ω to yield a global mass balance equation of the form,

$$P_e \iint_{\Omega} \frac{\partial h}{\partial t} d\Omega + \iint_{\Omega} \frac{\partial q_i}{\partial x_i} d\Omega = \iint_{\Omega} S_T \, d\Omega \qquad (6\text{-}34)$$

Applying the Divergence theorem and making use of Equation 6-6, the above equation transforms into,

$$P_e \frac{\partial}{\partial t} \iint_{\Omega} h \, d\Omega + \oint_{\partial\Omega} \sigma \, ds = \iint_{\Omega} S_T \, d\Omega \qquad (6\text{-}35)$$

Now, the introduction of a few definitions will render Equation 6-35 into a more familiar water-budget expression. Let,

$$V(t) = \iint_{\Omega} h(x, y, t) \, d\Omega \qquad (6\text{-}36)$$

be the amount of water stored in Ω at any time t,

$$Q(t) = \oint_{\partial\Omega} \sigma \, ds \qquad (6\text{-}37)$$

be the rate at which water enters or leaves Ω through the boundary $\partial\Omega$ of the domain and,

$$F(t) = \iint_{\Omega} S_r \, d\Omega \tag{6-38}$$

be the rate at which water is added or withdrawn from Ω through source terms. Then, introducing Equations 6-36 through 6-38 into Equation 6-35 yields

$$\frac{\partial V(t)}{\partial t} + \frac{1}{P_e} Q(t) = \frac{1}{P_e} F(t) \tag{6-39}$$

Time integration of Equation 6-39 provides a way to calculate a mass balance at a particular time interval, i.e.

$$\int_{t^n}^{t^{n+1}} \frac{\partial V(t)}{\partial t} dt + \frac{1}{P_2} \int_{t^n}^{t^{n+1}} Q(t)\, dt = \frac{1}{P_2} \int_{t^n}^{t^{n+1}} F(t)\, dt \tag{6-40}$$

where t^{n+1} and t^n indicate two consecutive time levels. If the second and the third integrals in Equation 6-40 are evaluated by means of the trapezoidal rule, the equation transforms into,

$$V^{n+1} = V_*^n - (Q^{n+1} + Q^n)\frac{\Delta t}{2P_e} + (F^{n+1} + F^n)\frac{\Delta t}{2P_e} \tag{6-41}$$

where V_*^n is calculated integrating the solution over the domain Ω, i.e.

$$V_*^n(t) = \iint_{\Omega} h(x, y, t^n)\, d\Omega \tag{6-42}$$

and $\Delta t = (t^{n+1} - t^n)$. A local truncation error or the numerical error committed in one time step, can be estimated as (Dahlquist and Bjorck 1974),

$$LTE = V^{n+1} - V_*^{n+1}$$

where $V_*^{n+1} = \iint_{\Omega} h(x, y, t^{n+1})\, d\Omega$. Then, the absolute error A_{err} is computed as follows,

$$A_{err} = \frac{V_*^{n+1} - V_*^n}{\Delta t} + Flux + Source$$

$$= \frac{V_*^{n+1} - V_*^n}{\Delta t} + \frac{(Q^{n+1} + Q^n)}{2P_e} - \frac{(F^{n+1} + F^n)}{2P_e} \qquad (6\text{-}43)$$

Mass balance computations are verified under steady-state as well as transient conditions. The following test serves to check the mass balance for steady-state conditions, and at the same time, it allows to compare the two algorithms for flux calculations previously described. The problem, originally implemented with MODFLOW (EPA 1993), consists of a two-dimensional coastal unconfined aquifer with a hydraulic conductivity of 1,340 *ft/day*. The aquifer is recharged at a rate of 25 *in/yr*. The maximum evapotranspiration rate for the area is 50 *in/yr*, the extinction depth is 8 *ft*, and the ET surface, coincident with the topographic surface, ranges from 18 *ft* at the low southwest corner to 0 *ft* at the coast. No flow boundaries surround the area to the north, south and west. The coastline, located along the entire east boundary is represented by a Dirichlet boundary ($h = 0$). More details can be found in EPA (1993). Figure 6.3 shows the potentiometric surface obtained, which matches the reported results remarkably well. Once the steady state is reached , the simulated evapotranspiration is 78 %, the discharge through the Dirichlet boundary calculated by differentiating the solution and using Equation 6-33 is 22 % and 24 %, respectively (Figure 6.4). Part of the disparity in the results obtained with the method discussed in Section 6.2.3 is due to the presence of multiple sharp corners on the Dirichlet boundary. As mentioned earlier (Carey *et al.* 1985), the normal and hence the flux at those points is not uniquely defined. In any case, this test shows the reliability of the derivative method when computing fluxes. Though in general less accurate, the

Figure 6.3: Mass balance test: problem boundary and potentiometric surface

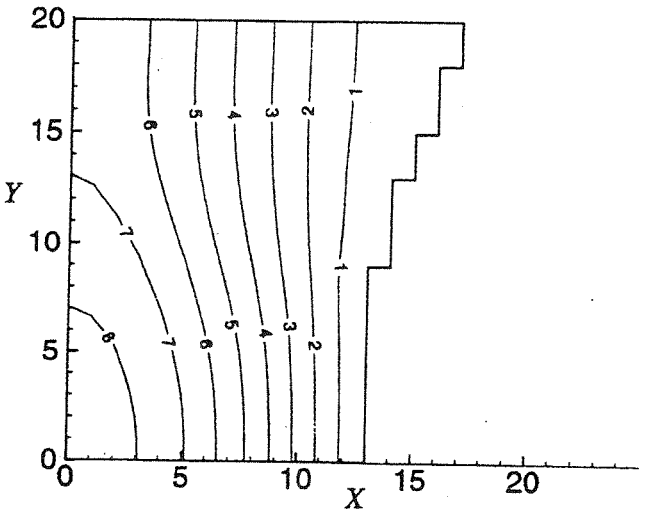

Figure 6.4: Mass balance test: flux components

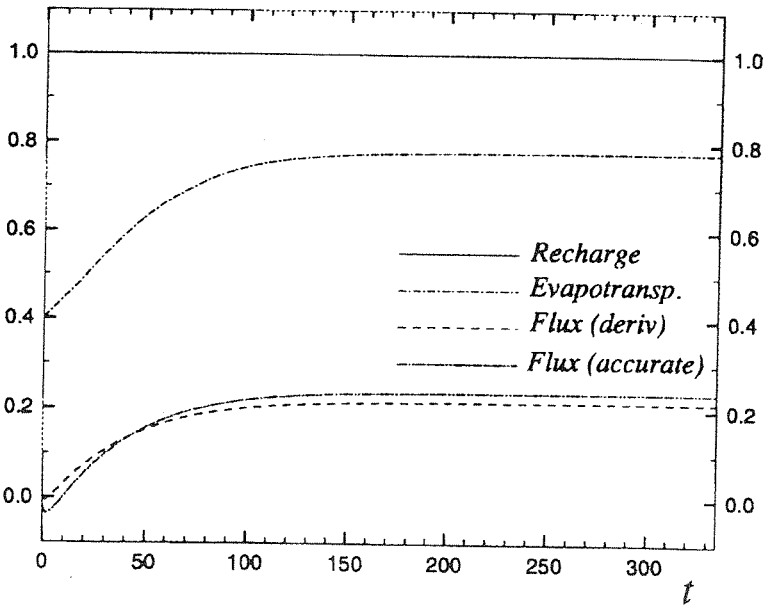

derivative method is robust. The mass balance for the problem was satisfied, with closure error of less than 1 %.

For the purpose of testing the mass balance under transient conditions, the following oscillatory problem is solved. A one dimensional, linear, semi-infinite homogeneous aquifer was subject to a no flow boundary condition at $x \to \infty$ and a periodic head-dependent boundary condition at $x = 0$. The problem has the following analytical solution (Carslaw and Jaeger 1959),

$$h = h_0 + \frac{Ca_u}{\beta^2 + \alpha^2}(\beta Cos(\alpha x - \omega t) - \alpha Sin(\alpha x - \omega t))e^{-\alpha x} \qquad (6\text{-}44)$$

where h_0 is the initial state; C is the conductance coefficient as previously defined; a_u is the amplitude of the stream stage oscillation; $\alpha = \sqrt{\frac{\omega}{2\kappa}}$ with $\omega = 2\pi/T_p$ the frequency of the oscillation, T_p is the period of the oscillation and κ the aquifer diffusivity; $\beta = C + \alpha$; $a = \sqrt{2\omega\kappa}$ is a damping coefficient and ω/a is the celerity of the wave within the aquifer. The set of parameters used in the test is shown in Table 6-1.

Table 6.1: Parameters for oscillation model

Parameter	Value
κ	0.05 m/s
h_o	10.0 m
a_u	1.5 m
T_p	21 days
C	2×10^{-3} m/s/m

Figure 6.5.a shows the numerical solution and the analytical solution as a function of time at three fixed locations. In absence of any other sources, the change in storage equals the flux from the stream (Figure 6.5.b), both exhibiting the oscillatory nature of the

Figure 6.5.a: Oscillatory problem: numerical solution (symbols) and analytical solution (line segments) at different locations as a function of time

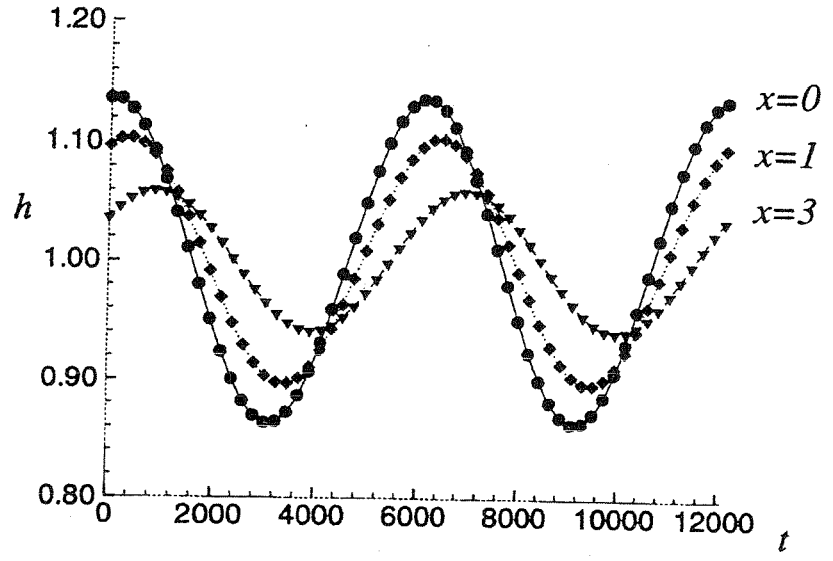

Figure 6.5.b: Oscillatory problem: river flux (Q_R) and storage ($\partial V/\partial t$)

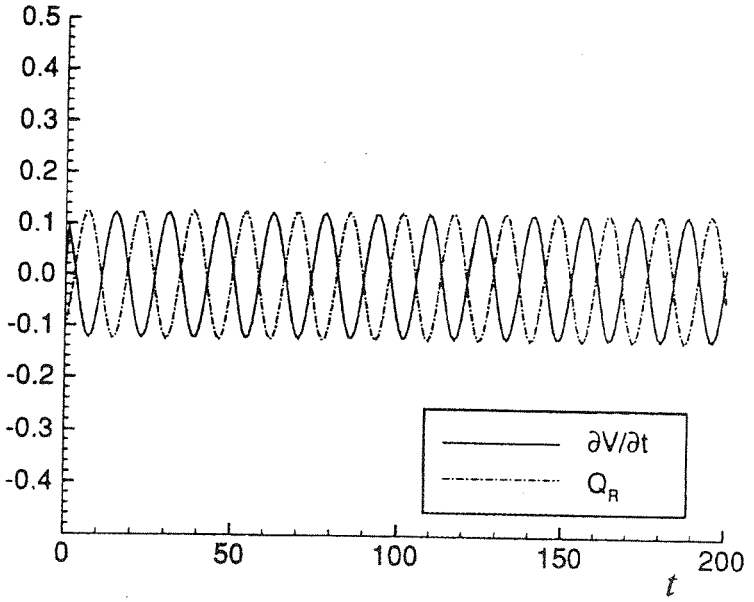

problem and the remarkable accuracy of the trapezoidal method. Indeed, for periodic problems this method is exact (Dahlquist and Bjorck 1974).

6.3. KINEMATIC WAVE MODEL

In the following sub-sections, the Petrov- Galerkin method is implemented for the hyperbolic kinematic wave equation.

6.3.1. Finite element formulation

Dupont (1973) stated that the classical Galerkin formulation produces very poor results when applied to propagation problems. The use of discontinous weighting functions that produce "upwind" effects but at the same time maintain the accuracy of the central difference scheme is a viable alternative to the traditional Galerkin scheme (Katopodes 1984). Many authors have contributed to the development of the technique and have been trying to establish the proper dissipation level, among them Raymond and Garder (1976), Baker and Soliman (1981), Hughes and Brooks (1982), Muñoz Carpena *et al.* (1994). As it is shown in Appendix A and later in this Chapter, the Petrov-Galerkin or the dissipative Galerkin method used in this work is able to dissipate any parasitic waves that may appear around flow discontinuities. Moreover, the scheme does not introduce smearing effects, and is able to cope with advection-diffusion problems with high accuracy.

The finite element formulation of the kinematic wave model (KWM) starts with the application of the method of weighted residuals (MWR) to obtain a system of

algebraic equations that can be solved for the variable A. Let the internal boundary Γ_R be discretized into NSR elements and $NSR+1$ nodes, and A be represented by the approximation,

$$A \approx A_\Delta \sum_{j=1}^{NSR+1} a_j(t)\phi_j(s) \tag{6-45}$$

over the partition Δ of the domain Γ_R. The $a_j(t)$ are the unknown nodal area values, and the $\phi_j(s)$ are appropriate interpolation functions, being s the arc-length along Γ_R. It is understood that $\phi_j(s) = \psi_j(\hat{x})$ whenever $\hat{x} \in \Gamma_R$. Substitution of Equation 6-45 into Equation 5-7 generates a residual that, according to the MWR, must vanish on a weighted average sense, i.e.

$$\int_{\Gamma_R} W\left[\frac{\partial A_\Delta}{\partial t} + \frac{5}{3}\gamma A_\Delta^{2/3}\frac{\partial A_\Delta}{\partial s} - \nu\frac{\partial^2 A_\Delta}{\partial s^2} - G(A_\Delta)\right]ds = 0 \tag{6-46}$$

where $W(s)$ is some weighting function, G is the coupling term, γ is the channel parameters ratio given by $\sqrt{S}/nP^{2/3}$ and ν is the coefficient of added diffusion, introduced for comparison purposes with known solutions of the generalized Burger's equation (Fletcher 1989).

The weak or variational form of Equation 6-46 is obtained with the aid of the standard integration by parts formula,

$$\int_{\Gamma_R}\left(W\left[\frac{\partial A_\Delta}{\partial t} + \frac{5}{3}\gamma A_\Delta^{2/3}\frac{\partial A_\Delta}{\partial s} - G(A_\Delta)\right] + \nu\frac{\partial A_\Delta}{\partial s}\frac{\partial W}{\partial s}\right)ds - \nu W\frac{\partial A_\Delta}{\partial s}\Bigg|_0^L = 0 \tag{6-47}$$

where L is the total length of the internal boundary Γ_R.

Galerkin's procedure is used to solve the ground-water flow problem. Given the quasi-hyperbolic nature of the equation, a consistent Petrov-Galerkin is employed to solve Equation 6-47 (Carey and Oden 1986). In this method, the weighting function W is set equal to the approximation function plus a perturbation term that is a function of the derivative of the approximation function, i.e.

$$w = \phi_i + p_i = \phi_i + \tilde{\alpha}\frac{\Delta s}{2}\frac{d\phi_i}{ds} \tag{6-48}$$

The upwinding coefficient $\tilde{\alpha}$ is usually set equal to its optimum value $2/\sqrt{15}$ (Raymond and Garder 1976). Usually, the determination of the optimum dissipation level requires some numerical experimentation. Replacing A_Δ in Equation 6-47 according to Equation 6-45 yields,

$$\int_{\Gamma_R}(\phi_i + p_i)\left[\sum_j \frac{\partial a_j}{\partial t}\phi_j + \frac{5}{3}\gamma\left(\sum_j a_j\phi_j\right)^{2/3}\sum_k a_k\frac{\partial\phi_k}{\partial s} - \sum_j G_j\phi_j\right]ds$$

$$+\int_{\Gamma_R}\nu\sum_j\frac{\partial\phi_i}{\partial s}\frac{\partial\phi_j}{\partial s}a_j\,ds \qquad i = 1,\cdots,NSR+1 \tag{6-49}$$

Since $W(0) = 0$ ($A(0,t)$ is prescribed) and the natural boundary condition $\partial A/\partial s = 0$ is chosen at $s = L$, the boundary term in Equation 6-47 has been dropped. By varying the subindex i from 1 to $NSR+1$, the following matrix equation is obtained,

$$\mathbb{D}\cdot\frac{\partial\hat{a}}{\partial t} + \hat{c}(\hat{a}) + \mathbb{V}\cdot\hat{a} = \mathbb{D}\cdot\hat{G} \tag{6-50}$$

For one-dimensional elements, the above matrices and vectors are given as follows,

$$D_{ij} = \int_0^{\Delta s}\phi_i\phi_j\,ds + \tilde{\alpha}\frac{\Delta s}{2}\int_0^{\Delta s}\frac{\partial\phi_i}{\partial s}\phi_j\,ds = \frac{\Delta s}{12}\begin{bmatrix}4-3\tilde{\alpha} & 2-3\tilde{\alpha}\\ 2+3\tilde{\alpha} & 4+3\tilde{\alpha}\end{bmatrix} \tag{6-51}$$

$$c_i = \frac{5}{3}\bar{\gamma}\sum_k \frac{\partial \phi_k}{\partial s} a_k \left[\int_0^{\Delta s} (\phi_i + p_i)\left(\sum_j a_j \phi_j \right)^{2/3} ds \right] \tag{6-52}$$

$$V_{ij} = \nu \int_0^{\Delta s} \frac{\partial \phi_i}{\partial s} \frac{\partial \phi_j}{\partial s} ds \tag{6-53}$$

$$G_i = Q_a B_1 (h_i - h_{b_i} - \varepsilon u_i) \tag{6-54}$$

where $\bar{\gamma}$ is computed using average values within the element.

6.3.2. Time integration

Given the nonlinearity of the problem, intrinsically represented in the vector $\hat{c}(\hat{a})$ of Equation 6-50, an iterative technique must be used to advance the solution in time. The Newton's method, implemented here, is a powerful technique with a quadratic rate of convergence when close to the solution (Fletcher 1989). The application of the Crank-Nicolson-Galerkin method to Equation 6-50 leads to the following system of equations,

$$\mathbf{D}\cdot\hat{a}^{k+1} - \frac{\Delta t}{2}\left[\mathbf{D}\cdot\hat{G}^{k+1} - \hat{c}(a^{k+1}) - \mathbf{V}\cdot\hat{a}^{k+1}\right] = \mathbf{D}\cdot\hat{a}^{k} + \frac{\Delta t}{2}\left[\mathbf{D}\cdot\hat{G}^{k} - \hat{c}(a^{k}) - \mathbf{V}\cdot\hat{a}^{k}\right] \tag{6-55}$$

Calling $\hat{e}(\hat{a}^k)$ the right hand side of Equation 6-55, the above equation can be rewritten as,

$$f(\hat{a}^{k+1}) = 0 \tag{6-56}$$

where

$$f(\hat{a}^{k+1}) = \mathbf{D}\cdot\hat{a}^{k+1} - \frac{\Delta t}{2}\left[\mathbf{D}\cdot\hat{G}^{k+1} - \hat{c}(a^{k+1}) - \mathbf{V}\cdot\hat{a}^{k+1}\right] - \hat{e}(\hat{a}^{k}) \tag{6-57}$$

Then, Newton's method can be expressed as,

$$\hat{a}^{r+1} = \hat{a}^{r} + \Delta a^{r} = \hat{a} - J^{-1}(\hat{a}^{r}) f(\hat{a}^{r}) \tag{6-58}$$

In Equation 6-58, r is the iteration level and $J(\hat{a}^r)$ is the Jacobian matrix with entries $J_{im} = \partial f_i / \partial a_m$. Expression (6-58) represents a linear system of equations that is to be solved for the correction vector $\Delta\hat{a}^r$ at each iteration.

The time stepping algorithm proceeds as follows:

Step 1: Assume that at time $t = t^k$, the area $\hat{a}^k$ is known

Step 2: Compute the vector $\hat{e}(\hat{a}^k)$

Step 3: Apply inflow boundary condition at first node $a^{k+1}(1) = a_{\text{inf}}^{k+1}$

Step 4: Initialize iteration loop, set $r = 0$ with $\hat{a}^r = \hat{a}^k$

Step 5: Compute $-f(\hat{a}^r)$ and $J(\hat{a}^r)$

Step 6: Solve $J(\hat{a}^r)\Delta\hat{a}^r = -f(\hat{a}^r)$

Step 7: Compute $\hat{a}^{r+1} = \hat{a}^r + \Delta\hat{a}^r$

Step 8: Has the desired accuracy been reached? i.e. $\|\Delta\hat{a}^r\| / \|\hat{a}^{r+1}\| \le \varepsilon_1$, where $\|x\| = \sum_{j=1}^{NSR+1} |x_i|$ is the chosen norm for any vector $\hat{x}$.

no $\rightarrow$ $r = r + 1$, return to *Step 5*

yes $\rightarrow$ Advance the solution $\hat{a}^{k+1} = \hat{a}^{r+1}$, obtain $\hat{u}^{k+1}$, and then continue with the ground-water model

Step 9: $t^{k+1} = t^k + \Delta t_k$. If $t^{k+1} < t + \Delta\tau_a$ return to *Step 1*, otherwise end kinematic wave propagation phase, go to GWM.

6.4. MODELING STRATEGY

The coupled model contains a multiple time stepping structure. The concept of multiple time steps stems from the fact that surface water flows occur in a matter of hours or days while ground-water phenomena occur in days or months. Even though this

disparity has been recognized by researchers (Yen and Riggins 1991), it is not until recently (Swain and Wexler 1993) that it has been incorporated into integrated modeling. Because of its intrinsic complexity, many modelers preferred the computationally cheaper single time step approach. However, the choice of a single time step is usually to the expense of a shorter simulation time, a poor representation of rapid occurring phenomena or a waste of resources when a small time step is used for slowly varying phenomena.

The disparity of time scales make it necessary to allow the model to run multiple time steps for the surface water portion for each time step of the ground-water portion. The scheme requires that the size of the kinematic wave interval be less or equal to the size of the ground-water time interval. Moreover, the ground-water time step must be an integral multiple of the kinematic wave time step. A third time interval is needed to represent a stress period, whose length is likely to be one month or four months. This allows one to model the seasonal character of processes such as pumping, evapotranspiration and recharge. The scheme requires that the ground-water time interval be less or equal to the stress period. In addition, the length of a stress period must be an integral multiple of the ground-water time interval.

The coupling term is implicitly incorporated in both, the kinematic wave modulus and the ground-water flow modulus. During the multiple kinematic-wave time intervals within a ground-water time interval, the head in the aquifer is held constant and equal to the value obtained in the previous ground-water interval. In order to advance the solution one ground-water time step while preserving the mass conservation constraint, a temporal stream-stage average is calculated and passed on to the ground-water portion to compute leakage. The new aquifer hydraulic head is then used to run the multiple kinematic-wave

intervals within the next ground-water interval. This process continues until the desired simulation time is reached. For a better understanding of the time stepping structure, see Figure 6-6 below.

Figure 6.6: Time stepping structure of the coupled model

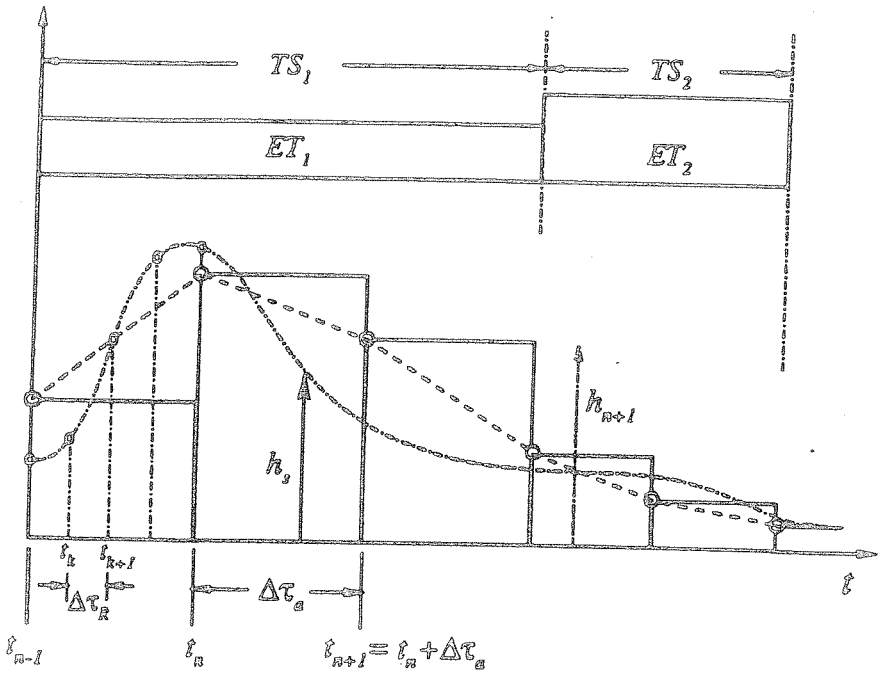

As it was previously mentioned, the surface water phase evolves in time according to the fully implicit Crank-Nicolson-Galerkin (CNG) algorithm, whereas h is held fixed during a complete GWM time step. Then, the GWM is also advanced with the CNG scheme. Therefore the interacting flux for the kinematic wave propagation phase is defined as,

$$\sigma = B_1\left[h(s,t_n) - (h_b(s) + \varepsilon u(s,t))\right] \tag{6-59}$$

and for the ground-water phase as,

$$\sigma = B_I\left[h(s,t_n) - (h_b(s) + \varepsilon\overline{u}(s))\right] \tag{6-60}$$

where $\overline{u}$ is the temporal stream stage average over the entire time interval of the GWM, i.e.

$$\overline{u} = \frac{1}{\Delta\tau_a}\int_{t^n}^{t^n+\Delta\tau_a} u(s,t)\,dt \tag{6-61}$$

which is easily computed once the KWM was propagated one full GWM time step $\Delta\tau_a$.

In order to evaluate the performance of the coupled model developed in this work, a study case similar to the one analyzed by Pinder and Sauer (1971) is now discussed. For a rectangular domain 9,144 m long and 2,438 m wide, the finite element mesh is generated with uniform stepsize $\Delta x = \Delta y = 304.8\ m$ yielding 279 nodes and 480 linear triangular elements. The characteristic values of the parameters are: $L_0 = 100\,m$, $V_0 = 2\ m/s$, $S_0 = 0.001$, $b_0 = 10\ m$, $K_0 = 0.01\ m/s$, $h_0 = 100\ m$, $S_y = 0.1$. A resistance factor $R_f = 5\times10^3\ s$ is used.

The final configuration is obtained by running the model for a sufficiently long time with a steady flow of 41.21 m^3/s ($A = 30\ m^2$) until equilibrium is reached. As it can be seen in Figure 6.7.a and Figure 6.7.b, the river switches from a loosing condition upstream to a gaining condition downstream. This situation is represented not only by the change of the sign in the flux (Figure 6.7.b) but also by the mound and the depression on the water table configuration of Figure 6.8.

Now, the configuration depicted in Figure 6.8 is used as initial condition to route the input hydrograph shown in Figure 6.9 ($a(0,t)$). The time structure of the simulation is as follows,

Table 6.2: Simulation time structures

Stress Period	Duration (sec)	$\Delta\tau_a$ (sec)	$\Delta\tau_R$ (sec)	$\Delta\tau_a/\Delta\tau_R$
1	9000	1500	30	50
2	6600	550	50	11
3	4000	2000	100	20

$\Delta\tau_a$ *is the aquifer modulus time step*

$\Delta\tau_R$ *is the kinematic wave modulus time step*

The model is run 20 ground-water time steps and 472 kinematic wave time steps.

As the wave moves through the channel, interaction with the underlying aquifer takes place and the hydrograph shows bank storage effects. Figure 6.9. depicts the flood hydrograph with leakage and without leakage at a point located 8,229.6 *m* from the upstream boundary, the latter obtained with the method of characteristics (MOC). Figure 6.10 contains three-dimensional views of the water table surface at different times. The graphs follow the passage of the wave through the system and the magnitude of its effect on the aquifer. If the hydrograph rises so does the head in the aquifer, and vice versa. It is worth noting that bank storage effects decrease rapidly with distance from the channel. Another way to visualize the results is by means of a plot of the aquifer head at river nodes and stream stage at the same times as the three-dimensional views previously discussed (Figure 6.11).

Figure 6.7.a: Stream stage $h_s(s)$, area a(s) and aquifer head h(s) at river nodes

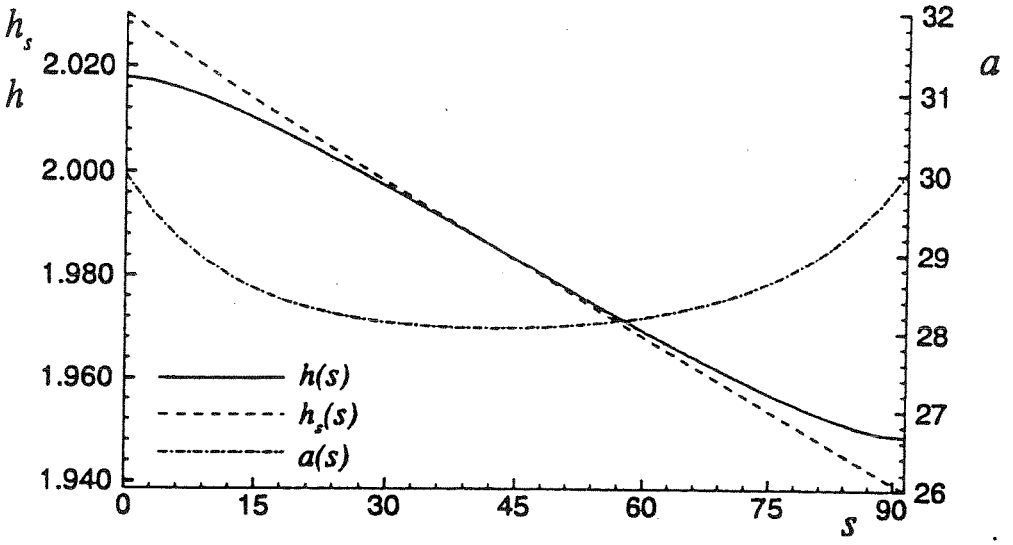

Figure 6.7.b: Steady state river flux

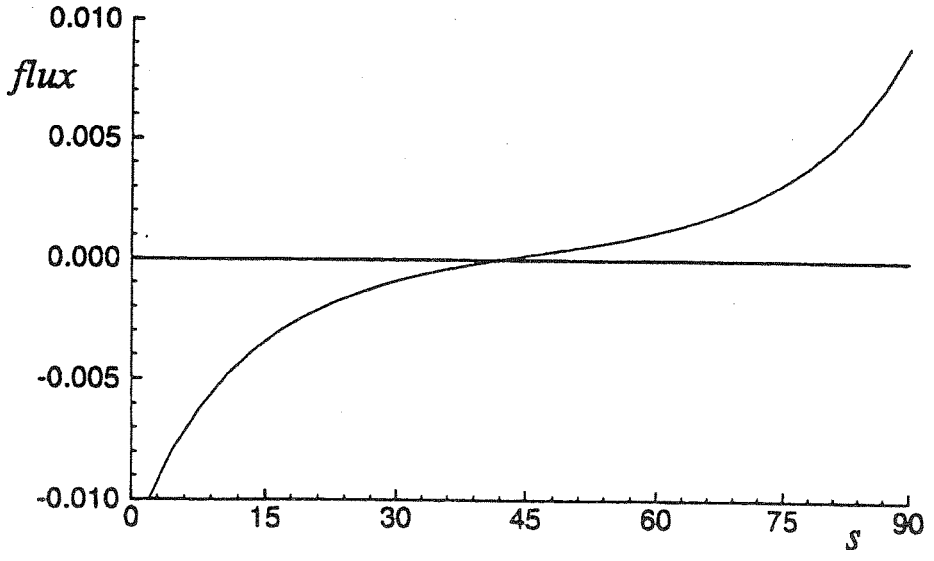

Figure 6.8: Aquifer head initial condition

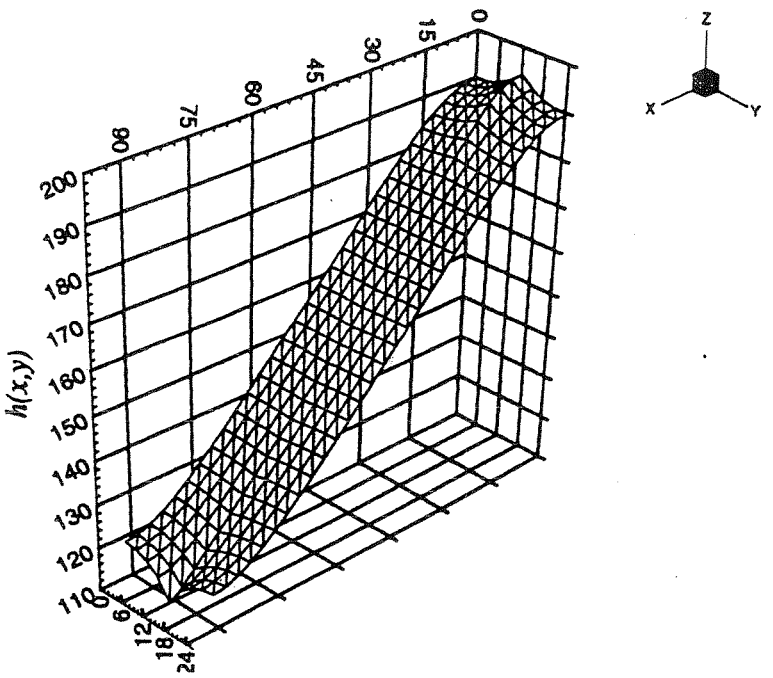

Figure 6.9 - Hydrographs with leakage (dashed line) and without leakage (dash-dot line) Solid line: input hydrograph

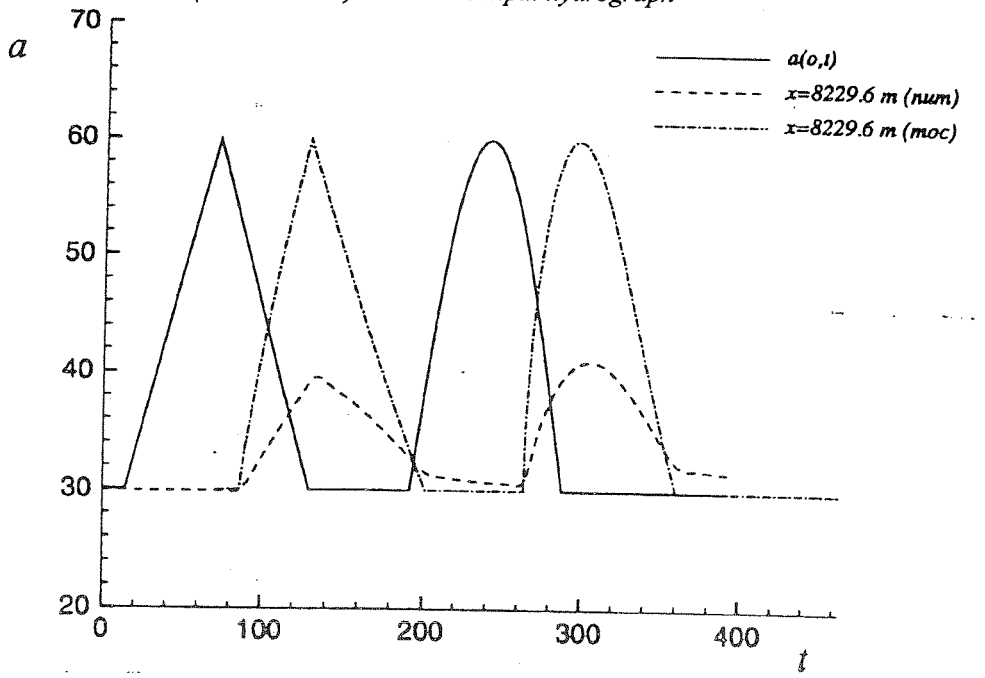

Figure 6.10: Three-dimensional views of the aquifer at different times
a) t=3,000 s; b) t=7,500 s; c) t=12,850 s; d) t=19,600

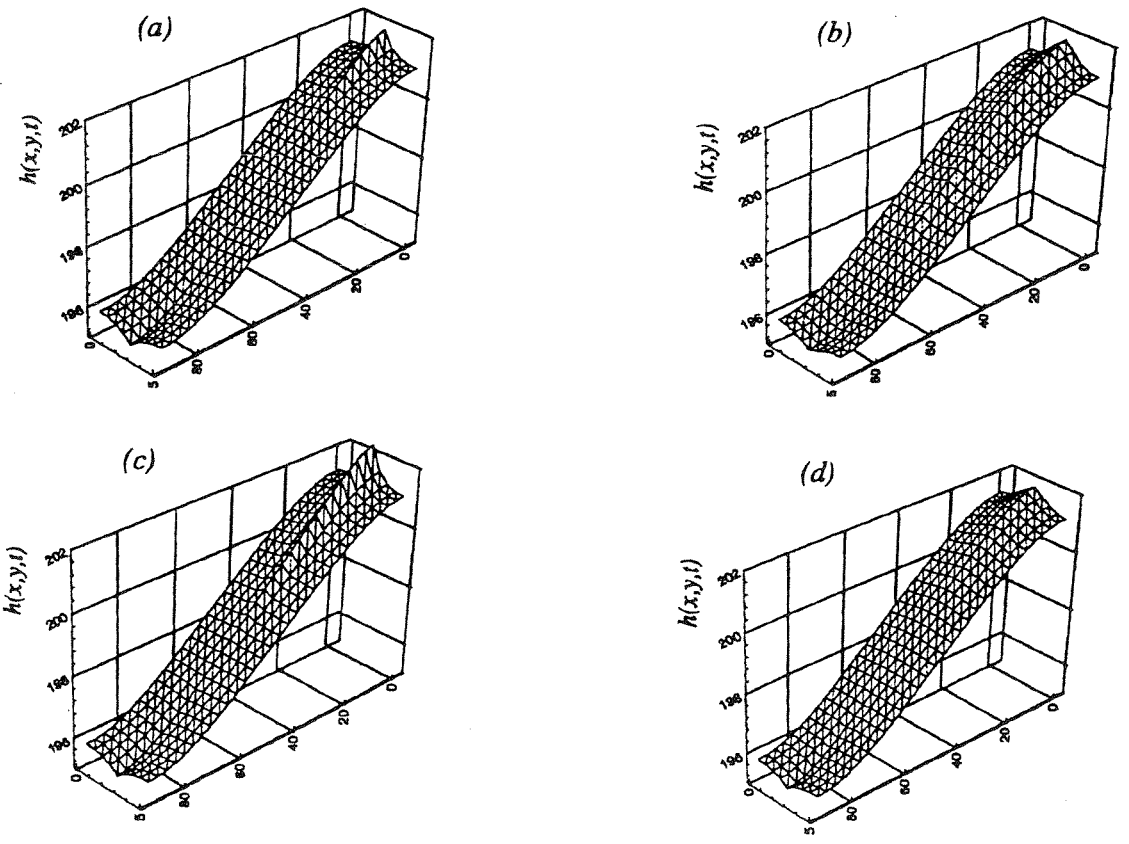

Figure 6.11: Stream stage and aquifer head at river nodes at different times
a) t=3,000 s; b) t=7,500 s; c) t=12,850 s; d) t=19,600

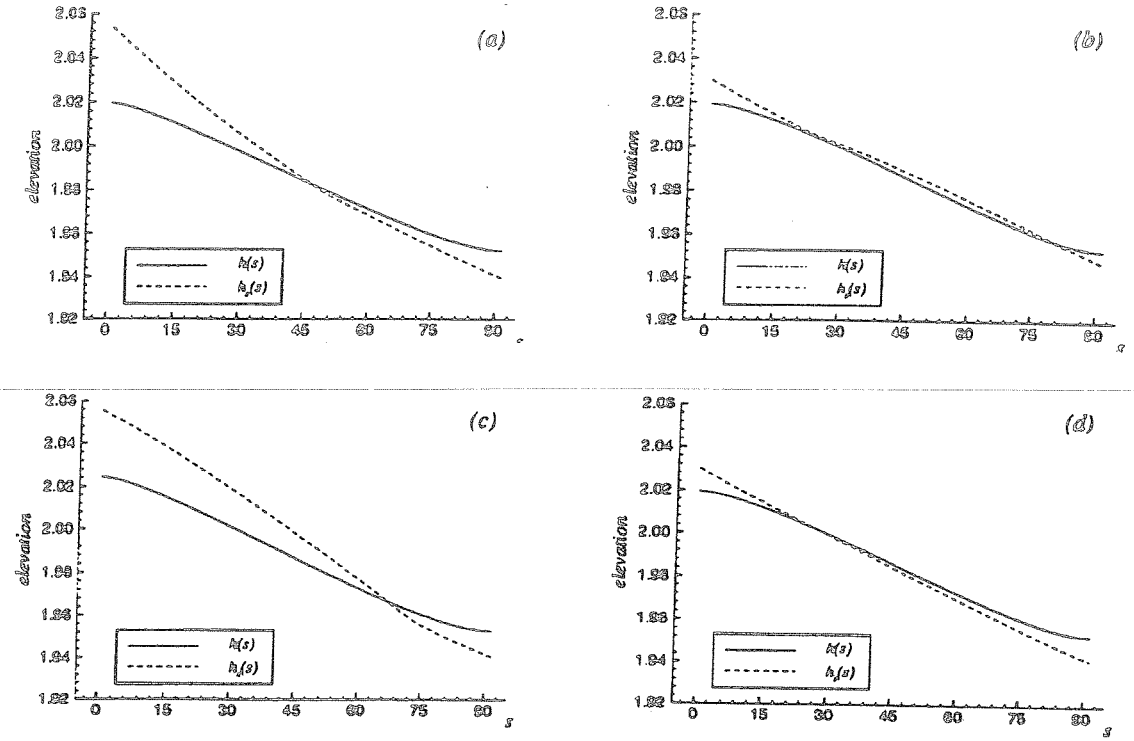

CHAPTER 7

MODEL SIMULATIONS

7.1. INTRODUCTION

The four previous chapters deal with the formulation of the ground-water flow governing equation, the kinematic wave governing equation, the dimensionless form of the governing equations and their discretizations with the finite element method. In this chapter, the implementation of the coupled model in the Lower Bill Williams River Basin is presented. The work includes the conceptualization of the system, the definition of initial conditions, boundary conditions and aquifer properties, and the specification of all data related to the stream characterization. Results from two steady state runs and a 7 year transient simulation are discussed.

7.2. MODEL VALIDATION

The coupled model is not site specific and, within its capabilities and limitations, could be applied to a variety of situations. Reproducing past and present hydrologic conditions and predicting future stresses are all goals within the modeling process. Consequently, it is crucial to assess the degree of confidence that can be placed on model predictions. The confidence level will depend largely on the calibration, sensitivity analysis, and verification of the model. Matching model results to field data is a validation process *per-se*. However, the lack of field data in the study area limits the comparison

between model results and observed values. It follows that any matching can only be established on a qualitative basis.

The validation of the mathematical model mostly relies on a series of study cases specially developed to verify the two main components of the model, i.e. the ground-water flow modulus and the kinematic wave modulus, and its interacting capability as well. All tests are fully documented on Chapter 6 and Appendix A.

7.3. MODEL GRID

The discretization of the physical domain represents an important stage in the finite element modeling process. In discretizing a domain, consideration must be given to an accurate representation of the boundaries, point sources, distributed sources, and material and geometric properties. Therefore, the basic idea is to choose a discretization that will be general enough to model the irregular domain at hand with elements simple enough such that computational error and cost are minimized. Computational cost means here computer time and storage requirements. Judgment should be used in discretizing the area of interest into sufficiently small elements so that steep gradients of the solution can be accurately calculated. Triangular and/or quadrilateral elements can be used for this purpose. In particular, triangles are attractive because there is a natural correspondence between the number and location of nodal points in an element and the number of terms used in the local polynomial approximation (Reddy 1993). Perhaps the most appealing feature of the FEM is the generality and ease with which very irregular meshes and boundary conditions are treated. However, while uniform meshes are simple to generate by simple algorithms, very general meshes are not. A description of the available

techniques for mesh generation is beyond the scope of this work. For an in-depth explanation on the subject the reader may consult the article by Eiseman (1985). In the following paragraphs the mesh generation procedure used in this work is explained.

The approximate boundary of the alluvial aquifer underlying the Bill Williams River and portions of its major tributaries, digitized from topographic maps, defines the boundary of the physical domain. The mesh is carefully refined within the Refuge, is shown in Figure 7.1. Overall it contains 387 nodes and 604 triangular elements. The boundary of the mesh encloses an area of 84.6 km^2. Physical boundaries are followed as closely as possible, preserving an adequate ratio between areas of contiguous elements. On a west-east direction the domain extends for about 55 km. Lateral development of the mesh ranges from about 500 m at the eastern boundary up to about 9,000 m in the Planet Ranch area. This extension represents the flattened saddle area bounded by the Rawhide Mountains to the east and the Little Black mountains to the west. The northern boundary of the alluvial aquifer is located far enough from the stream and the pumping center to minimize boundary effects. The river is discretized into 70 nodes approximately 600 m apart within the Refuge and 900 m apart elsewhere. As shown in Figure 7.1, river nodes follow the actual river path very closely.

7.4. GROUND-WATER MODEL CONCEPTUALIZATION

In this section, the aquifer parameters and characteristic, boundary conditions, evapotranspiration characteristics, and pumping withdrawals are presented and discussed.

Figure 7.1: Finite element grid

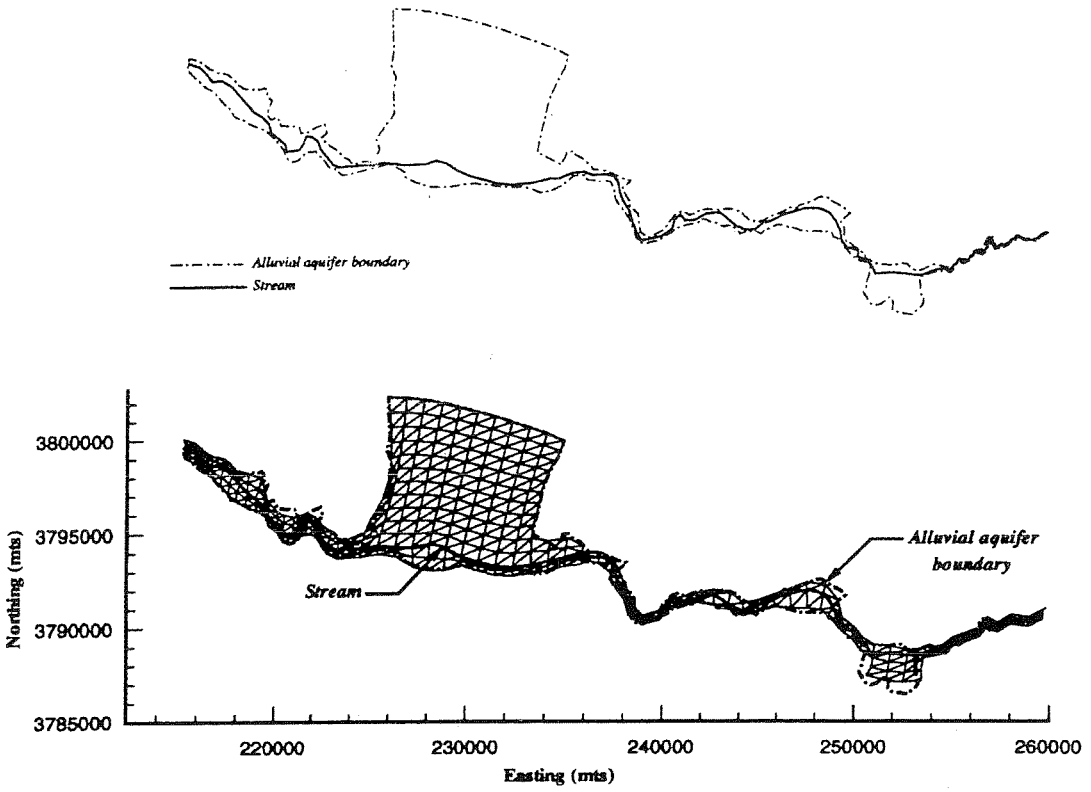

7.4.1. Aquifer characteristics

According to the information presented in Chapter 2, Section 2.4, the aquifer system is modeled as a single unconfined layer whose bottom was reconstructed from scattered thickness information. The lowest point, located in the Planet Ranch area, reaches 100 a.m.s.l., and the highest point, close to the dam site, is at 282 a.m.s.l. Figure 7.2 shows a three-dimensional view of the aquifer bottom along with a contour level projection. A cross-sectional view of the aquifer along river nodes is plotted in Figure 7.3. The elevation of the top of the aquifer was defined by the elevation of the stream bottom,

Figure 7.2: Aquifer bottom

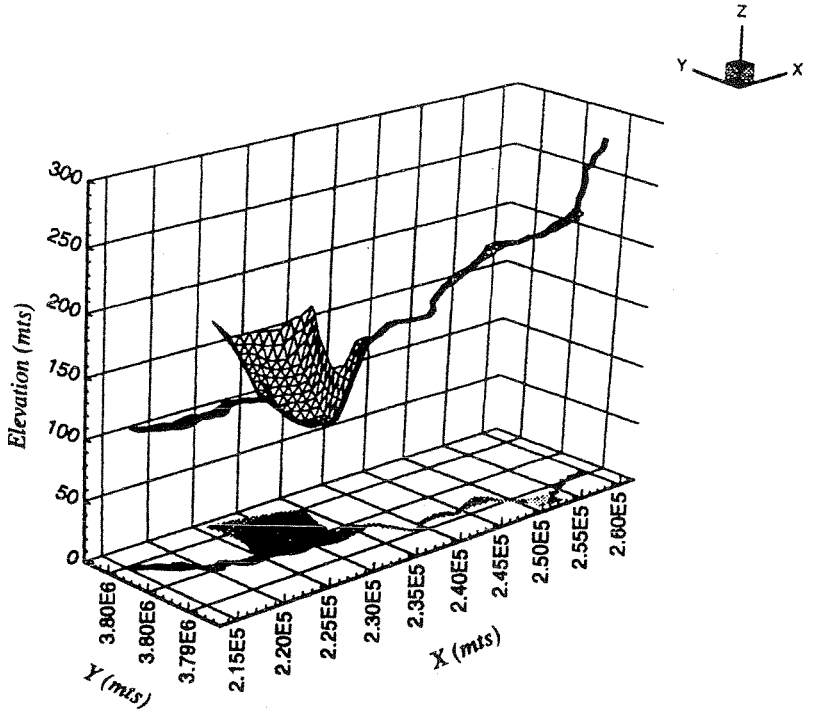

Figure 7.3: Cross-sectional view of the aquifer along river nodes

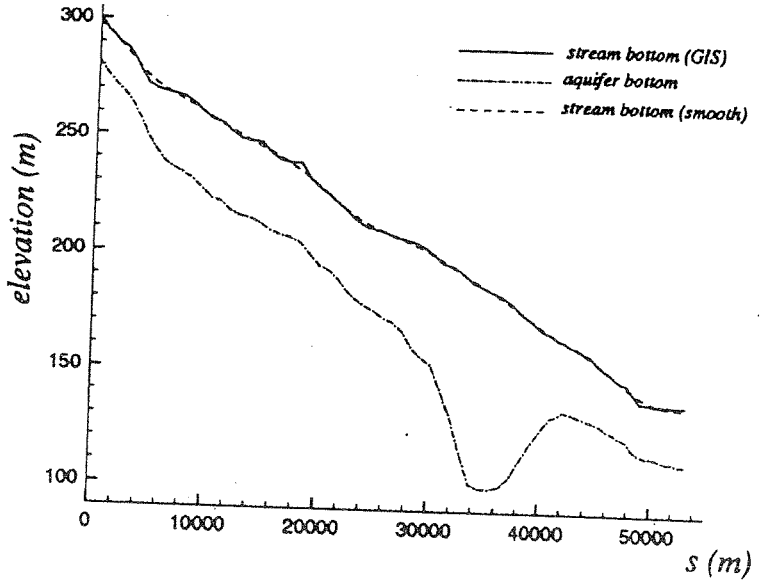

originally interpolated from Digital Elevation Models (DEM) of the study area and later smoothed out for modeling purposes.

Hydraulic conductivity values reported for the area are very disparate and exceedingly high, even for a clean sand aquifer, and greatly differ from aquifer properties estimated in nearby areas and around other alluvial basins throughout Arizona. Therefore, a mean hydraulic conductivity value of 1×10^{-3} *m/s* is adopted. The specific yield S_y of the aquifer is assumed constant and equal to 0.2.

7.4.2. Boundary conditions

Although the geology of the basin is relatively complex, the boundary conditions for the model are fairly simple. For the most part, the aquifer is bounded by fractured hard rock with little or none leakage to a regional aquifer system. The southern boundary of the model is bounded by the Buckskin Mountains and is considered a no-flow boundary. No flow boundaries also occur along the northern boundary of the model, except at the edge of the flattened saddle area. A prescribed flux boundary condition is set at this location whose magnitude is estimated through a solution obtained with a prescribed head boundary. Precipitation occurs in very small amounts, therefore, mountain front recharge plays a minor role in the overall hydrologic budget. Sporadic rainy episode may provide some runoff waters through the main washes to feed the shallow alluvial aquifer. Nevertheless, the amount of recharge is considered "meager" (Rivers West 1990).

Lake Havasu, located at the western boundary, is first represented by a prescribed head condition of 136.5 *m*, which is approximately equal to the normal level operation of

Parker Dam. The outflow at this boundary turns out to be equal to 0.01712 m^3/s and is later used as a prescribed flux at this location. Likewise, the effect of Alamo Reservoir at the eastern end of the model is represented by a constant head of 300 m.

7.4.3. Evapotranspiration

In the model, evapotranspiration losses (ET) are simulated upstream of the Planet Ranch and at the Refuge. In accordance with the aerial coverage of riparian vegetation and the ET estimates given in Chapter 2, three ET zones are defined. Table 7.1 includes the parameters used in the steady state simulations. Following the common practice in ground-water flow modeling, the extinction depth is set equal to 4.57 m in all three areas. Each ET element is assigned an average ground surface elevation computed using the ground surface elevation at the each corner node extracted from digital elevation models of the study area.

Table 7.1: Model parameters for evapotranspiration

ET zone	# of finite elements with ET	ET model area (km^2)	ET rate (m/s)
Upstream of Planet Ranch	40	6.04	9.75×10^{-8}
Wildlife Refuge excluding marsh	72	6.10	1.73×10^{-7}
Marsh	18	1.21	1.02×10^{-7}

For the transient simulation, the ET average annual rates are broken down into monthly rates. Monthly values are determined by multiplying the annual ET rate by the scaling factors presented in Figure 7.4. Those scaling factors are defined as the monthly ET loss

by volume, calculated by means of the Blaney-Criddle method, divided by the annual ET loss by volume.

Figure 7.4: Scaling factors for monthly evapotranspiration rate

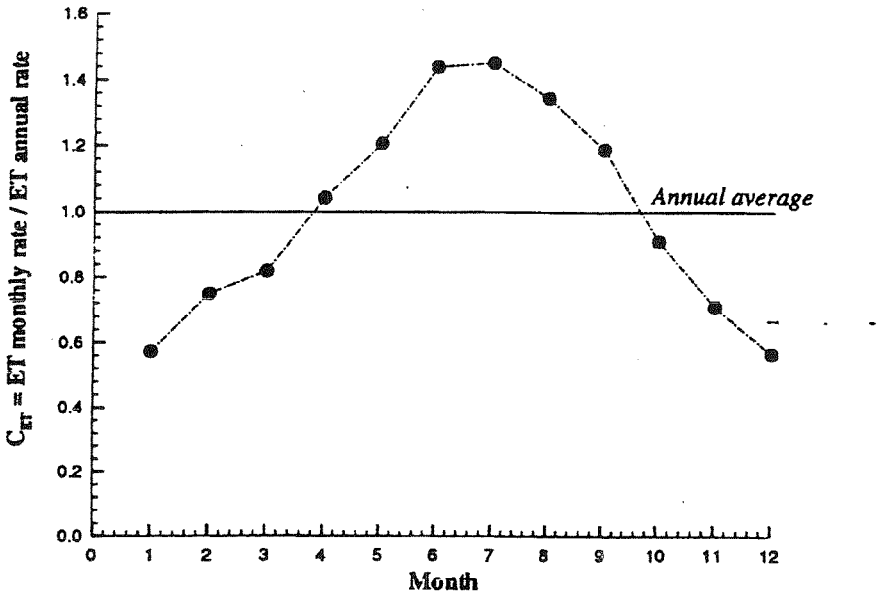

7.4.4. Pumping

Ground-water is extracted at an annual rate of $1.8503\times10^{7}\ m^{3}$ (see Section 2.6.4.2). For the steady state simulation this figure is divided evenly over the 13 commercial wells in operation at the Planet Ranch. Each well yields an average annual pumping rate of 0.0453 m^3/s. Figure 7.5 shows the location of the wells on the finite element grid.

The monthly pumping distribution for transient simulations is determined from the seasonal pumping schedule given by Harshman and Maddock (1993). As it can be seen in Figure 7.6, monthly pumping rates range from a minimum of $4.73\times10^{-4}\ m^{3}/s$ per well during the months of November through February up to a maximum of $9.2\times10^{-2}\ m^{3}/s$ per well during the months of May through August.

Figure 7.5 - Location of wells on the finite element grid

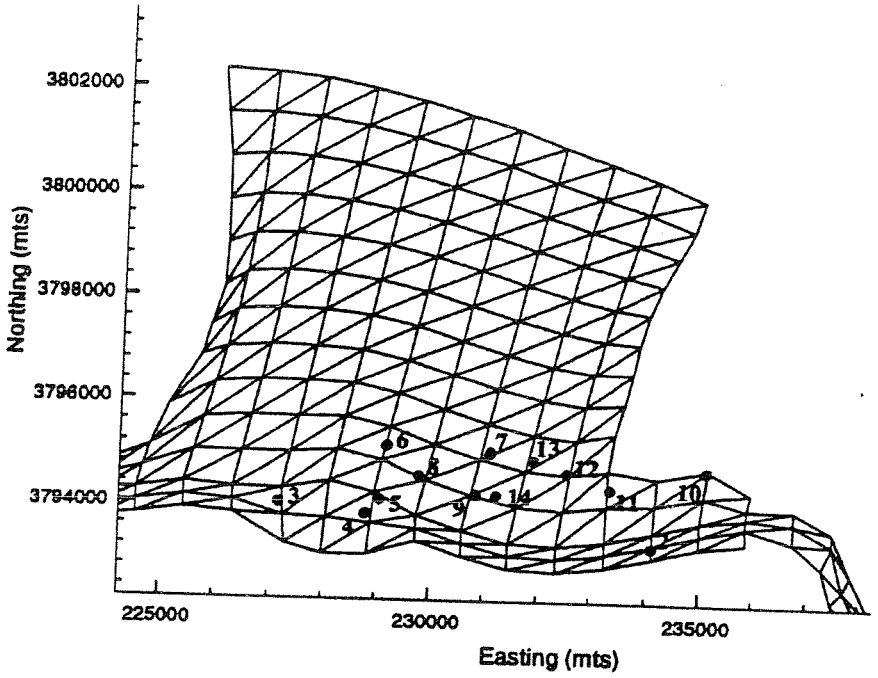

Figure 7.6: Monthly pumping distribution

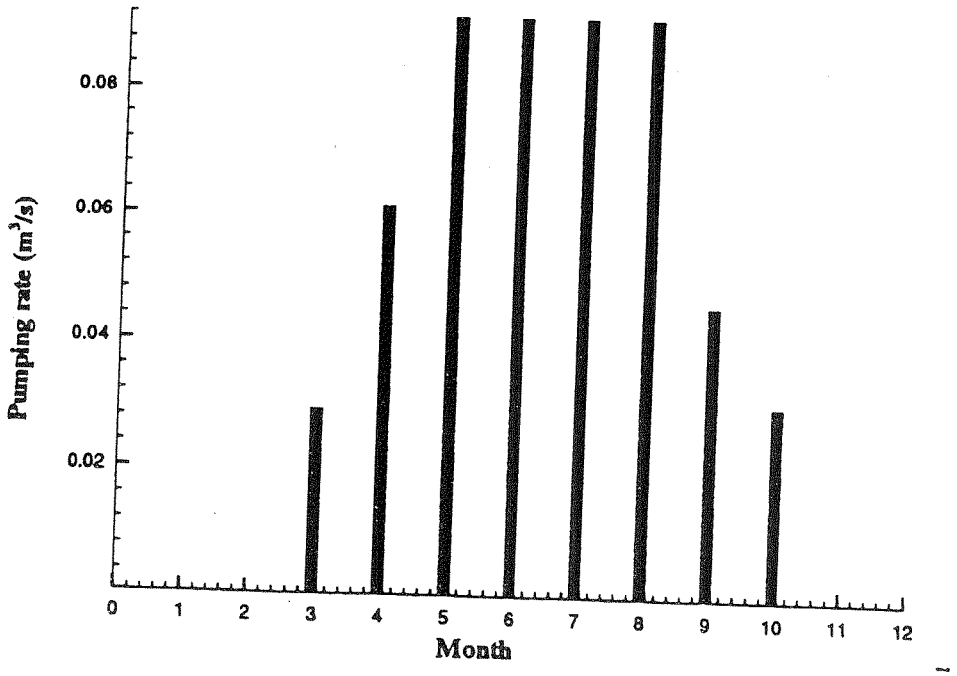

7.5. STREAM CONCEPTUALIZATION

The stream is discretized into 70 nodes and 69 reaches. Parameters such as stream width b, Manning's roughness coefficient n, resistivity factor R_f and streambed slope S are all defined by river reach while streambed elevations are given by river node. The calibrated values for all these parameters appear on Appendix B.

Not much field data exists on localized transects. Downstream from Alamo Dam the Bill Williams river traverses through a narrow channel confined between canyon walls. It also passes through the 9.7 *km* reach at the Planet Ranch where it widens substantially. When the river enters the refuge its width reduces considerably. Consequently, given the information available, the rectangular cross-section assumption seems be appropriate except during periods of high floods when overbanking occurs.

7.6. DEFINITION OF SCALES

According to the dimensional analysis presented in Chapter 5, the model requires the definition of a set of appropriate scales. There is one group of fundamental scales that must be specified by the model user; these are L_0, S_0, S_y, b_0, v_0, K_0 and h_0. Those scales associated with the surface-water system are chosen to represent normal flow conditions while those associated with the ground-water system are such that they typify aquifer conditions. The second group, composed by τ, A_0, n_0, u_0, E^*, R^* and Q^*, is automatically defined once the first group is selected.

The fundamental scales used in this work are $L_0 = 100\ m$, $S_0 = 0.002$, $S_y = 0.2$, $b_0 = 10\ m$, $v_0 = 0.5\ m/s$, $K_0 = 0.02\ m/s$ and $h_0 = 10\ m$. Then, the scales of the second

group are $\tau = 200\ s$, $u_0 = 0.2\ m$, $A_0 = 2\ m^2$, $n_0 = 0.0306$, $R^\circ = 2 \times 10^{-4}\ m/s$, $E^\circ = 2 \times 10^{-4}\ m/s$, $Q^\circ = 1\ m^3/s$.

7.7. SIMULATIONS

Model simulations include two steady-state runs for average annual conditions and one transient run for a period of seven consecutive years running from 1984 to 1990.

The two steady-state simulations differ from each other in that one simulates ground-water development and the other does not. These two runs intend to evaluate the model performance in reproducing the general dynamics of the system. The lack of extensive field data allows only for a qualitative calibration of the model. Nevertheless ground-water level data presented in Section 2.6.3 and field observations by the Fish and Wildlife Service and the author are used during the calibration process. Some of the aspects considered are: 1) the general ground-water flow patterns as reproduced from 1979 data; 2) the disappearance of surface flows in the region of Planet Ranch and in the region immediately upstream of the river confluence with Lake Havasu under fully developed conditions; 3) the magnitude of the streamflows within the Refuge before and after ground-water pumping at Planet Ranch; 4) estimates of the consumptive use by riparian vegetation in the whole study area.

The transient run intends to show the behavior of the hydrologic system when all the processes are modeled using the time scale at which they actually occur. This is accomplished using monthly pumping rates and monthly evapotranspiration rates and daily Alamo Dam releases as the inflow hydrograph to the model.

7.7.1. Steady state simulations

The first steady-state simulation does not incorporate pumping, therefore, results from this run are comparable to the conditions prevailing in the system prior to 1985, when no major ground-water development existed. Boundary conditions for this run include a constant head of 300.13 *m* at the eastern model boundary, a constant flux of 0.01712 m^3/s evenly distributed along the downstream boundary, and a constant head of 198 *m* at the northern boundary limiting the saddle area at the Planet Ranch. A constant streamflow of 1.287 m^3/s representing an average dam release is used for the simulation.

The second steady-state run is aimed at examining the influence of pumping over downstream flows. Total annual pumping is distributed as explained in Section 7.4.4 and the surface inflow is maintained at 1.287 m^3/s. The prescribed head boundary condition to the north is switched to a prescribed flux boundary whose magnitude is determined from the previous steady state run when a prescribed head and no wells are present. The magnitude of that flux calculated by the model is equal to 0.7579 m^3/s.

Figure 7.7 shows the simulated stream discharge and the simulated flux through the streambed along the river for both steady state runs. The model successfully reproduces the streamflow patterns observed in the Bill Williams. When all the wells are in operation downstream flows are reduced from a maximum of 0.5-0.6 m^3/s to a maximum of 0.32-0.36 m^3/s. For this pumping scenario the river dries up before joining Lake Havasu. These results are in agreement with the results previously reported by Harshman and Maddock (1993). The graph showing fluxes through the streambed highlights the fact that most of the stream-aquifer interaction is circumscribed to the Planet Ranch area and a few kilometers downstream, where water resurfaces.

Figure 7.7: Simulated stream discharge and simulated flux through the streambed

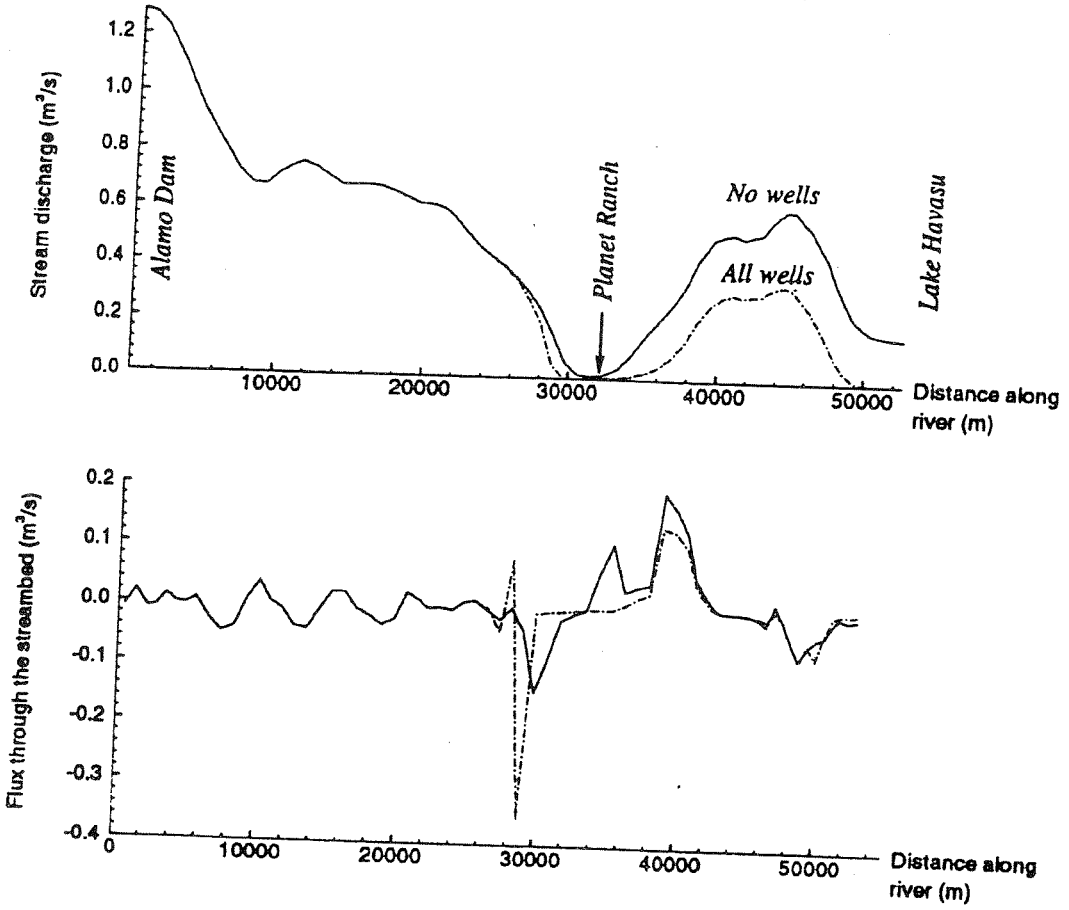

Water-level contours for both scenarios are depicted in Figure 7.8. As it can be seen, the model is able to reproduce the general ground-water flow pattern in the system (see Figure 2.5). Moreover, the distortion of the contour lines pattern in the Planet Ranch area clearly show the starting of pumping.

Most of the hydrologic components in the study area are not quantified. Evapotransporation losses is perhaps the only estimate readily available for comparison purposes. The steady-state run with no pumping yields the volumetric rates shown in Table 7.2 . In this table, QD_1 is the flow at the eastern boundary, QD_2 is the flow at the

Table 7.2: Volumetric rates for steady-state run with no pumping

Inflows (m^3/s)	Outflows (m^3/s)
QD_1=0.06875	ET=0.73962
QD_2=0.75786	QR=0.0659
	QD_3=0.01712

Figure 7.8: Water level contours for both steady-state runs

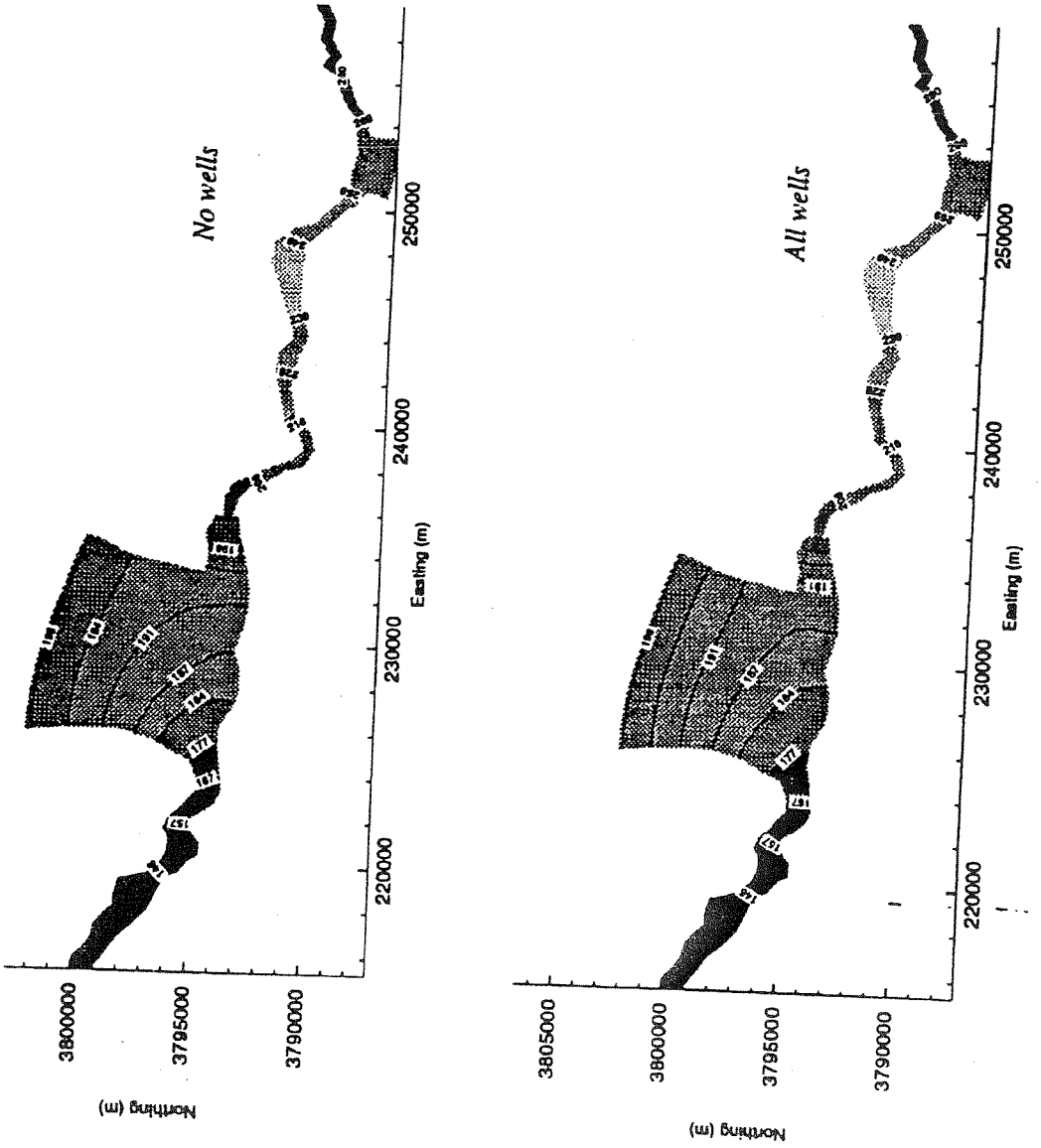

northern boundary, QD_3 is the flow at the western boundary, ET is the evapotranspiration loss and QR is the net flux through the streambed. The mass balance error for this run is 0.5 %. ET calculated by the model differs only by 6 % from the ET estimates presented in Chapter 2. Those estimates are based on an approximate 75 % vegetation density upstream of the Planet Ranch, a value that may overestimate the actual vegetation coverage. If a 65 % density is adopted instead, the agreement between simulated ET and previous estimates is quite good, the difference being close to 1 %.

7.7.2. Transient simulation

The transient simulation runs from December 1983 to December 1990, with ground-water development introduced in January 1985. Results from the steady state run with no pumping are used as initial condition for this run. Stress periods and time steps are chosen according to the guidelines stated in Section 6.4. The ground-water time step is set at 8 hours and the kinematic wave time step is set at 24 minutes. This implies that the model performs 7,761 ground-water flow calculations and 155,220 kinematic wave calculations.

As previously explained, evapotranspiration and pumping are defined on a monthly basis, with the length of each stress periods equal to the actual number of days on each month. The monthly values for ET rates repeat year after year and so do pumping rates. Streamflows at Alamo Station are used as inflows to the model (Figure 7.9). Daily steramflows are linearly interpolated to provide the model with data every 24 minutes, which is the time step of the kinematic wave modulus.

Figure 7.9: Input hydrograph

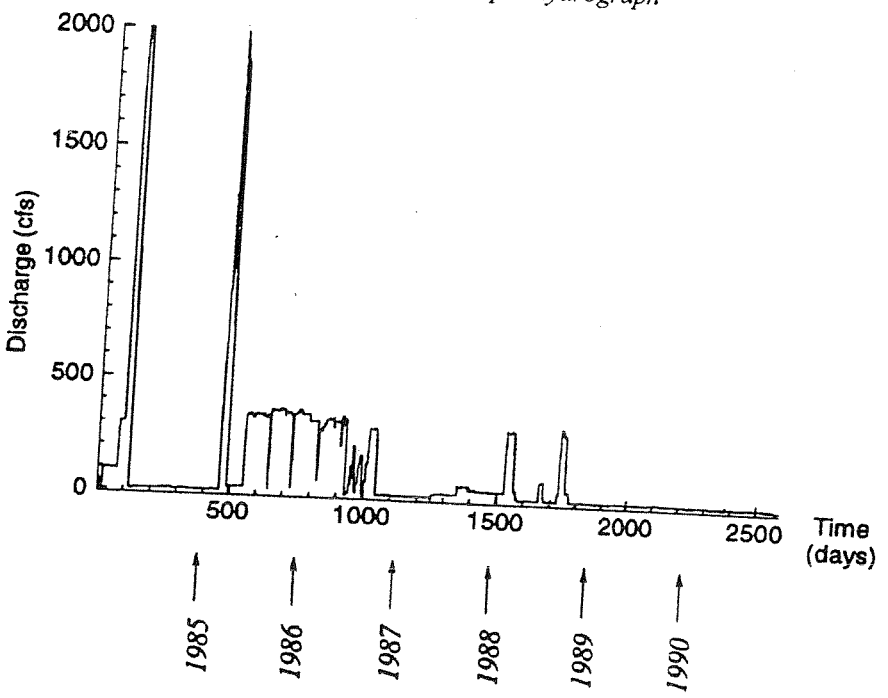

The simulated stream discharge at various times is plotted as a function of the distance along the river (Figure 7.10). The top graph shows those cases where the input to the model is significant, in which case the Planet Ranch area is flooded and its attenuator capacity is overshadowed by the magnitude of the surface flows. The bottom graph shows cases with much smaller surface inflows. The September 1987 curve resembles the results of the second steady state simulation previously discussed. It is interesting to note that after two years of pumping, there are flows all along the Refuge (December 86 curve). In December 1986 and June 1989 the upstream inflow is quite similar, however the June 89 curve shows the effects of four and a half years of continuous pumping with the resulting disappearance of surface flows before the river reaches Lake Havasu. This result would indicate that the most severe impact to the Refuge is caused by the pumping at the Planet Ranch.

Figure 7.10: Simulated discharge along the stream for various times

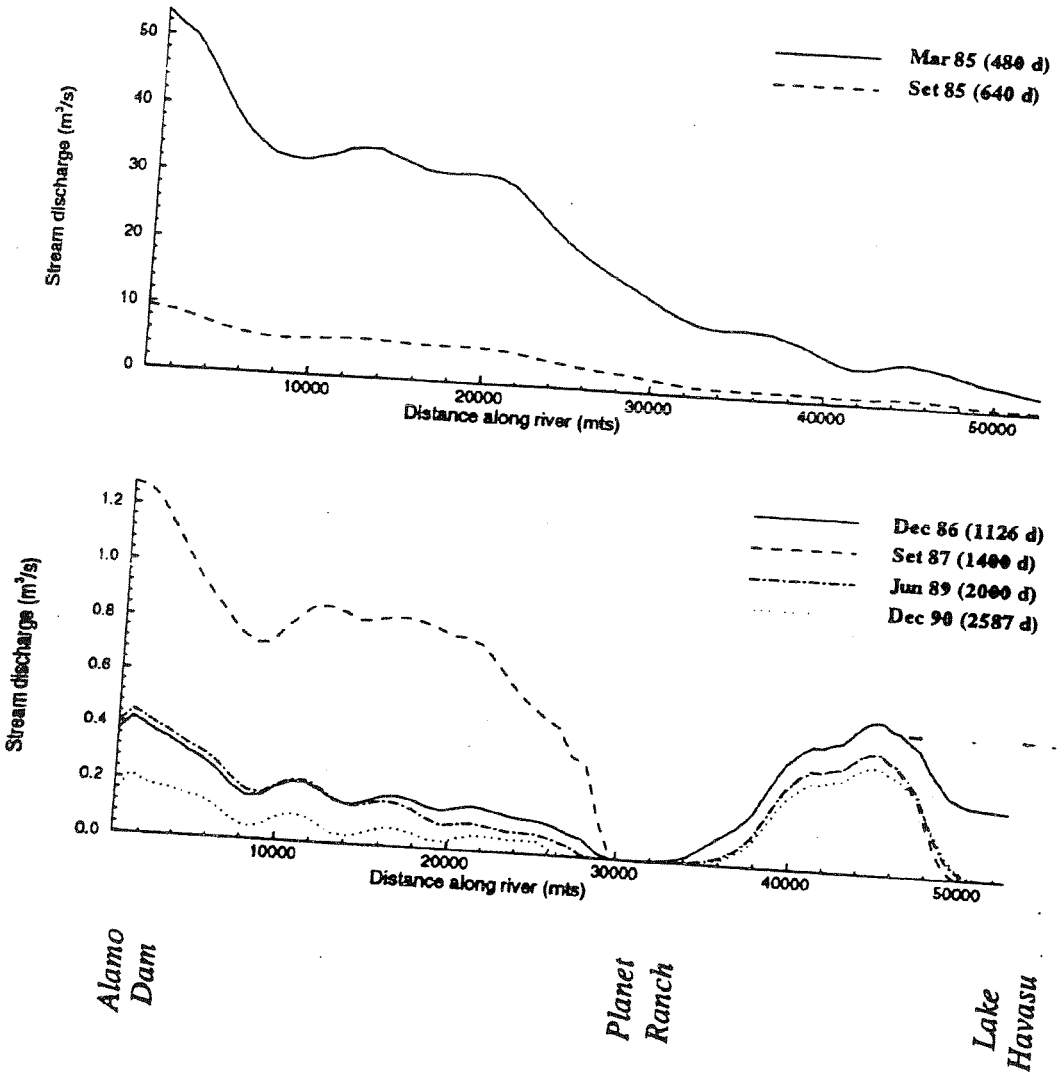

Simulated streamflows are evaluated at three locations (Figure 7.11). The first of them, 4,460 *m* downstream from Alamo Station, lies between canyon walls. The second one, 31,099 *m* downstream from Alamo Station, is situated within the Planet Ranch zone. The third point, 48,283 *m* downstream from Alamo Station, is located within the Refuge. Along the first 4.5 *km*, transmission losses are relatively small to moderate. This is reflected on the top hydrograph, which resembles the input hydrograph (see Figure 7.9). At the second location, the river is dry most of the time flowing sporadically in response

Figure 7.11: Simulated stream discharge at three locations

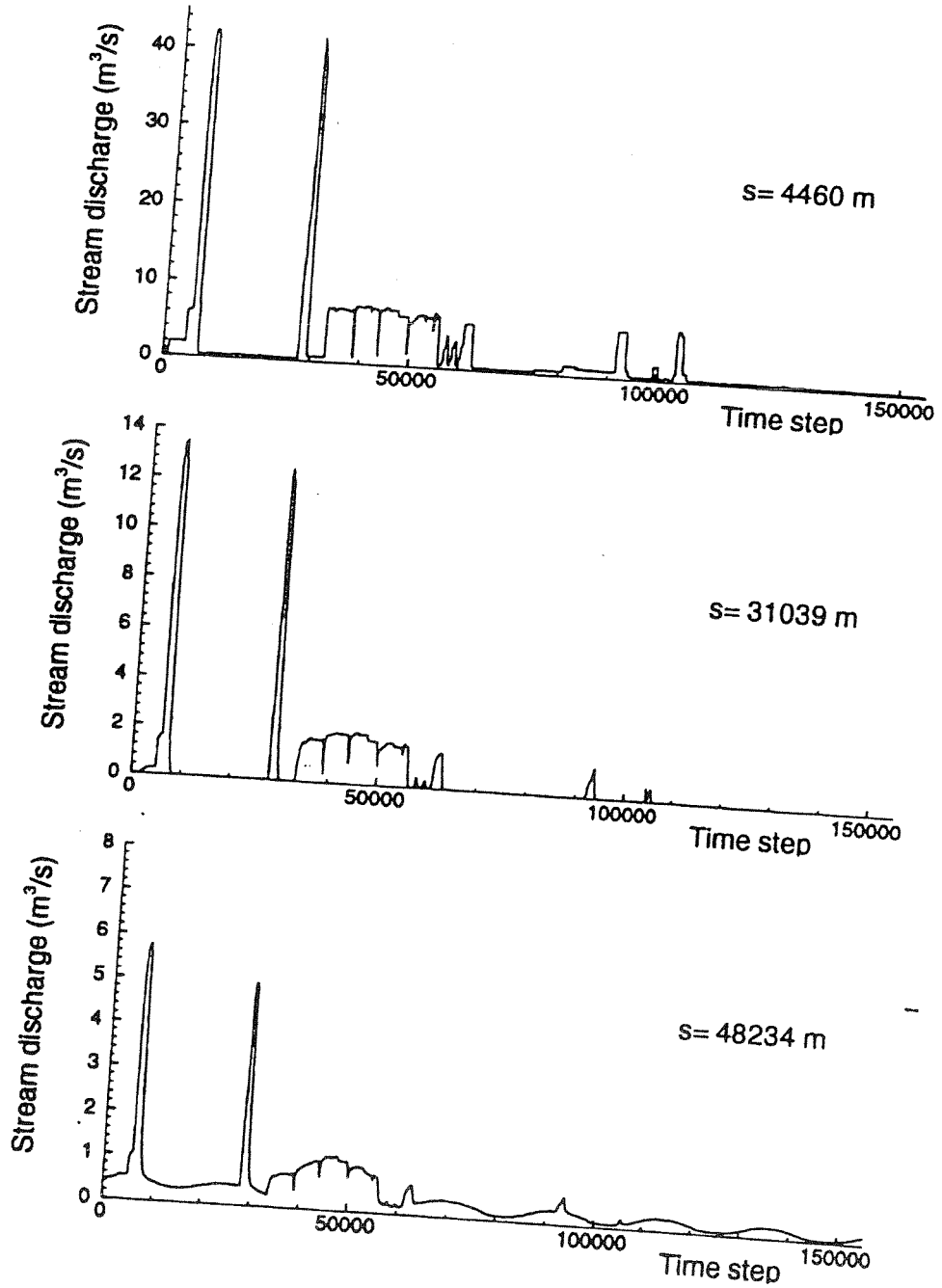

to high upstream streamflows. Within the Refuge an interesting phenomenon occurs. Streamflows clearly respond to the frequency of the input hydrograph, however, they also show an additional frequency imposed by the annual cycle of evapotranspiration and pumping. This effect manifests itself as a smooth modulation on the bottom graph. Also noticeable is the decrease in streamflows at the Refuge as a consequence of the combined effect of pumping and low dam releases since 1989.

If now the stream wetted area is plotted at the three locations, the comments above are still more evident (Figure 7.12). The major difference between the area plot and the discharge plot is that the magnitude of the area peaks is almost preserved at all three locations while the magnitude of the discharge peaks attenuates considerably as the waves travel downstream. Parameters such as stream width, slope and Manning coefficient are all intervening factors in the stream discharge computation whereas the area is the variable convected by the kinematic wave model. The highest peaks are in phase at all three points, however floods of smaller magnitude reach downstream locations within a lag time. The wave celerity is a function of the stream area, and as the area increases, so does the wave celerity.

The analysis of the mass balance components provides an additional mean to interpret model results. Figure 7.13 shows the inflow hydrograph once again, the net flux through the streambed, the change in storage, pumping and evapotranspiration as a function of time. Both, the flux through the streambed and the change in storage reflect the fast effect of streamflows on the ground-water system. In addition to this high frequency response, the storage also exhibits the influence of seasonal processes which impose a modulation over the system. The change in storage is out of phase with the

Figure 7.12 - Simulated wetted area at three locations

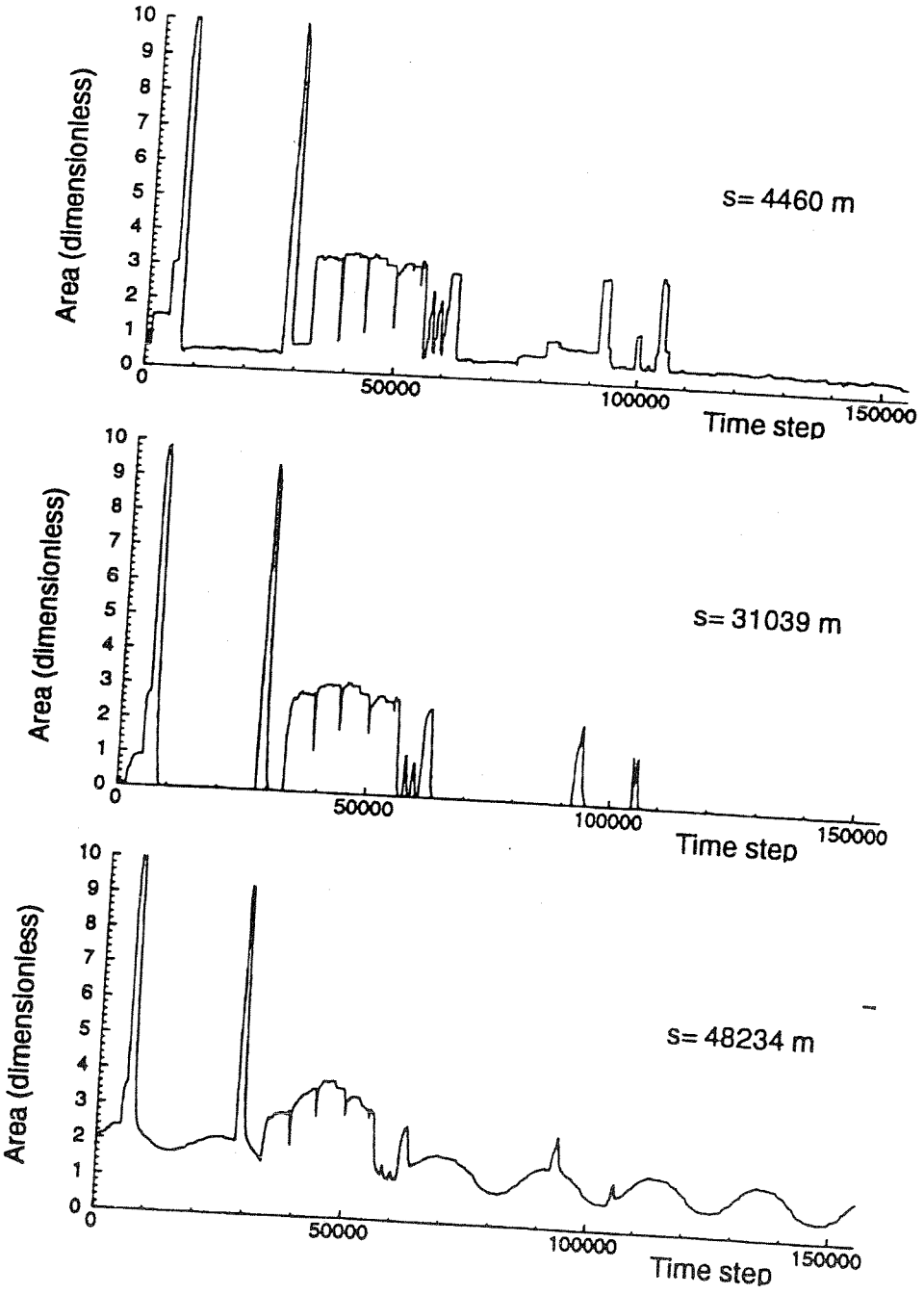

Figure 7.13 - Simulated mass balance components
Top: inflow hydrograph. Middle: net flux through the streambed (solid line) and change in storage DV/DT (dash-dot line). Bottom: Evapotranspiration (solid line) and pumping (dash-dot line)

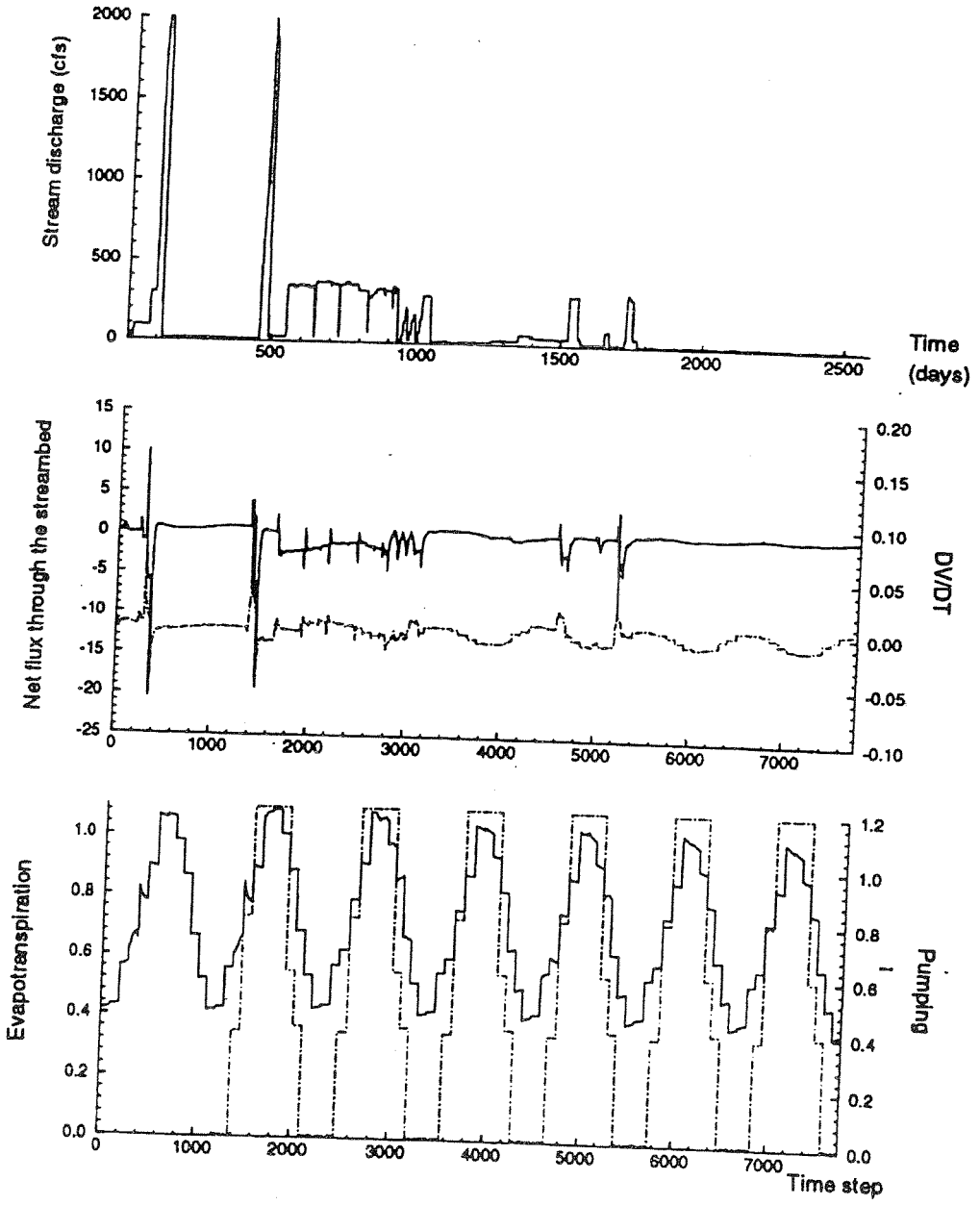

pumping and the evapotranspiration. It attains a negative maximum when natural and cultural stresses in the system are at their maximum, and it recuperates when the losses from the system are at their minimum. The combination of pumping and the occurrence of low dam releases toward the end of the simulation produces a decline in ET losses.

In general, simulated hydraulic heads are overestimated by about 10-12 *m*. In spite of that, the model reproduces water level fluctuations in response to surface flows remarkably well. Figure 7.14 illustrates the drawdown observed at well #2 since pumping started along with simulated drawdown.

Figure 7.14 - Simulated and observed drawdown at well #2

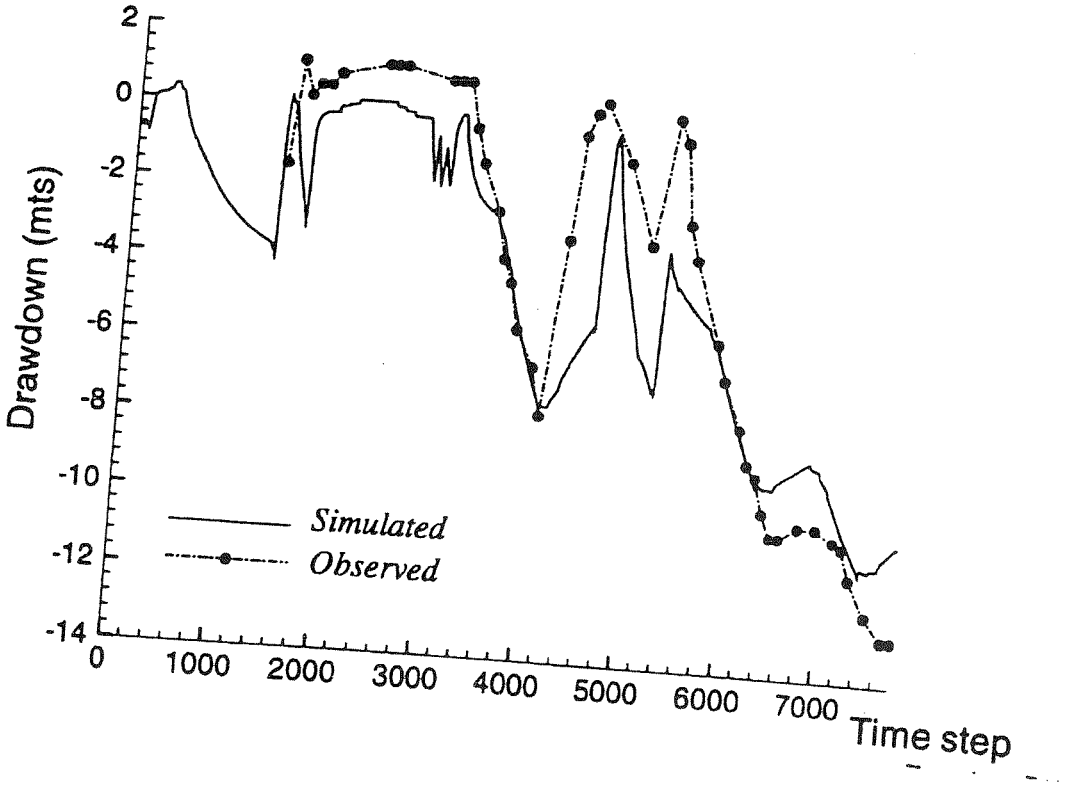

CHAPTER 8

CONCLUSIONS

A fairly complete survey of the different approaches available currently to model the interaction between surface-water and ground-water has been presented. In general, such modeling is accomplished by means of either a single model or a coupled model. However, in situations where highly variable and dynamic seasonal effects are present, it is vital that the stream-aquifer interaction be simulated with an adequate degree of accuracy and a coupled model can provide such degree of adequacy.

The primary goal of the present work was the development of a robust finite element code for the simultaneous representation of ground-water flows and surface-water flows along with their interaction. The coupled model developed is able to capture the observed dynamics of the study area, to maintain full coupling between surface flows and ground-water flows, and to combine the time scales characteristic of both components.

An overview of the main features involved in wave propagation in open channels has been provided. It was shown that the kinematic wave assumption simulates open channel flow in the study site remarkably well, making the coupling between the two flow components extremely easy to implement with the finite element method.

The two components of the integrated model are linked through a coupling term, mathematically represented by an expression analogous to Ohm's law. In employing such a relationship, it has been assumed that all infiltrated water is instantaneously recharged to

the aquifer, that channel loss equals recharge to the aquifer, and that the transfer of water is controlled by saturated flow through low permeability streambed sediments. Nonetheless, this formulation provided satisfactory results for a basin scale application like the Bill Williams case.

The surface-water component was solved using a Petrov-Galerkin formulation while the ground-water component was treated with a Bubnov-Galerkin approximation. In this work, the coupling term is not explicitly included in the ground-water flow equation, but ratter is treated through a boundary flux integral that arises naturally in the weak form of the governing equations. It has been shown that, in order to have a single connected domain for the case of a fully penetrating stream, it is necessary to introduce a branch cut in the domain along the internal boundary that represents the stream.

On the other hand, the characteristic time-scales of the transient response for both systems were clearly established, leading to the definition of three dimensionless parameters, namely, a Peclet number that inherits the disparity between both time scales, a flow number that relates the pumping rate and the streamflow, and a Biot number that relates the conductance at the river-aquifer interface to the aquifer conductance. It was shown that when modeling transient interconnected surface-water and ground-water systems, the rapid unsteady open channel motion can affect the ground-water regime. In this sense, encouraging results have been obtained using multiple time-steps in the simulation process.

Finally, a reasonable qualitative approximation to the sparse field data available in the study site was obtained. During the steady state simulations the model successfully reproduced the streamflow patterns observed in the Bill Williams River and the overall

ground-water flow pattern reconstructed from 1979 data. Results from these runs confirmed the relative impact that pumping at the Planet Ranch had on downstream streamflows. Upstream ground-water development seemed to have more pronounced adverse effects on flows at downstream locations than controlled flows. It was also shown that the system responded to the various frequencies imposed to it. This result could not be obtained with a traditional single model approach.

Even though the model successfully reproduced the general hydrologic characteristics of the study area, a finer calibration and a sensitivity analysis are recommended before any future prediction is undertaken. Particular attention should be given to the resistivity factor, perhaps the parameter that carries the greatest uncertainty and whose influence in computing fluxes through the streambed is undoubtedly important.

It is desirable that the results obtained from this study and a previous modeling effort in the same area be combined to develop a comprehensive monitoring plan to measure water table elevations and surface flows and to survey vegetation species and densities. Continuous recording of surface flows has already started, however ground-water level data and vegetation densities are lacking. Such a plan would serve multiple purposes. On one hand, water table data collected at strategic locations within the Refuge would provide the Fish and Wildlife Service with information on the water table evolution, so critical for vegetation development. On the other hand, such information would contribute to improve the present calibration of the model, which was basically done on a qualitative basis.

CHAPTER 9

REFERENCES

Akan A.O. and B.C. Yen, Mathematical model of shallow water flow over porous media, *J. Hydraul. Div. ASCE*, 107 (HY4), 479-494, 1981.

Anderson T.W., G.W. Freethey and P. Tucci, Geohydrology and water resources of alluvial basins in South-Central Arizona and parts of adjacent states. USGS Professional Paper 1406-B, 1992.

Baker A.J. and M.O. Soliman, On the accuracy and efficiency of a finite element tensor product algorithm for fluid dynamic applications, *Comp. Meth. Appl. Mech. Engrg.*, Vol. 27, 215-237, 1981.

Bear J., *Dynamics of Fluids in Porous Media*. Dover Publications, INC. New York, 1972.

Bear J. and A. Verruijt, *Modeling groundwater flow and pollution*. Theory and Applications of Transport in Porous Media. D. Reidel Publishing Company, 1987.

Besbes M. and G. De Marsily, From infiltration to recharge: use of a parametric transfer function, *J. Hydrol.* 74, 271-293, 1984.

Blaney H.F. and W.D. Criddle, Determining water requirements in irrigated areas from climatological and irrigation data. USDA (SCS) TP-96, p.48, 1950.

Borah D.K., S.N. Prasad and C.V. Alonso, Kinematic wave routing incorporating shock fitting, *Water Resour. Res.*, 16(3), 529-541, 1980.

Bouwer H., Unsaturated flow in ground-water hydraulics, *J.Hydraul. Div. Amer. Soc. Civil. Eng.*, 90 (HY5), 121-144, 1964.

Bouwer H., Rapid field measurement of air entry value and hydraulic conductivity of soil as significant parameters in flow system analysis, *Water Resour. Res.*, 2(4), 729-738, 1966.

Bouwer H., *Groundwater hydrology*, McGraw-Hill, 1978.

Bouwer H., Predicting reduction in water losses from open channels by phreatophyte control, *Water Resour. Res.*, 11(1), 96-101, 1975.

Bureau of Land Management, USDI, Assessment of water resources conditions in support of instream rights, Bill Williams River, Arizona, 1988.

Bureau of Land Management, USDI, Bill Williams Riparian Management Area Plan, 1989.

Carey G.F., Derivative calculation from finite element solutions, *Comput. Meths. Appl. Mech. Engrg.*, 35, 1-14, 1982.

Carey G.F., S.S. Chow and M.K. Seager, Approximate boundary-flux calculations, *Comput. Meths. Appl. Mech. Engrg.*, 50, 107-120, 1985.

Carey G.F. and J.T. Oden, *Finite elements: Fluid Mechanics*. Volume VI. Prentice-Hall, 1986.

Carslaw H.S. and J.C. Jaegger, *Conduction of head in solids*. Oxford University Press, 1959.

Chow V.T., D.R. Maidment and L.W. Mays, *Applied hydrology*. McGraw-Hill Book Company, 1988.

Cooley R.L., A modular finite-element model (MODFE) for areal and axisymetric ground-water flow problems, Part 2: Derivation of finite-element equations and comparisons with analytical solutions. Techniques of Water-Resources Investigations of the U.S. Geological Survey. Book 6. Chapter 4, 1992.

Corp of Engineers, General design for Alamo Reservoir. Colorado River Basin, Bill Williams River, Ariz., Flood Control. Design Memorandum N°3, 1964.

Cox W.B. and D.B. Stephens, Field study of ephemeral stream-aquifer interaction. Proceedings of FOCUS Conference on Surface Water Groundwater Issues (NWWA), 337-358, 1988.

Crebas J.I., B.H. Gilding and J.W. Wessling, Coupling of groundwaer and open-channel flow, *J. Hydrol.*, 72, 307-330, 1984.

Cunningham A.B. and P.J. Sinclair, Application and analysis of a coupled surface and groundwater model, *J. Hydrol.*, 43, 129-148, 1979.

Cunningham B.A., C.J. Anderson and H. Bouwer, Effects of sediment-laden flow on channel bed clogging, *J. Irrig. Drain. ASCE*, Vol. 113, No. 1, 106-118, 1987.

Dahlquist G. and A. Bjorck, *Numerical methods*. Prentice-Hall Inc., 1974.

Davis L.A. and S.P. Neuman, Documentation and user's guide: UNSAT2 - Variably saturated flow model. Final report. Water, Waste & Land, Inc. Consulting Engineers ans Scientists. Fort Collins, co. 1983.

Defina A. and B. Matticchio, A coupled 2D model for interacting surface and groundwater flows, *2nd International Conference on River Flood Hydraulics*, York, England, 1994.

De Marsily G., *Quantitative hydrogeology*. Groundwater hydrology for engineers. Academic Press, Inc., 1986.

Dillon P.J. and J.A. Liggett, An ephemeral stream-aquifer interaction model, *Water Resour. Res.*, 19(3), 621-626, 1983.

Dupont T., Galerkin methods for first-order hyperbolics: an example, *SIAM J. Num. Anal.*, Vol. 10, 890-899, 1973.

Eiseman P.R., Grid generation for fluid mechanics computations, *Ann. Rev. Fluid Mech.*, 17, 487-522, 1985.

EPA. A manual for instructional problems for the USGS Modflow Model. EPA/600/R-93/010, 1993.

Fletcher C.A.J., *Computational techniques for fluid dynamics*, Vol.I. Fundamental and General Techniques, Springer-Verlag, 1989.

Fread D.L., Applicability criteria for kinematic and diffusion routing models. American Water Resources Association National Conference. San Antonio, Texas, 1983.

Freeze R.A., Role of subsurface flow in generating surface runoff. 1. Base flow contributions to channel flow, *Water Resour. Res.*, 8(3), 609-623, 1972.

Freeze R.A. and J.A. Cherry, *Groundwater*. Prentice Hall, 1979.

Freyberg D.L., Modeling the effects of a time-dependent wetted perimeter on infiltration from ephemeral channels, *Water Resour. Res.*, 19(2), 559-566, 1983.

Freyberg D.L., J.W. Reeder, J.B. Franzini and I. Remson, Application of the Green-Ampt model to infiltration under time-dependent surface water depths, *Water Resour. Res.*, 16(3), 517-528, 1980.

Glover K.C., A finite element model for simulating hydraulic interchange of surface and ground water. U.S. Geological Survey, Water Resources Investigations Report 86-4319, 1988.

Glover R.E. and G.G. Balmer, River depletion resulting from pumping a well near a river, *Trans. Amer. Geophys. Union*, 35 (3) 468-470, 1954.

Glover R.E., Transient ground water hydraulics. Dept. Civ. Eng., Colorado State University, Fort Collins, CO. 413 pp., 1974.

Hall F.R. and A.F. Moench, Application of the convolution equation to stream-aquifer relationships, *Water Resour. Res.*, (8)2, 487-493, 1972.

Hantush M.S., Analysis of data from pumping wells near a river, *Jour. Geophys. Res.*, 64 (11), 1921-1932, 1959.

Harshman C.A. and T. Maddock III, The hydrology and riparian restoration of the Bill Williams River near Parker, Arizona. HWR N° 93-040. Department of Hydrology and Water Resources, University of Arizona, 1993.

Henderson F.M., Flood waves in prismatic channels, *J. Hydraul. Div. ASCE*, 89, HY4, 39-67, 1963.

Hill R., Planet Ranch Manager, Personal communication, 1992.

Hughes T.J.R. and A.N. Brooks, A theoretical framework for Petrov-Galerkin methods with discontinuous weighting functions: application to the streamline-upwind procedure, *Finite elements in fluids*, Vol. 4, R.H. Gallagher *et al.*, eds., London, 1982.

Hunt B., An approximation for the bank storage effect, *Water Resour. Res.*, 26(11), 2769-2775, 1990.

Istok J., *Groundwater modeling by the finite element method*. AGU Water Resources Monograph 13, 1989.

Jones M.A. MODXX: A new modular groundwater flow model. M.S. Thesis (unpublished). Department of Hydrology and Water Resources, University of Arizona, 1993.

Katopodes N.D., A dissipative Galerkin scheme for open-channel flow, *J. Hydraul. Eng. ASCE*, Vol. 110, N° 4, 450-466, 1984.

Kraeger-Rovey C., Numerical model of flow in a stream-aquifer system. Hydrology paper No 74, Colorado State University, 1975.

Lacher L., Personnal communication, 1995.

Lane L.J., Transmission losses, National Engineering Handbook. Chapter 19, USDA, SCS, 1980.

Li W., Differential equations of hydraulic transients, dispersion, and groundwater flow. *Mathematical Methods in Water Resources*. Ed. Prentice-Hall, 1972.

Lighthill M.J. and G.B. Whitham, On kinematic waves. I: flood movement in long rivers, *Proceedings of the Royal Society of London*. Vol.229, 281-316, 1955.

Madlock, W.G., The effect of silt-ladden water on infiltration in alluvial channels, Ph.D. Dissertation, Department of Civil Engineering, University of Arizona, Tucson, Arizona, 1965.

McDonald M.G. and A.W. Harbaugh, A modular three-dimensional finite difference ground-water flow model. U.S. Geological Survey Techniques of Water - Resources Investigations Book 6, Chapter A1, 1988.

Mei C.C., The applied dynamics of ocean surface waves. *Advances series on Ocean Engineeering - Volume 1*. World Scientific, 1989.

Menendez A.N. and R. Norscini, Spectrum of shallow water waves: an analysis, *J. Hydraul. Div. A SCE.*, 108 (HY1), 75-94, 1982.

Miles J.C. and K.R. Rushton, A coupled surface water and groundwater catchment model, *J. Hydrol.*, 62, 159-177, 1983.

Miles J.C., Modeling the interaction between aquifer and rivers, *Advances in Water Engineering*. Ed. by T.H.Y. Tebbutt. Elsevier, 1985.

Morel-SeytouxH.J., From infiltration to aquifer recharge: a derivation based on the theory of flow of water in unsaturated soils, *Water Resour. Res.* 20(9), 1230-1240, 1984

Neuman S.P., Theory of flow in unconfined aquifers considering delayed response of the water table, *Water Resour. Res.*, 8, 1031-1045, 1972.

Neuman S.P., Finite element computer programs for flow in saturated-unsaturated porous media. Technion, Haifa, Israel, 87 pp., 1972.

Neuman S.P., Supplementary comments on theory of flow in unconfined aquifers considering delayed gravity response, *Water Resour. Res.*, 9, 1102-1103, 1973b.

Neuman S.P., Delayed drainage in a stream-aquifer system, *J. Irrig. Drain. Div., Proceedings ASCE*, Vol. 107, No. IR4, 407-410, 1982.

Neuman S.P., Class notes for Numerical Methods in Subsurface Hydrology, Department of Hydrology and Water Resources, The University of Arizona, 1992.

Pikul M.F., R.L. Street and I. Remson, A numerical model based on coupled one-dimensional Richards and Boussinesq equations. *Water Resour. Res.*, Vol. 10(2), 1974.

Pinder G.F. and W.G. Gray, *Finite element simulation in surface and subsurface hydrology*. Academic Press, New York, 1977.

Pinder G.F. and S.P. Sauer, Numerical simulation of a flood wave modification due to bank storage effects, *Water Resour. Res.*, 7(1), 63-70, 1971.

Ponce V.M. and D.B. Simons, Shallow wave propagation in open channel flow, *J. Hydraul. Div. ASCE*, 103 (HY12), 1461-1476, 1977.

Ponce V.M., R.M. Li and D.B. Simons, Applicability of kinematic and diffusion models, *J. Hydraul. Div. ASCE*, 104 (HY3), 353-360, 1978.

Ponce V.M., The kinematic wave controversy, *J. Hydraul. Eng.*, Vol. 117, No. 4, 511-525, 1991.

Prudic D.E., Documentation of a computer program to simulate stream-aquifer relations using a modular, finite-difference, ground-water flow model. U.S. Geological Survey Open-File Report 88-729, 1989.

Putman F., K. Mitchell and G. Bushner, Water Resources of the Upper San Pedro Basin, Arizona, Arizona Department of Water Resources, Hydrology Division, 1988.

Raymond W.H. and A. Garder, Selective dumping in a Galerkin method for solving wave problems with variable grids, *Mon. Wea. Rev.*, 104, 1583-1590, 1983.

Reddy J.N., *An introduction to the finite element method*. McGraw-Hill, Inc, 1993.

Reeder J.W., D.L. Freyberg, J.B. Franzini and I. Remson, Infiltration under rapidly varying surface water depths, *Water Resour. Res.*, 16(1), 97-104, 1980.

Reid M.E. and S.J. Dreiss, Modeling the effects of unsaturated, stratified sediments on groundwater recharge from intermittent streams, *J. Hydrol.*, 114, 149-174, 1990.

Rivers West Inc., Water resources assessment: Bill Williams Unit, Havasu National Wildflife Refuge. Document prepared for U.S. Fish and Wildlife Service, Region 2, Albuquerque NM, 89 p., 1990.

Ruchton K.R. and L.M. Tomlinson, Possible mechanisms for leakage between aquifers and rivers, *J. Hydrol.*, 40, 49-65, 1979.

Singh V.P., *Hydrologic systems*, Volume I: Rainfall-Runoff Modeling. Prentice Hall, 1988.

Smith R.E. and J.Y. Parlange, A parameter-efficient hydrologic infiltration model, *Water Resour. Res.*, 14(3),533-538, 1978

Sophocleus M., A. Koussis, J.L. Martin and S.P. Perkins, Evaluation of simplified stream-aquifer depletion models for water rights administration, *Groundwater*, Vol. 33, N° 4, 1995.

Sophocleous M. and S.M. Perkins, Calibrated models as management tools for stream-aquifer systems: the case of Central Kansas, USA. *J. Hydrol.*, 152, 31-56, 1993.

Sophocleous M., M.A. Townsend, L.D. Vogler, T.J. McClain, E.T. Marks and G.R. Coble, Experimental studies in stream-aquifer along the Arkansas River in Central Kansas - field testing and analysis, *J. Hydrol.*, 98, 249-273, 1988.

Spencer J.E. and S.J. Reynolds, Geology and mineral resources of the Buckskin and Rawhide Mountains, West Central Arizona. Arizona Geological Survey, Bulletin 198, 1989.

Streltsova T.D., Method of additional seepage resistances-Theory and application, *J. Hydraul. Div. ASCE*, 100, HY8, 1119-1131, 1974.

Streltsova T.D., Unsteady unconfined flow into a surface reservoir, *J. Hydrol.*, 27, 95-110, 1975.

Swain E.D. and E.J. Wexler, A coupled surface-water and ground-water model. In *Irrigation and drainage*, Proceedings of ASCE Conference. Editor: W.F. Ritter. Honolulu, Hawai, 1991.

Swain E.D. and E.J. Wexler, A coupled surface-water and ground-water flow model for simulation of stream-aquifer interaction. U.S. Geological Survey Open- File Report 92-138, 162 pp., 1993.

Thames F.C., J.F. Thompson, C.W. Mastin and R.L. Walker, Numerical solutions for viscous and potential flow about arbitrary two-dimensional bodies using body-fitted coordinate systems, *J. Comput. Phys.*, 24, 3, 245-273, 1977.

Theis C.V., The effect of a well on the flow of a nearby stream, *Trans. Amer. Geophys. Union*, 734-738, 1941.

Thompson J.F., F.C. Thames and C.W. Mastin, TOMCAT - A code for numerical generation of boundary-fitted curvilinear coordinate systems on field containing any number of arbitrary two-dimensional bodies, *J. Comput. Phys.*, 24, 3, 274-283, 1977.

Trescott P.C., G.F. Pinder and S.P. Larson, Finite-difference model for aquifer simulation in two dimensions with results of numerical experiments. Book 7, Chapter 1. Techniques of Water-Resources Investigations of the U.S. Geological Servey, 1976.

Turner S.F., Water resources of the Planet Ranch on Bill Williams River, Mohave and Yuma Counties, Arizona. Arizona Ranch and Metals Co., 47 pp., 1962.

Vasiliev O.F., System modelling of the interaction between surface and ground waters in problems of hydrology, *Hydrological Sciences Journal*, 32, (3) 297-311, 1987.

Verma R.D. and W. Brutsaert, Unsteady free surface ground water seepage, *J. Hydraul. Div. ASCE*, 97 (HY8), 1213-1229, 1971.

Vionnet L.B., Modeling of ground-water and surface/ground-water interaction for the San Pedro River Basin, Cochise County, Arizona. Master's Thesis. University of Arizona, 1992.

Vionnet L.B. and T. Maddock III, Modeling of ground-water and surface/ground-water interaction for the San Pedro River Basin, Part 1, Mexican border to Farbank, Arizona. HWR No. 92-010. Department of Hydrology and Water Resources, University of Arizona, Tucson, Arizona, 1992.

Wilson L.G., Monitoring the movement of Anfo detonation products in soils and ground water of the Planet Ranch. Final Report on Contract N° 29611, submitted to G.E. Tempo, 1979.

Wilson L.G. and K.J. De Cook, Field observations on changes in the subsurface water regime during influent seepage in the Santa Cruz River, *Water Resour. Res.*, 4(6), 1219-1234, 1968.

Wolcott H.N., H.E. Skibitzke and L.C. Halpenny, Water resources of Bill Williams River Valley near Alamo, Arizona. USGS Water-Supply Paper 1360-D, 1956.

Woolhiser D.A. and J.A. Liggett, Unsteady, one-dimensional flow over a plane - the rising hydrograph, *Water Resour. Res.*, Vol. 3(3), 1967.

Woolhiser D.A., R.E. Smith and D.C. Goodrich, KINEROS, a kinematic runoff and erosion model, documentation and user manual. Agricultural Research Service ARS-77, 1990.

Yen B.C. and R. Riggins, Time scales for surface-subsurface flow modeling. In: Irrigation and drainage, Proceedings of ASCE Conference, Editor: W.F. Ritter. Honolulu, U.S.A., 1991.

Zitta V.L. and J.M. Wiggert, Flood routing in channels with bank storage, *Water Resour. Res.*, 7(5), 1341-1345, 1971

APPENDIX A

MODEL VALIDATION

A.1 INTRODUCTION

A good agreement between numerical results and field data would support the validity and reliability of the model to replicate the overall hydrologic conditions within the study area. Nevertheless, each component of the coupled model is validated separately by performing simple tests for which either an analytical solution is known or some published results are available to compare with. This appendix documents the series of tests performed, first on the ground-water flow model and second, on the kinematic wave model.

A.2. GROUND-WATER MODEL

Six ground-water test problems are presented to demonstrate the applicability of the ground-water flow model.

A.2.1. Homogeneous, anisotropic confined aquifer with two wells and a losing stream

The case of a two-dimensional homogeneous, anisotropic, confined aquifer defined over the domain $0 \le x \le 3000\ m$, $0 \le y \le 1500\ m$ is integrated forward in time until steady

state conditions are achieved. To this aim, an initial condition $h(x,y,0) = 200\ m$ is set. The boundary conditions for the problem are,

$$h(0,y,t) = h(3000,y,t) = 200\,m$$

$$\frac{\partial h(x,0,t)}{\partial y} = \frac{\partial h(x,1500,t)}{\partial y} = 0$$

The values of K_x and K_y are set to 40 *m/day* and 20 *m/day*, respectively. Additional data for the test include the presence of two wells, one located at (1000,670) and pumping at a rate of 1200 m^3 */day* and another one located at (1900,900) pumping at a rate of 2400 m^3 */day*. A river traverses the region from point (2000,0) to point (1000,1500), introducing a constant infiltration rate of 0.24 m^3 */day/*m^3.

A mesh of 64 triangular elements and 45 nodes is used to represent the domain and the river is modeled as an internal line source. Figure A.1 portrays the hydraulic head contour lines, which agree very closely with the results reported by Reddy (1993).

Figure A.1: Hydraulic head contour lines

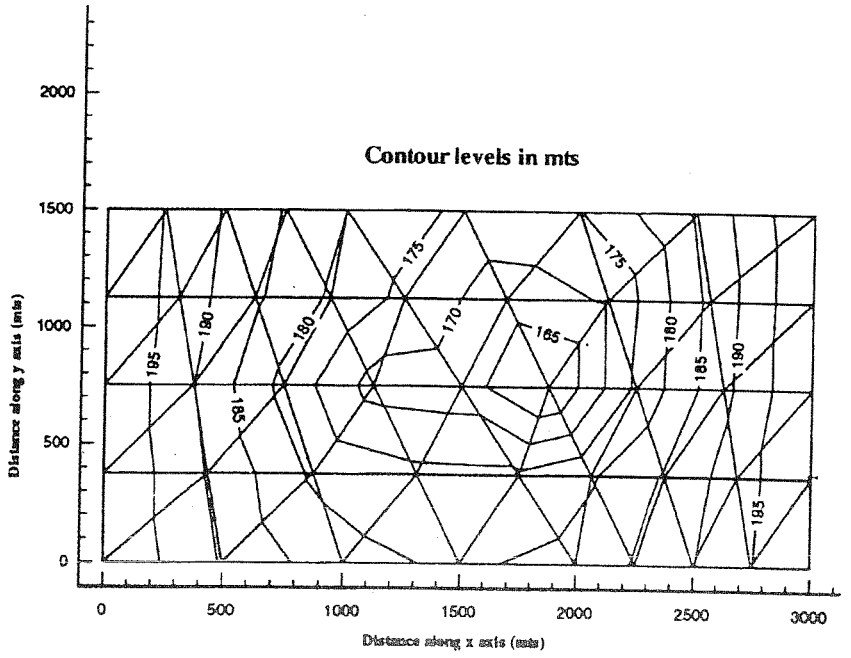

A.2.2. Homogeneous, isotropic confined aquifer over a square domain

This test solves the case of a two-dimensional confined, isotropic and homogeneous aquifer under transient conditions defined over the domain $0 \le x \le 1$, $0 \le y \le 1$ and subject to the following boundary conditions (Neuman 1992),

$$h(1, y, t) = h(x, 1, t)$$

$$\frac{\partial h(0, y, t)}{\partial x} = \frac{\partial h(x, 0, t)}{\partial y} = 0$$

both for $t > 0$, and the initial codition,

$$h(x, y, 0) = 0$$

The exact solution to the problem is given by,

$$h(x, y, t) = 1 - \sum_{n=1}^{\infty} \sum_{m=1}^{\infty} C_{nm} \cos\left[\frac{1}{2}(2n-1)\pi x\right] \cdot \cos\left[\frac{1}{2}(2m-1)\pi y\right] \cdot$$

$$\exp\left\{\frac{-\pi^2 t}{4}\left[(2n-1)^2 + (2m-1)^2\right]\right\} \qquad \text{(A-1)}$$

with

$$C_{nm} = \frac{16(-1)^{n+1}(-1)^{m+1}}{\pi^2 (2n-1)(2m-1)}$$

The rectangular domain is discretized into a 200 triangular element mesh with 121 nodes, with uniform stepsize $\Delta x = \Delta y = 0.1$. The test is run with a $\Delta t = 0.0025$ until the relative change between two successive time steps solution is less than some prescribed tolerance, i.e. the stopping criteria is set as follows,

$$\left\| \frac{h^{n+1} - h^n}{h^{n+1}} \right\| < \varepsilon_{tol} \qquad \text{(A-2)}$$

where $\|h\| \equiv \sum_{j=1}^{N} |h_j(t)|$

Figure A.2 compares numerical results obtained with the Crank-Nicolson-Galerkin time steping algorithm versus the analytical values obtained with (A-1) at point (0.9, 0.1) over the whole simulation interval. The agreement between both computations is quite remarkable.

Figure A.2: Numerical and analytical solution

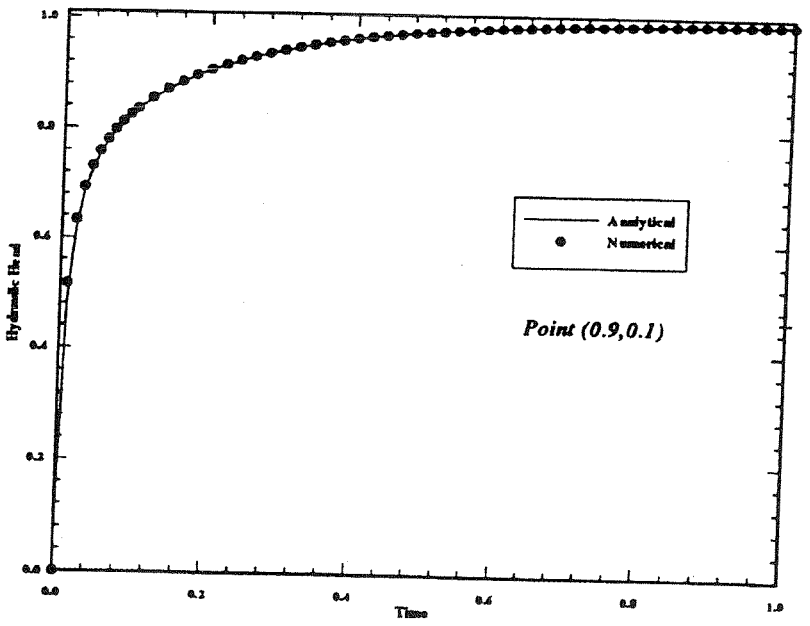

A.2.3. Homogeneous, isotropic aquifer with a uniform recharge - Dirichlet conditions

The third test deals with a one-dimensional homogeneous, isotropic aquifer under steady state conditions which receives a uniform recharge from the top. Both cases, confined and unconfined are analyzed. Assuming boundary conditions of the Dirichlet type at both ends of the domain of length L, the exact solution for the problem takes the form (Bear 1972),

$$h = h_0 + (h_L - h_0)\frac{x}{L} + \frac{R}{2T}(L - x)x \qquad \text{(A-3)}$$

for the linear case, and

$$h^2 = h_0^2 + (h_L^2 - h_0^2)\frac{x}{L} + \frac{R}{K}(L - x)x \qquad \text{(A-4)}$$

for the non-linear case. In the above expressions, , and is an uniform recharge rate. The following set of parameters is used in the simulation,

$h_0 = 1.0$ $T = 1.0$ $h_L = 0.5$ $K = 1.0$ $L = 8$ $R = 0.5$

Figures A.3*a*. and A.3*b*. depict the results obtained. The graphs show an excellent agreement between numerical and analytical results.

Figure A.3.a: Linear case

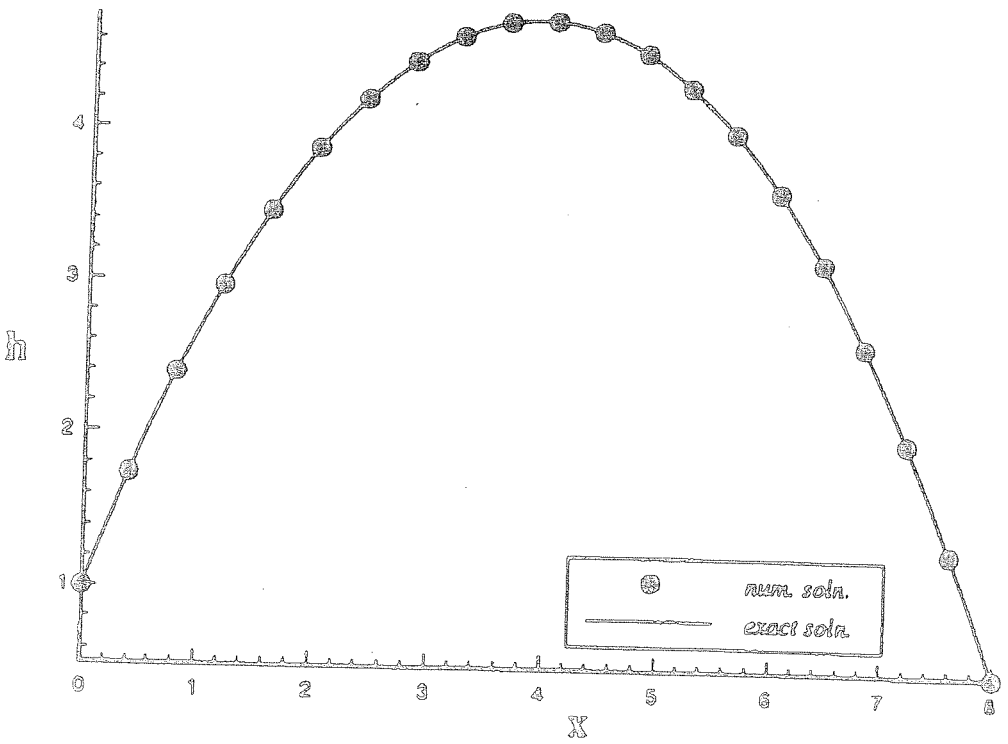

Figure A.3.b: Non-linear case

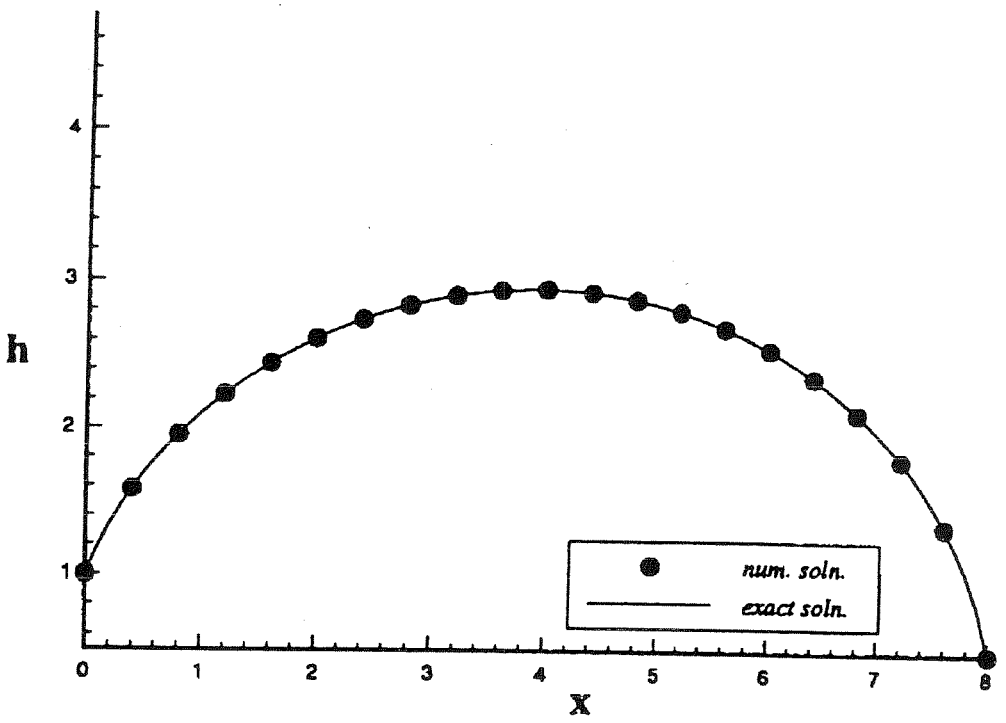

A.2.4. Stream-aquifer interaction with a constant stage stream

The fourth test maintains the characteristics of the third one except the boundary conditions. In this case, a no flux boundary condition is set at $x = L$ and a mixed boundary condition of the type $\partial h(0)/\partial x = \beta(h - h_s)$ is set at $x = 0$, with $h_s = 2$. The exact solution for the linear and non-linear case are,

$$h = h_s + \frac{RL}{T}\left(\frac{1}{\beta} + x - \frac{x^2}{2L}\right) \qquad \text{(A-5)}$$

and

$$h^2 = h_0^2 - \frac{Rx^2}{K} + \frac{2RL}{K}x \qquad \text{(A-6)}$$

with

$$h_0 = \frac{h_s}{2} + \sqrt{\left(\frac{h_s}{2}\right)^2 + \frac{RL}{\beta K}}$$

respectively. The values T, R, K and L are as in the previous case, with $\beta = 1$. A comparison between numerical results and exact solutions can be seen in Figure A.4.*a* and Figure A.4.*b*.

Figure A.4.a: Non-linear case

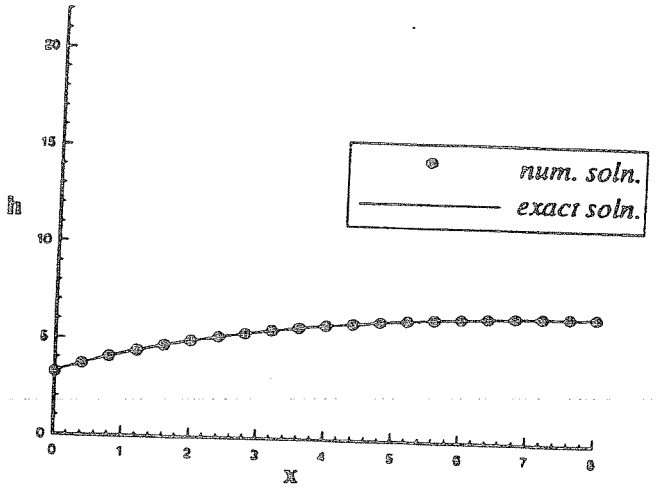

Figure A.4.b: Linear case

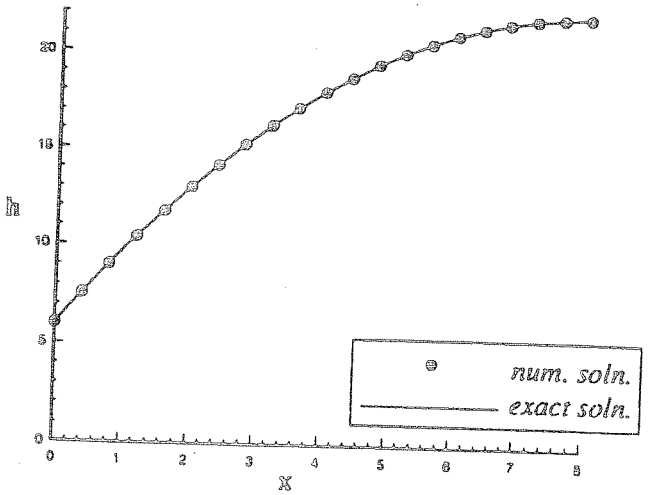

A.2.5. Homogeneous, isotropic, steady state, confined aquifer with a line source

A line source of constant intensity q is introduced in the problem set up of test A.1.4. for the linear case. The source is located at a distance x_0 from the left boundary of the domain. The exact solution is given by

$$h = h_s + \frac{RL - q}{\beta T} + \frac{RL}{T}x - \frac{q}{T}x - \frac{R}{2T}x^2 \qquad x \le x_0 \qquad \text{(A-7)}$$

$$h = h_s + \frac{RL - q}{\beta T} + \frac{RL}{T}x - \frac{q}{T}x_0 - \frac{R}{2T}x^2 \qquad x > x_0 \qquad \text{(A-8)}$$

The values of the parameters for this test are identical to those used in tests A.1.3 and A.1.4, with the addition of $q = 3$, located at $x_0 = 2.8$. Results from numerical and analytical computations are depicted in Figure A.5.

Figure A.5: Numerical and analytical solutions

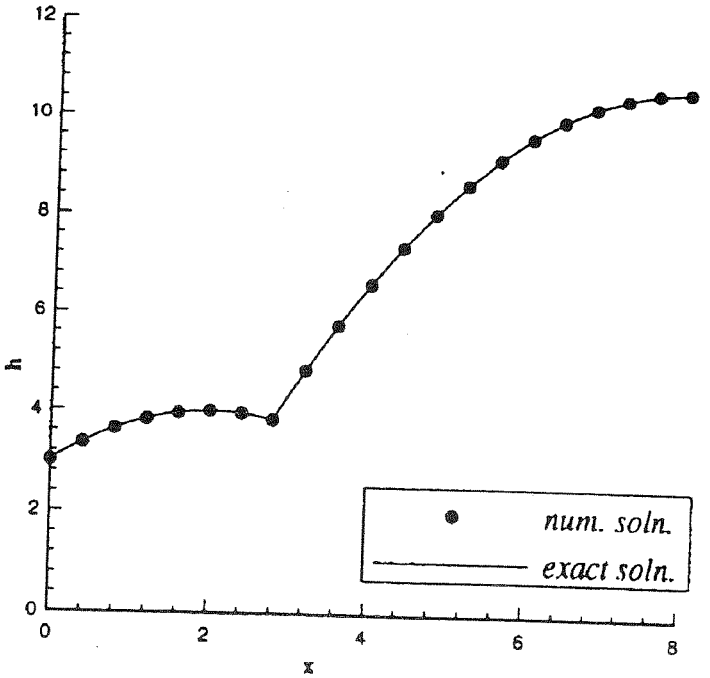

A.2.6. Isotropic, homogeneous, unconfined aquifer with uniform recharge

The test here described is conducted to validate the transient response of the model for the non-linear case (Li 1972, Bear 1972). A weakly non-linear equation of the form,

$$\frac{\partial^2 h^2}{\partial x^2} + \frac{2R}{K} = \frac{1}{T}\frac{\partial h^2}{\partial t} \qquad \text{(A-9)}$$

subject to boundary conditions,

$$\frac{\partial h(0,t)}{\partial t} = 0, \qquad h(L,t) = h_0$$

and initial condition $h(x,0) = h_0$ is solved over the domain $[0,L]$. The recharge is equal to R for $0 \le x \le L_R$ and equal to zero for $L_R \le x \le L$. Parameters for the simulations include $L = 20$, $L_R = 5$, $K = 1$ and $R = 0.02$. Upon applying the Laplace Transform method to equation (A-9), the approximate analytical solution is,

$$h(x,t) = d^2 + \frac{RTt}{K}\left[\frac{1}{2} + \left(1 + \frac{a^2}{2t}\right)\operatorname{erfc}\left(\frac{a}{2\sqrt{t}}\right) - \frac{a}{\sqrt{\pi t}}\exp\left(\frac{-a^2}{4t}\right)\right.$$

$$\left. - \left(1 + \frac{b^2}{2t}\right)\operatorname{erfc}\left(\frac{b}{2\sqrt{t}}\right) - \frac{b}{\sqrt{\pi t}}\exp\left(\frac{-b^2}{4t}\right)\right] \quad \text{for } 0 \le x \le L_R \qquad \text{(A-10)}$$

and

$$h(x,t) = d^2 + \frac{RTt}{K}\left[\frac{1}{2} + \left(1 + \frac{c^2}{2t}\right)\operatorname{erfc}\left(\frac{c}{2\sqrt{t}}\right) - \frac{c}{\sqrt{\pi t}}\exp\left(\frac{-c^2}{4t}\right)\right.$$

$$\left. - \left(1 + \frac{b^2}{2t}\right)\operatorname{erfc}\left(\frac{b}{2\sqrt{t}}\right) - \frac{b}{\sqrt{\pi t}}\exp\left(\frac{-b^2}{4t}\right)\right] \quad \text{for } L_R \le x \le \infty \qquad \text{(A-11)}$$

where $a = L_R - x/\sqrt{t}$, $b = L_R + x/\sqrt{t}$ and $x = x - L_R/\sqrt{t}$.

Expressions A-10 and A-11 are valid depending on how well the following two assumptions are met: 1) R is small compared to T; 2) h should not depart greatly from h_0, otherwise the hypothesis of T constant ceases to hold.

Figures A.6 and A.7 illustrate the results obtained for $T = 1$ and $T = 1.1$, respectively, for $t = 5$, 10, and 15. It can be noticed that, as h departs from $h_0 = 1$, the discrepancy between numerical and analytical values starts to increase (Figure A.6). A higher value of T (Figure A.7) causes the numerical solution to improve for larger t. The values of T obtained under such conditions are listed in Table A.1. Identical results are reproduced for $\Delta t = 1$ and $\Delta t = 0.5$.

Table A.1: Table of higher t values obtained for larger T

t	T
5	1.025
10	1.050
15	1.075

Figure A.6: Numerical results for T=1

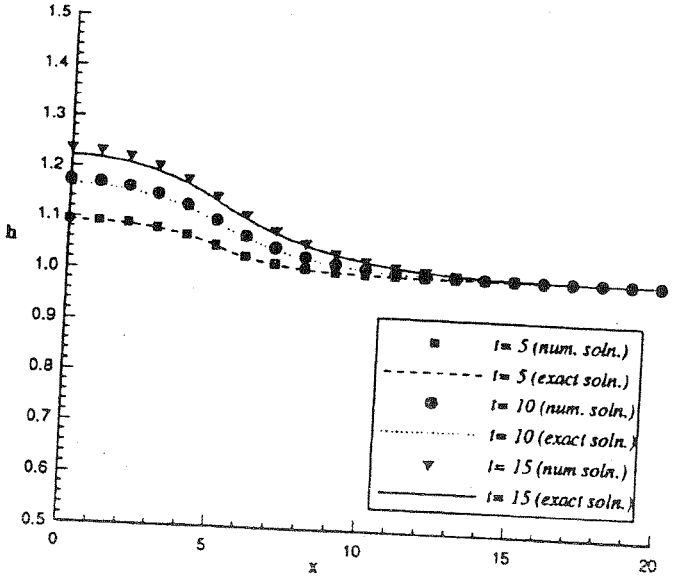

Figure A.7: Numerical results for T=1.1

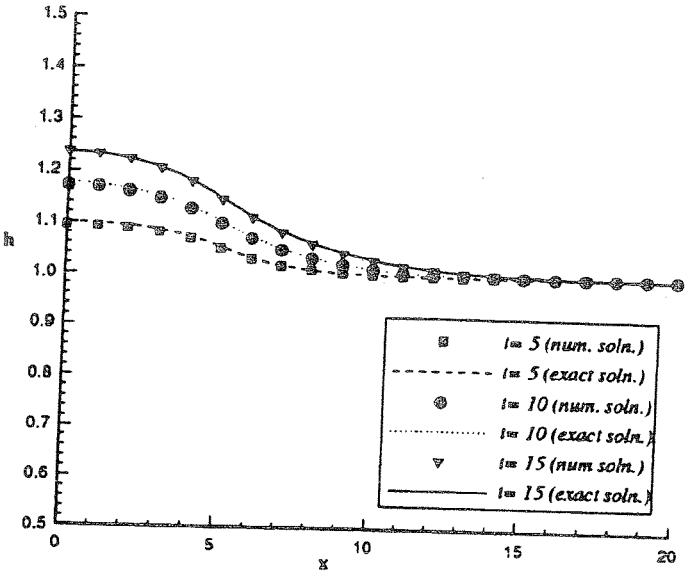

A.3. KINEMATIC WAVE MODEL

Two surface-water test problems are presented to demonstrate the applicability of the surface-water flow model.

A.3.1. Forced nonlinear convection

In this test, the following nonlinear problem is solved (Raymond and Garder 1976),

$$\frac{\partial u}{\partial t} + u\frac{\partial u}{\partial x} = g(x,t) \qquad \text{for } 0 < x < l,\ t > 0 \qquad \text{(A-12)}$$

subject to $u(x,0) = f(x)$, $u(0,t) = f(-t)$

where $f(x) = \exp\left[-(x-10)^4/4\right]$

The solution of Equation (A-12) is $u(x,t) = f(x-t)$, provided that,

$$g(x,t) = \frac{1}{2}(x-t-10)f(x-t)[x-f(x-t)]$$

The system of nonlinear ordinary differential equations derived from the application of the method of weighted residuals and the Petrov-Galerkin method to equation A-12 is solved by the Crank Nicolson method utilizing a Newton iterative technique. The nonlinear Gaussian wave, initially centered at $x = 10$, is allowed to propagate through a computational domain 50 units long, with $\Delta x = 0.5$, and $\Delta t = 0.1$. All the scales for the problem are set equal to one. Numerical results along with the exact solution and the initial condition are plotted in Figure A.8 as time goes on. Numerical calculations match the exact solution very closely, showing neither numerical dispersion nor numerical attenuation. In addition, the result of the computations show no undesired reflections as the wave leaves the computational domain, where the natural boundary condition $\partial u(x = 50)/\partial x$ is imposed.

Figure A.8: Numerical and analytical results at various times (Dashed line is numerical solution, solid line is exact solution)

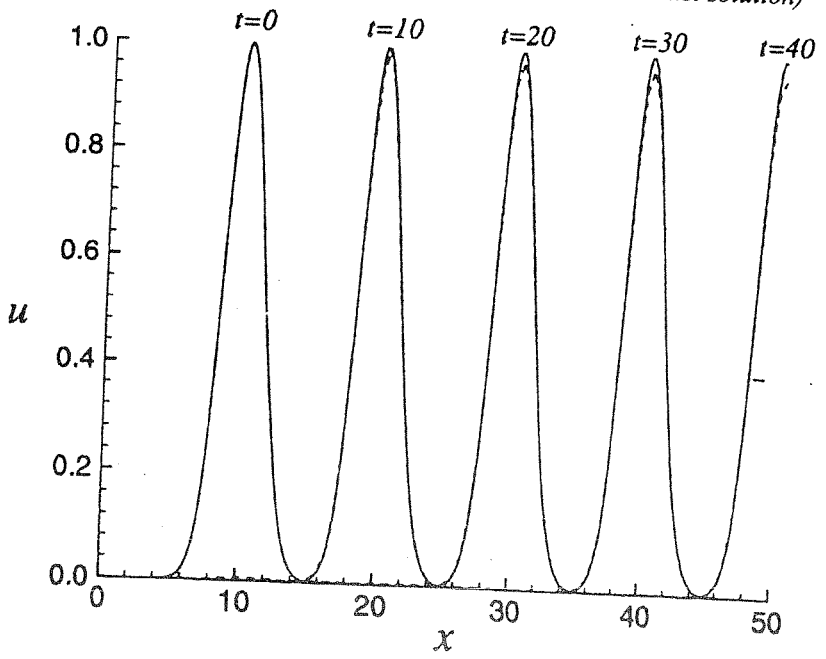

A.3.2. Triangular kinematic wave

A triangular shaped wave is routed through a rectangular channel 9,144 m long. The general set up for the test is obtained from Chow et al. (1989), however some parameter values are slightly changed. The channel characteristics are: Manning's coefficient = 0.035, slope = 1%, and width = 60 m. There is no lateral flow and the initial condition is a uniform area of 30 m^2, equivalent to a discharge of 53.4 m^3/s. The input area hydrograph is given by,

$$a = 30 \ m^2 \qquad 0 \le t \le 12 \ min$$

$$a = \left(\frac{5}{4} - \frac{t}{2880}\right)30 + \left(-\frac{1}{4} + \frac{t}{2880}\right)60 \qquad 12 \ min < t \le 60 \ min$$

$$a = \left(\frac{9}{4} - \frac{t}{2880}\right)60 + \left(-\frac{5}{4} + \frac{t}{2880}\right)30 \qquad 60 \ min < t \le 108 \ min$$

$$a = 30 \ m^2 \qquad t > 108 min \ min$$

The test is performed over a 30 evenly spaced element size of $\Delta x = 304.8 \ m$, and with a $\Delta t = 30 \ s$. Two different sets of appropriate scales are chosen for this problem as shown in Table A.2,

Table A.2: Scale sets

Scale	Set 1	Set 2
L_0	1219.2 m	--
u_0	--	1 m
V_0	4.064 m/s	2 m/s
$\bar{S}$	0.01	0.01
b_0	60 m	60 m

and the remaining scales are immediately derived and are shown in Table A.4,

Table A.3: Remaining scales

Scale	Set 1	Set 2
L_0	--	100 m
u_0	12.19 m	--
τ_r	300 s	60 s
n_0	0.13	0.05

Figure A.9.*a* and Figure A.9.*b* depict the wave amplitude as a function of time at different locations, and the wave profile as a function of at different times, respectively, obtained when the first set of scales is used. Numerical results are compared with analytical values obtained by means of the method of characteristics (Figure A.9.*a*). The agreement between the simulated values and the exact solution is remarkable. This test shows that the Petrov-Galerkin scheme implemented here is perfectly able to eliminate the typical and unwelcome numerical oscillations of the traditional Galerkin method. Besides that, the scheme introduces virtually no artificial diffusion, characteristic commonly associated with finite difference solutions.

In order to detect any model sensibility to the selection of the proper set of scales, a second run is performed with a second set of scales (see above). Although not shown here, the results obtained are identical to those presented in Figure A.9.*a* and Figure A.9.*b*. This demonstrates the model independence to the choice of scales.

Finally, the use of $\Delta t = 60\ s$ (maximum Courant number = 0.93) still produces good results, however when Δt is tripled, i.e. $\Delta t = 3\ min$, some wiggles develop on the numerical solution. In this later case, the maximum Courant number is 2.78. Although the scheme is unconditionally stable, the use of values greater than one for the Courant number is unadvisable because of an excessive loss of accuracy. Note that when peak

values are used, the kinematic wave applicability criterium stated in Equation (4-15) is violated, as well as the criterium set forth by Lighthill and Witham (1955) as the Froude number $F_o = V_0/\sqrt{gu_0}$ is close to one. Therefore, this example represents a marginal condition as far as the kinematic wave model applicability is concerned, contrary to the belief of the authors (Chow et al. 1989).

Figure A.9.a: Wave amplitude as a function of time at different locations (Solid line: numerical solution. Dashed line: analytical solution)

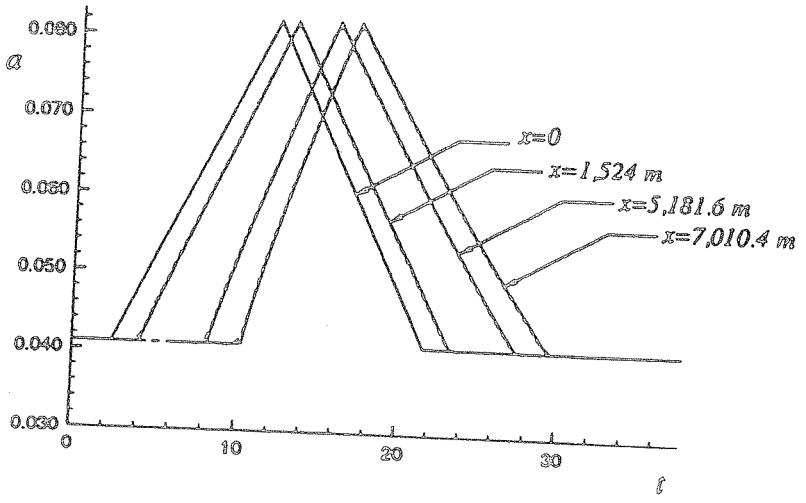

Figure A.9.b: Wave profile as a function of at different times

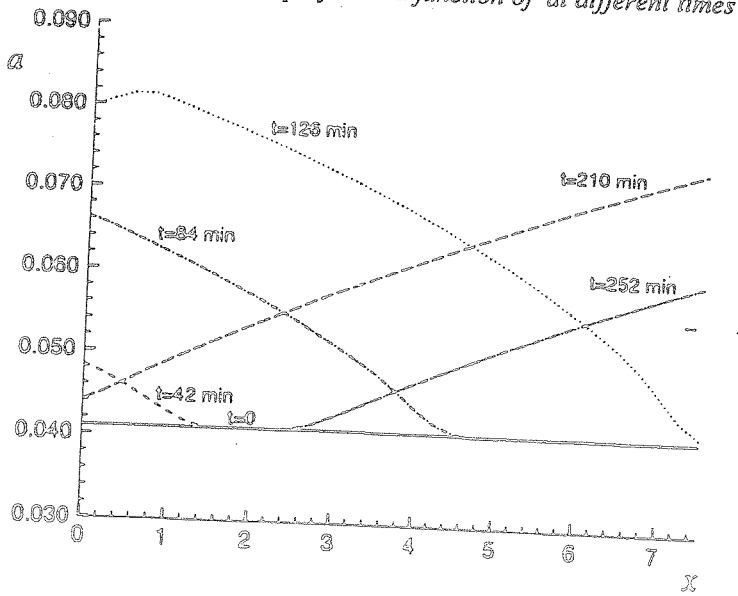

APPENDIX B

STREAM PARAMETERS

Reach #	Width (m)	Rf (s)	n	Slope	Elevation (m) (*)
1	1.508E1	1.00E3	3.00E-2	5.63E-3	3.000E2
2	1.519E1	1.00E3	3.00E-2	5.48E-3	2.945E2
3	1.546E1	1.00E3	3.00E-2	5.19E-3	2.892E2
4	1.595E1	1.00E3	3.00E-2	4.96E-3	2.856E2
5	1.674E1	1.00E3	3.00E-2	4.64E-3	2.824E2
6	1.789E1	1.00E3	3.00E-2	4.33E-3	2.792E2
7	1.898E1	1.00E3	3.00E-2	3.98E-3	2.761E2
8	2.010E1	1.00E3	3.00E-2	3.68E-3	2.732E2
9	2.070E1	1.00E3	3.00E-2	3.38E-3	2.707E2
10	2.113E1	1.00E3	3.00E-2	3.16E-3	2.680E2
11	2.078E1	1.00E3	3.00E-2	3.01E-3	2.655E2
12	2.046E1	1.00E3	3.00E-2	2.92E-3	2.630E2
13	1.958E1	1.00E3	3.00E-2	2.88E-3	2.604E2
14	1.898E1	1.00E3	3.00E-2	2.86E-3	2.579E2
15	1.770E1	1.00E3	3.01E-2	2.83E-3	2.557E2
16	1.698E1	1.00E3	3.04E-2	2.82E-3	2.533E2
17	1.602E1	1.00E3	3.13E-2	2.82E-3	2.508E2
18	1.582E1	1.00E3	3.24E-2	2.85E-3	2.484E2
19	1.540E1	1.00E3	3.41E-2	2.92E-3	2.460E2
20	1.516E1	1.00E3	3.60E-2	3.03E-3	2.435E2
21	1.483E1	1.00E3	3.77E-2	3.18E-3	2.409E2
22	1.456E1	1.00E3	3.90E-2	3.34E-3	2.381E2
23	1.446E1	1.00E3	3.96E-2	3.48E-3	2.352E2
24	1.461E1	1.00E3	4.00E-2	3.58E-3	2.320E2
25	1.514E1	1.00E3	4.00E-2	3.60E-3	2.286E2
26	1.612E1	1.00E3	3.98E-2	3.54E-3	2.252E2
27	1.720E1	1.00E3	3.96E-2	3.44E-3	2.218E2
28	1.926E1	1.00E3	3.88E-2	3.21E-3	2.196E2
29	2.182E1	1.00E3	3.79E-2	2.94E-3	2.169E2
30	2.412E1	1.00E3	3.70E-2	2.73E-3	2.142E2
31	2.727E1	1.00E3	3.60E-2	2.52E-3	2.123E2
32	3.121E1	1.00E3	3.48E-2	2.39E-3	2.102E2
33	3.664E1	1.02E3	3.34E-2	2.33E-3	2.083E2
34	4.375E1	1.12E3	3.21E-2	2.36E-3	2.065E2
35	5.320E1	1.51E3	3.09E-2	2.44E-3	2.046E2
36	6.370E1	2.27E3	3.03E-2	2.55E-3	2.025E2

Reach #	Width (m)	Rf (s)	n	Slope	Elevation (m) (*)
37	7.455E1	3.67E3	3.00E-2	2.66E-3	2.002E2
38	8.377E1	1.14E4	3.00E-2	2.77E-3	1.978E2
39	9.168E1	3.20E4	3.00E-2	2.86E-3	1.952E2
40	9.621E1	1.45E5	3.00E-2	2.93E-3	1.926E2
41	9.927E1	13.51E5	3.00E-2	2.99E-3	1.899E2
42	1.001E2	18.07E5	3.00E-2	3.05E-3	1.872E2
43	1.005E2	11.32E6	3.00E-2	2.97E-3	1.845E2
44	9.983E1	11.96E6	3.00E-2	2.81E-3	1.817E2
45	9.834E1	12.42E6	3.00E-2	2.32E-3	1.790E2
46	9.522E1	2.79E6	3.03E-2	1.85E-3	1.761E2
47	9.100E1	2.93E6	3.10E-2	1.29E-3	1.731E2
48	8.546E1	3.00E6	3.26E-2	9.29E-4	1.702E2
49	7.967E1	2.94E6	3.41E-2	7.56E-4	1.674E2
50	7.230E1	2.84E6	3.60E-2	6.48E-4	1.656E2
51	6.241E1	2.55E6	3.76E-2	5.93E-4	1.639E2
52	5.188E1	2.17E6	3.98E-2	5.32E-4	1.622E2
53	4.177E1	1.60E6	4.13E-2	5.06E-4	1.605E2
54	3.402E1	1.13E6	4.35E-2	4.83E-4	1.587E2
55	2.987E1	7.16E5	4.42E-2	4.55E-4	1.569E2
56	2.706E1	4.39E5	4.50E-2	4.24E-4	1.552E2
57	2.568E1	2.26E5	4.50E-2	3.72E-4	1.533E2
58	2.427E1	1.17E5	4.48E-2	3.32E-4	1.514E2
59	2.291E1	4.47E4	4.45E-2	2.70E-4	1.493E2
60	2.149E1	1.50E4	4.38E-2	2.30E-4	1.472E2
61	2.029E1	3.79E3	4.30E-2	1.75E-4	1.451E2
62	1.921E1	1.23E3	4.20E-2	1.46E-4	1.431E2
63	1.837E1	1.00E3	4.11E-2	1.16E-4	1.414E2
64	1.776E1	1.00E3	4.04E-2	1.06E-4	1.399E2
65	1.736E1	1.00E3	4.01E-2	1.00E-4	1.387E2
66	1.709E1	1.00E3	4.00E-2	1.00E-4	1.378E2
67	1.690E1	1.00E3	4.00E-2	1.00E-4	1.372E2
68	1.673E1	1.00E3	4.00E-2	1.00E-4	1.368E2
69	1.662E1	1.00E3	4.00E-2	1.00E-4	1.364E2
					1.360E2

(*) elevation given by river node